# We need high resolution imaging and spectroscopy from optical to IR

Content

- The kinematics of massive star forming regions.
- HII galaxies and Giant HII regions. Cosmology
- Circumstellar regions
- 30 Dor (NGC2070) The giant HII region prototype

# Giant HII regions and HII galaxies: Measuring the distance scale and the Dark Energy Equation of State

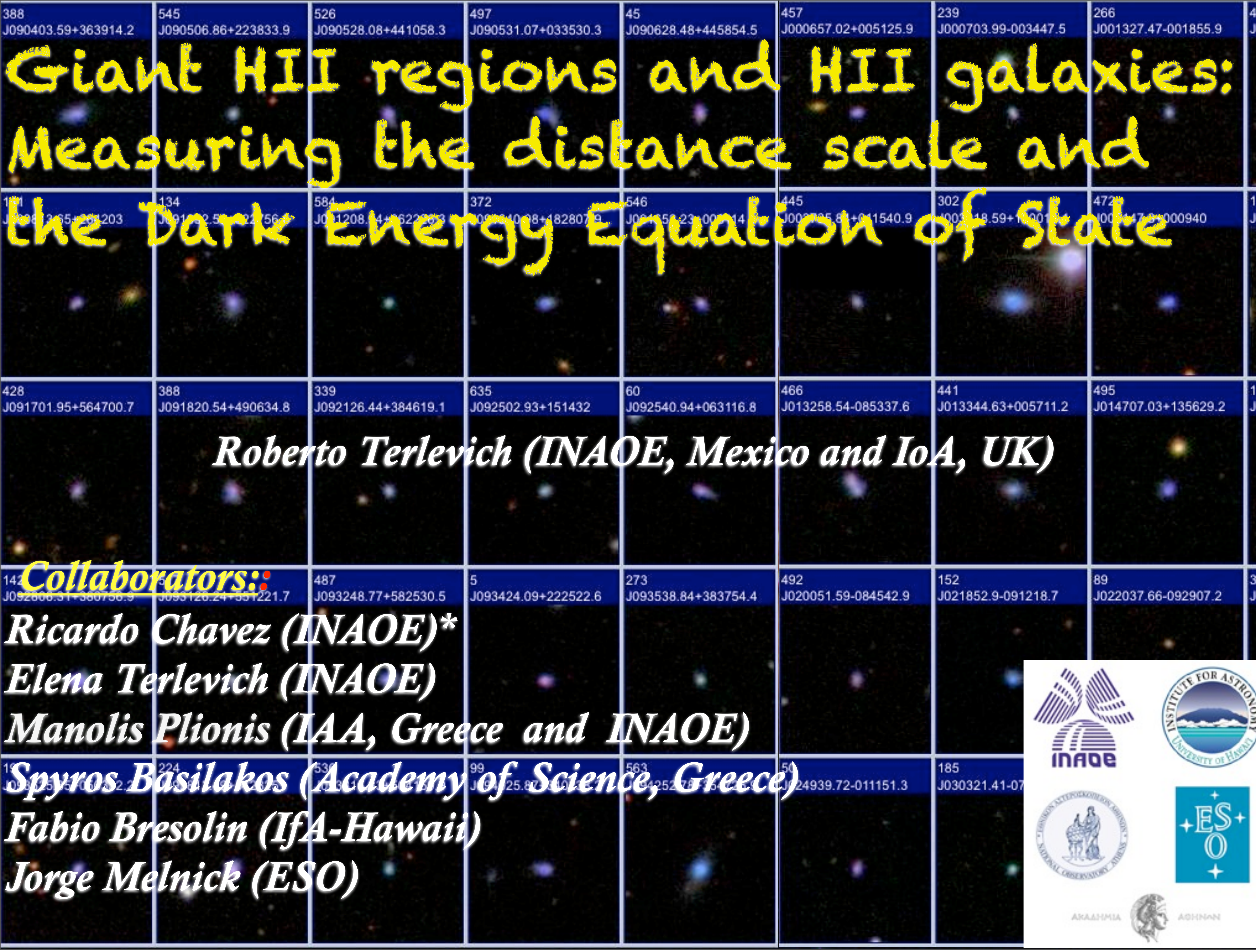

*Roberto Terlevich (INAOE, Mexico and IoA, UK)*

Collaborators::

*Ricardo Chavez (INAOE)**
*Elena Terlevich (INAOE)*
*Manolis Plionis (IAA, Greece and INAOE)*
*Spyros Basilakos (Academy of Science, Greece)*
*Fabio Bresolin (IfA-Hawaii)*
*Jorge Melnick (ESO)*

# *Cosmology Breakthroughs in Recent Past*

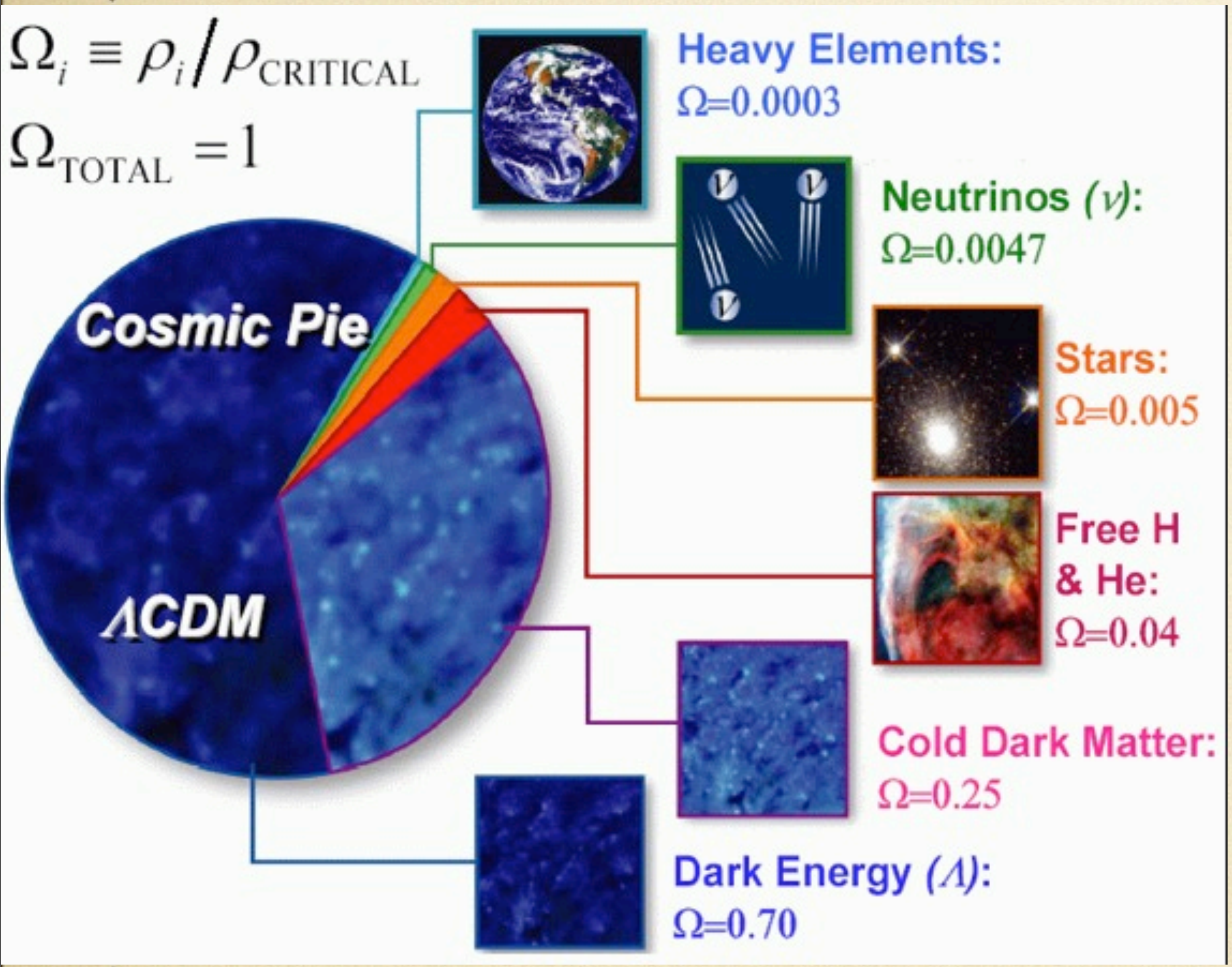


**"Dark Energy"** and **Dark Matter** are the dominant constituent of the Universe => 95% of the Universe is in forms unknown to us!

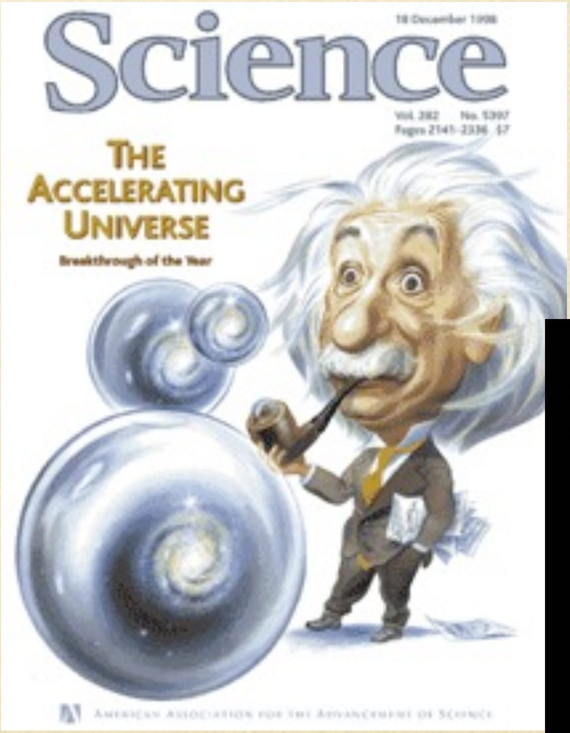


*1998 Science breakthrough of year*


*2003 Science breakthrough of year*

# *Cosmology Breakthroughs in Recent Past*

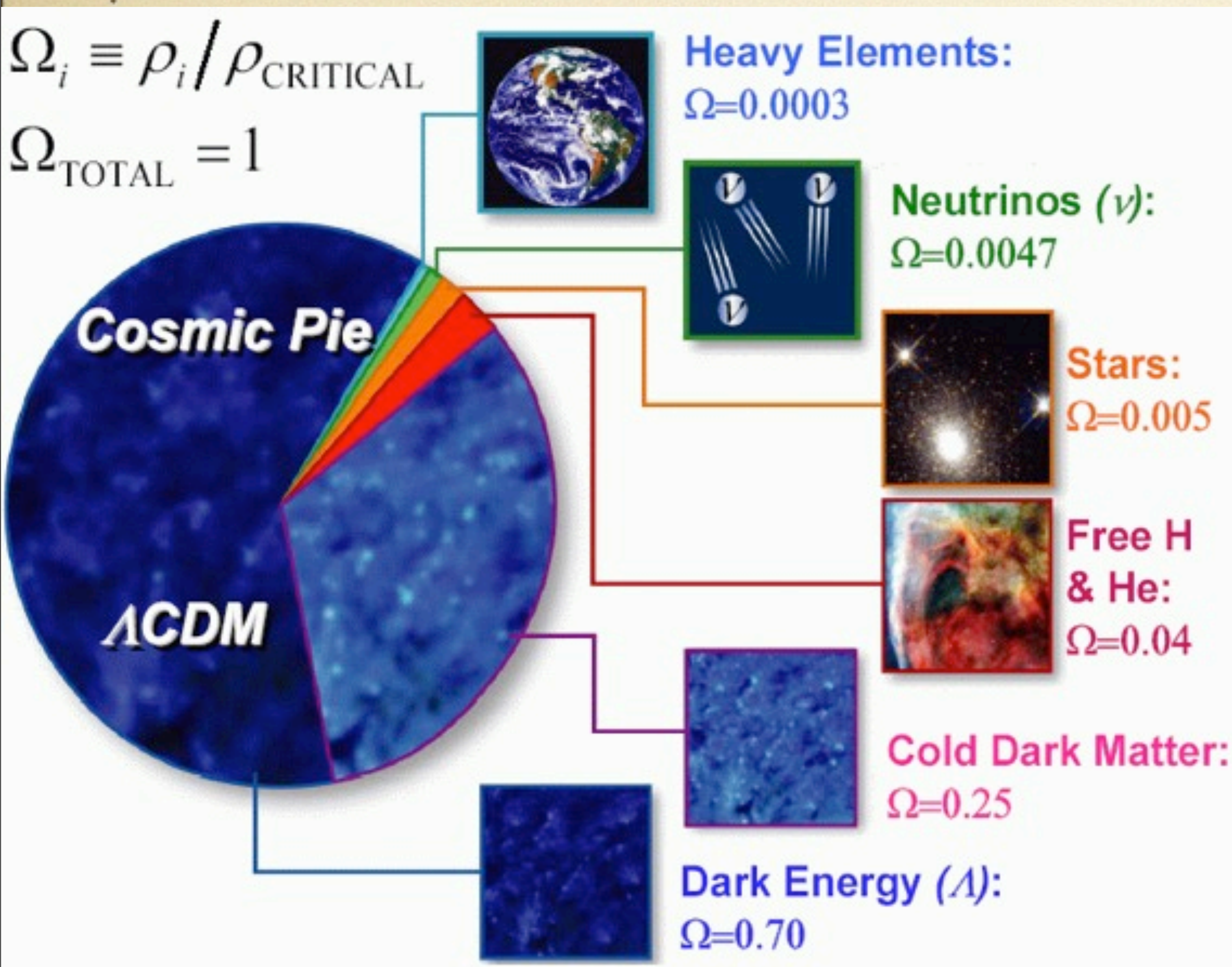


**"Dark Energy"** and **Dark Matter** are the dominant constituent of the Universe => 95% of the Universe is in forms unknown to us!

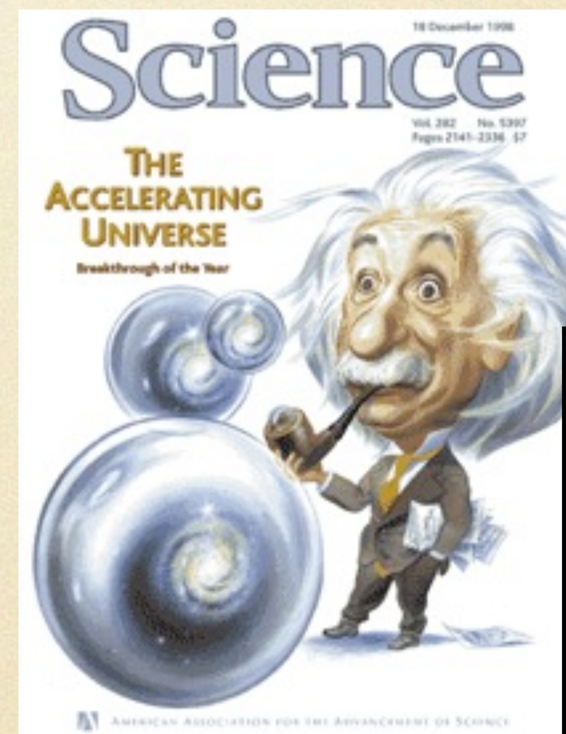


*1998 Science breakthrough of year*

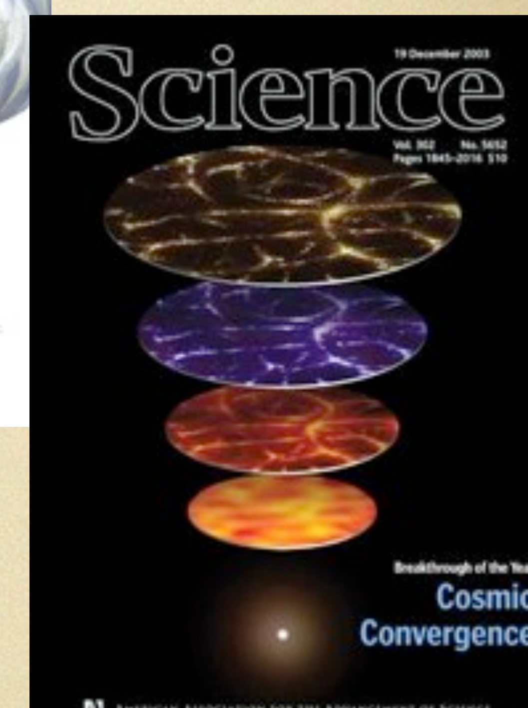


*2003 Science breakthrough of year*

➢ **"Dark Energy"** is **TOP PRIORITY** for future research: Outcome of 2 very extensive, recently released reports, "Report of the Dark Energy Task Force (advising DOE, NASA and NSF), Albrecht et al. (2006), and "Report of the ESA/ESO Working Group on Fundamental Cosmology", Peacock et al. (2006)

# *The Observational Landscape*

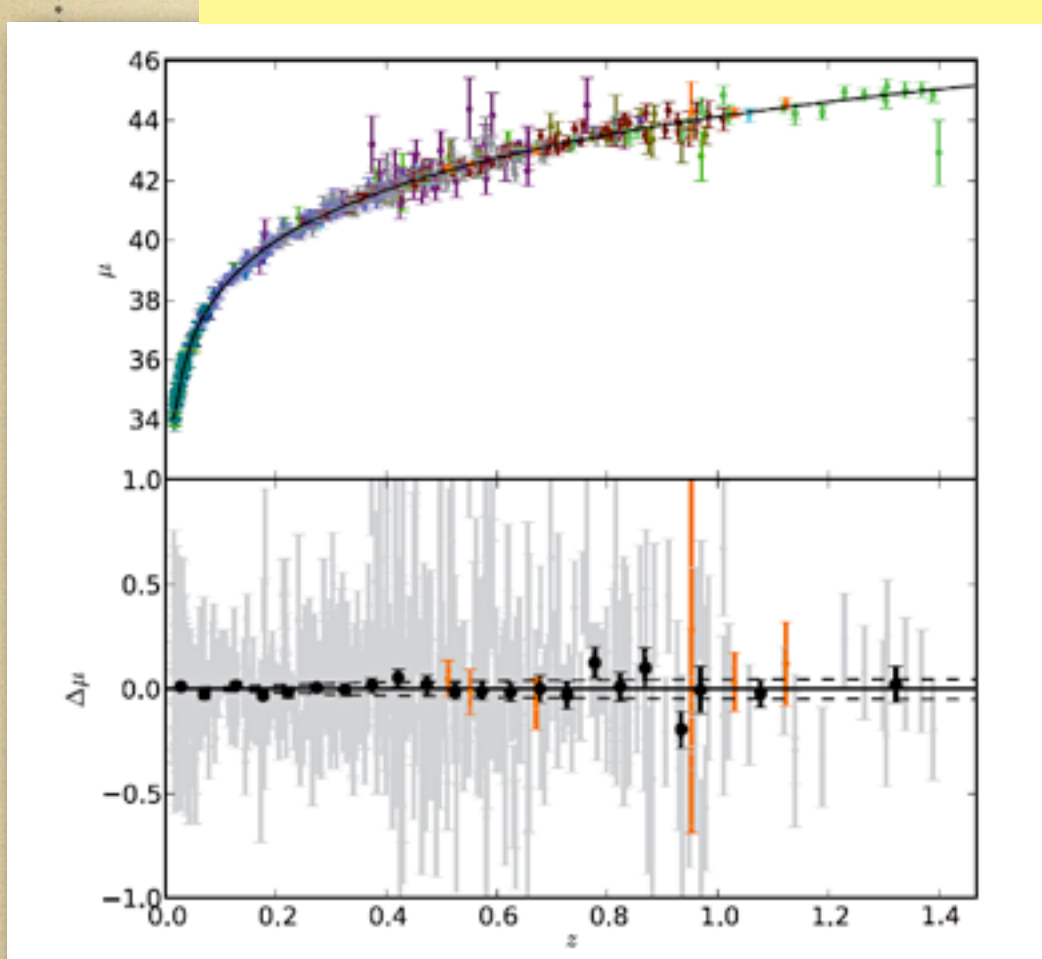


From Amanullah et al. 2010

Union2: 557 SNe Ia

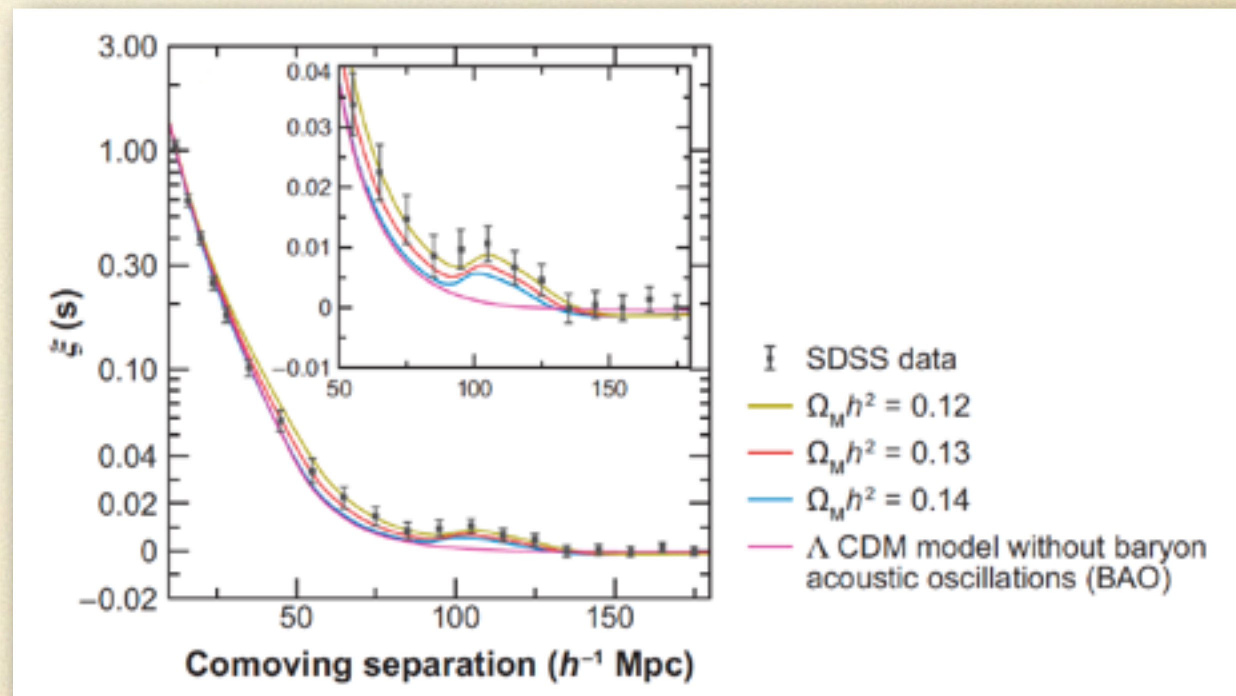


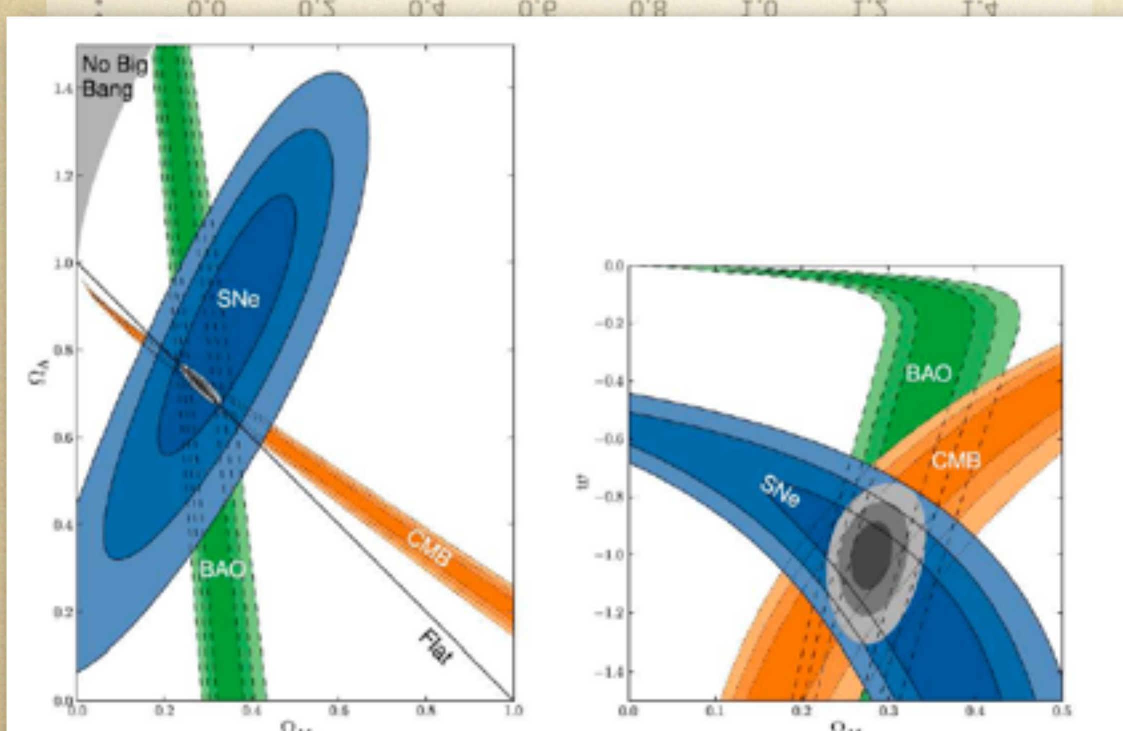


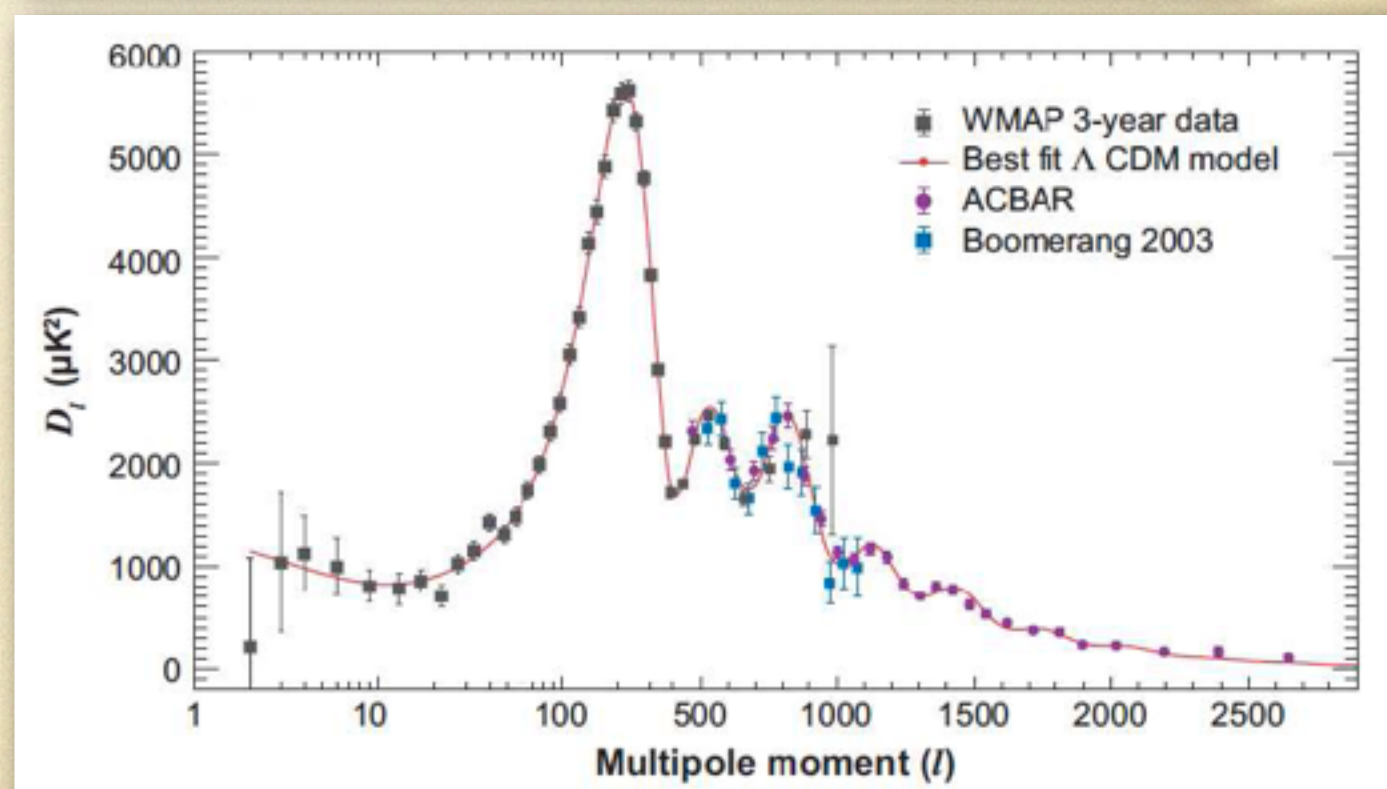


From Frieman et al. 2008

# *Measuring Dark Energy*

***Dark Energy*** is manifested in the expansion rate of the Universe, via:

$$H^2(z) = H^2_0[\Omega_m(1+z)^3 + \Omega_R (1+z)^4 + \Omega_{DE} (1+z)^{3(1+w)} ]$$

matter radiation dark energy

Equation of state parameter $w$ measures the evolution of the density of dark energy with redshift.

For $\Lambda$ cosmology: $w = -1$ ($p_{VAC} = -w\rho_{VAC} = -\Lambda/8\pi G$).

$w$ is currently constrained to ~20% by WMAP, SDSS, and SN Ia.

**Variable, time-dependent equations of state are possible:**

$$w(z)=w_0+w_a [z/(1+z)]$$

# *Measuring Dark Energy*

**Standard Candles** (e.g., SN Ia) measure luminosity distance:

$$d_L = (1+z) \int dz/H(z)$$

observationally we have: $d_L = 10^{(\Delta M - 25)/5}$ with $\Delta M = m - M$.

**Standard Rulers** (eg. CMB, BAO) measure angular diameter distance:

$$d_a = (1+z)^{-1} \int dz/H(z)$$

**SN Ia: Best tracer of H(z) to date, but.....**

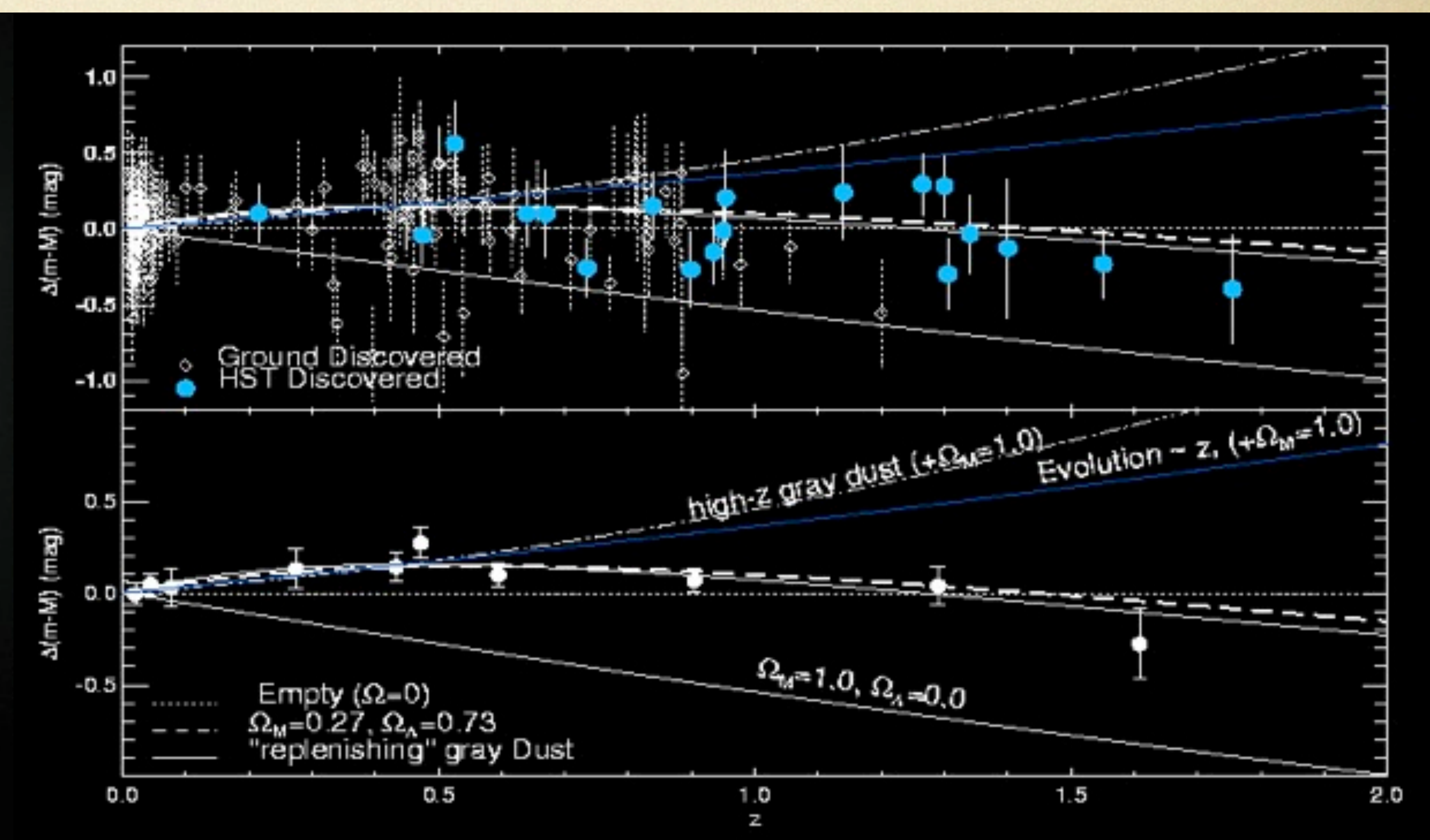

# *Manifestations of different Dark Energy models*

**What are the expected Distance Modulus variations of different models ?**

Assuming a nominal model ($w$=-1, $\Omega_m$=0.27) we plot below the relative distance modulus, $\Delta(m-M)$, between different models. Evidently we have:

1. **Maximum variation occurs at $z > 2$ (out of current SN Ia reach) !**
2. **There is a degeneracy between $w$ and $\Omega_m$**
3. **For $z<0.2-0.5$ differences are insignificant**

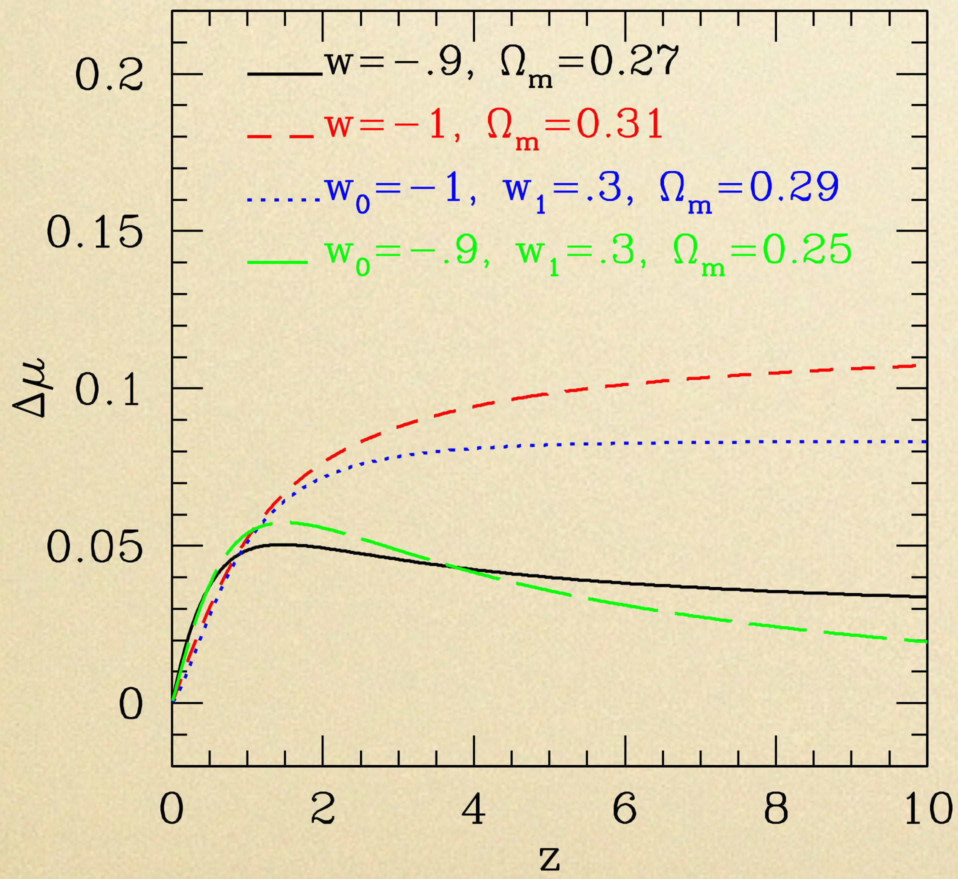

# *Manifestations of different Dark Energy models*

**What are the expected Distance Modulus variations of different models ?**

Assuming a nominal model ($w$=-1, $\Omega_m$=0.27) we plot below the relative distance modulus, $\Delta(m-M)$, between different models. Evidently we have:

**1. Maximum variation occurs at $z > 2$ (out of current SN Ia reach) !**

**2. There is a degeneracy between $w$ and $\Omega_m$**

**3. For $z<0.2-0.5$ differences are insignificant**

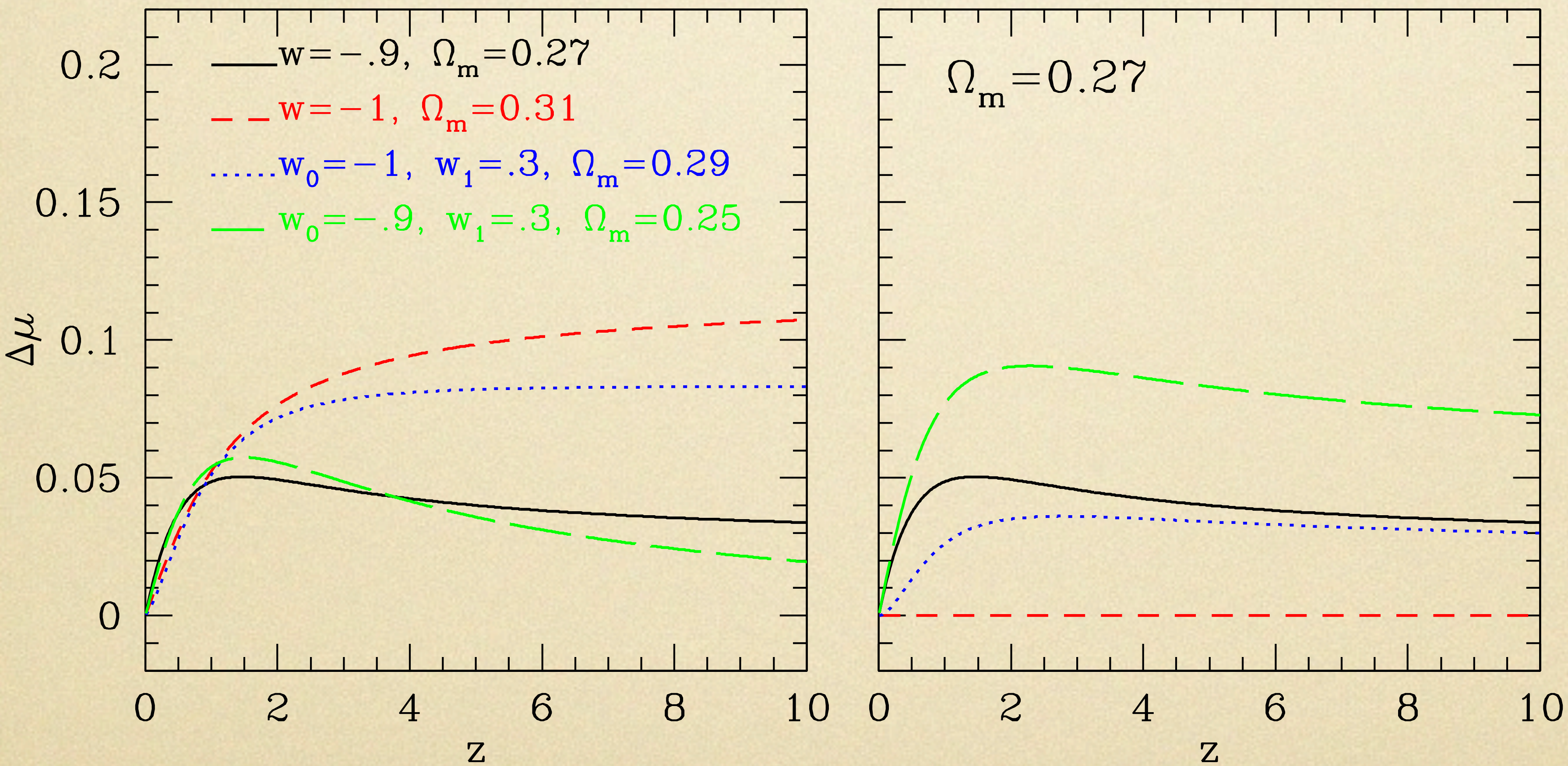


**see Plionis etal 2011, MNRAS.416.2981**

Even when $\Omega_m$ is fixed there are significant $\Delta(m-M)$, differences due to $w$ variations

# *Recent SN Ia based Results*

## 307 SN Ia: Large Homogeneous Sample (Kowalski et al. 2008)

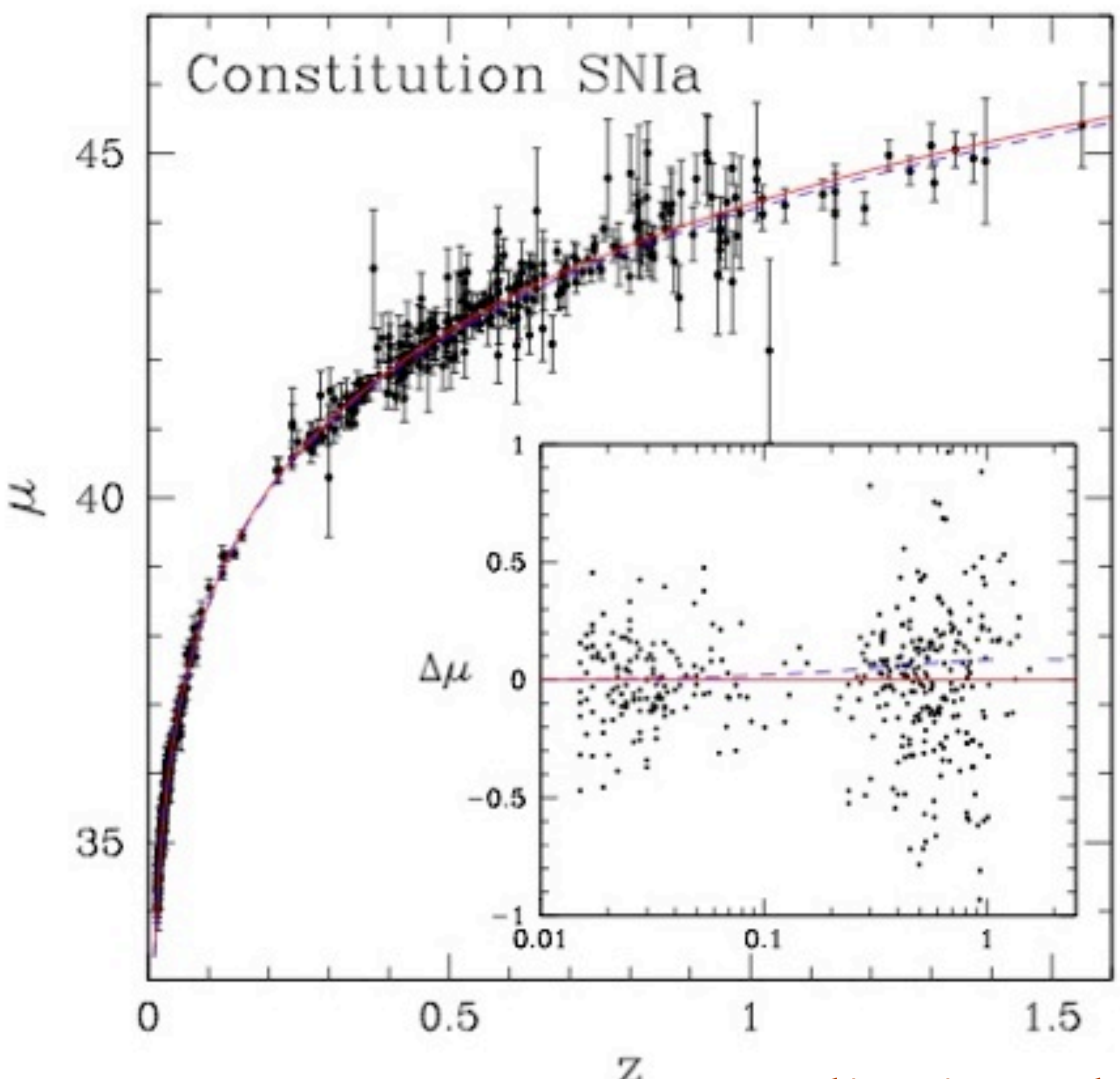


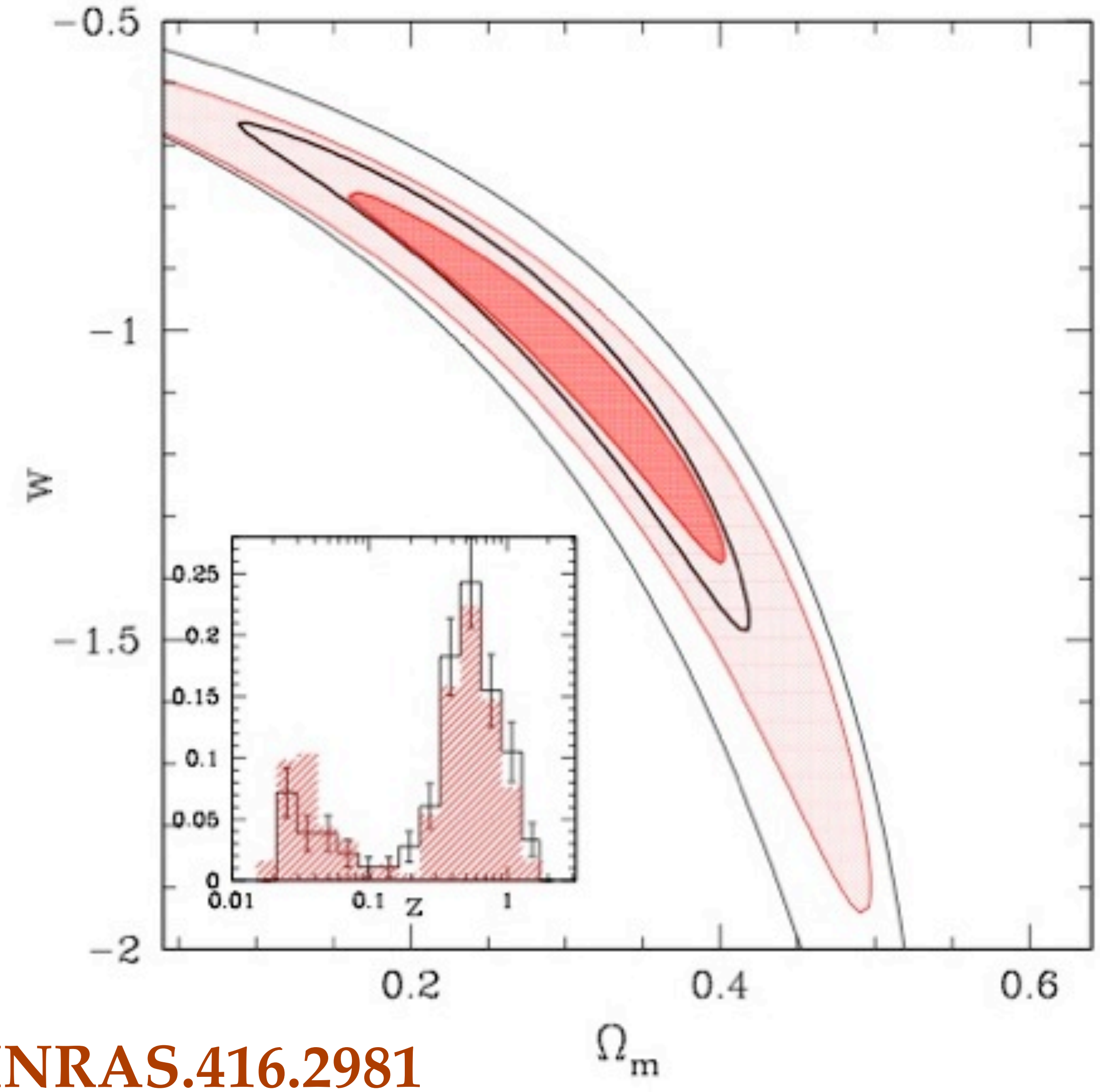


**see Plionis etal 2011, MNRAS.416.2981**

**Figure 4.** SNIa distance moduli as a function of redshift. *Inset Panel:* Distance moduli difference between the best fit model (see Table 1) and the SNIa data. The blue dashed line is the corresponding difference between the reference (red-continuous line) $(\Omega_m, w) = (0.3, -1.04)$ and the $(\Omega_m, w) = (0.3, -0.85)$ *dark-energy* models.

**Figure 5.** Cosmological parameter solution space using either of the two SNIa data sets (*Constitution*: red shaded contours and *D07*: black contours). Contours corresponding to the 1 and $3\sigma$ confidence levels are shown (ie., plotted where $-2\ln\mathcal{L}/\mathcal{L}_{\max}$ is equal to 2.30 and 11.83, respectively). *Inset Panel:* Normalized redshift distributions of the two SNIa data sets (the shaded histogram corresponds to the *Constitution* set).

# *SN Ia based Results (After 2008)*

**$\chi^2$ minimization procedure between models and data (Plionis etal 2011, MNRAS.416.2981)**

$$\mathcal{L}^{\rm SNIa}(\mathbf{c}) \propto \exp[-\chi^2_{\rm SNIa}(\mathbf{c})/2]$$

with:

$$\chi^2_{\rm SNIa}(\mathbf{c}) = \sum_{i=1}^{172}\left[\frac{\log D_{\rm L}^{\rm th}(z_i,\mathbf{c}) - \log D_{\rm L}^{\rm obs}(z_i)}{\sigma_i}\right]^2$$

where $D_{\rm L}(z)$ is the dimensionless luminosity distance

$$D_{\rm L}(z) = H_{\rm o} d_{\rm L} = H_{\rm o}(1+z)x(z)$$

Increasing the number of SNIa from 181 to 307 does not provide more stringent constraints !

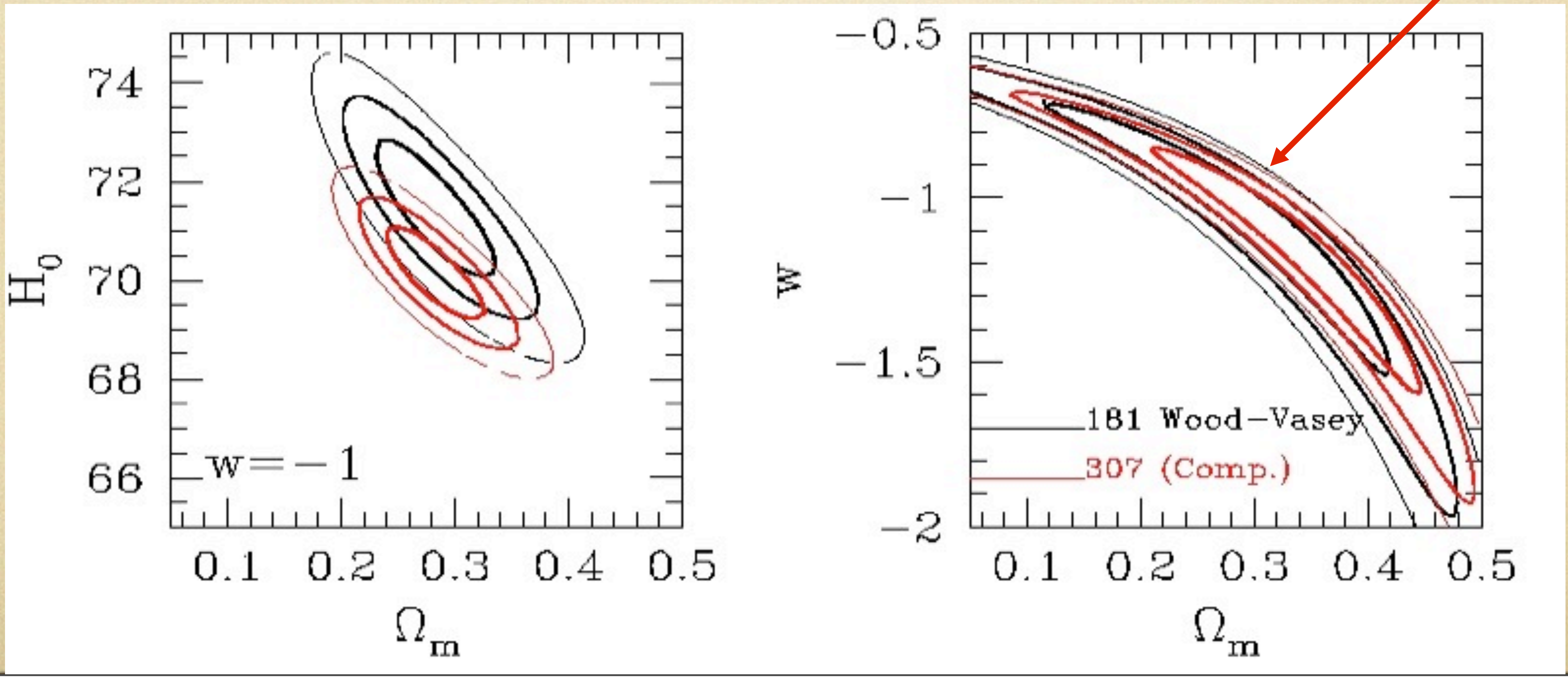

# *How to proceed to reduce uncertainties in the* $w$-$\Omega_m$

**We model the SNIa distance modulus error distribution so that we obtain the same type of $w$-$\Omega_m$ constraints as with the real data.**

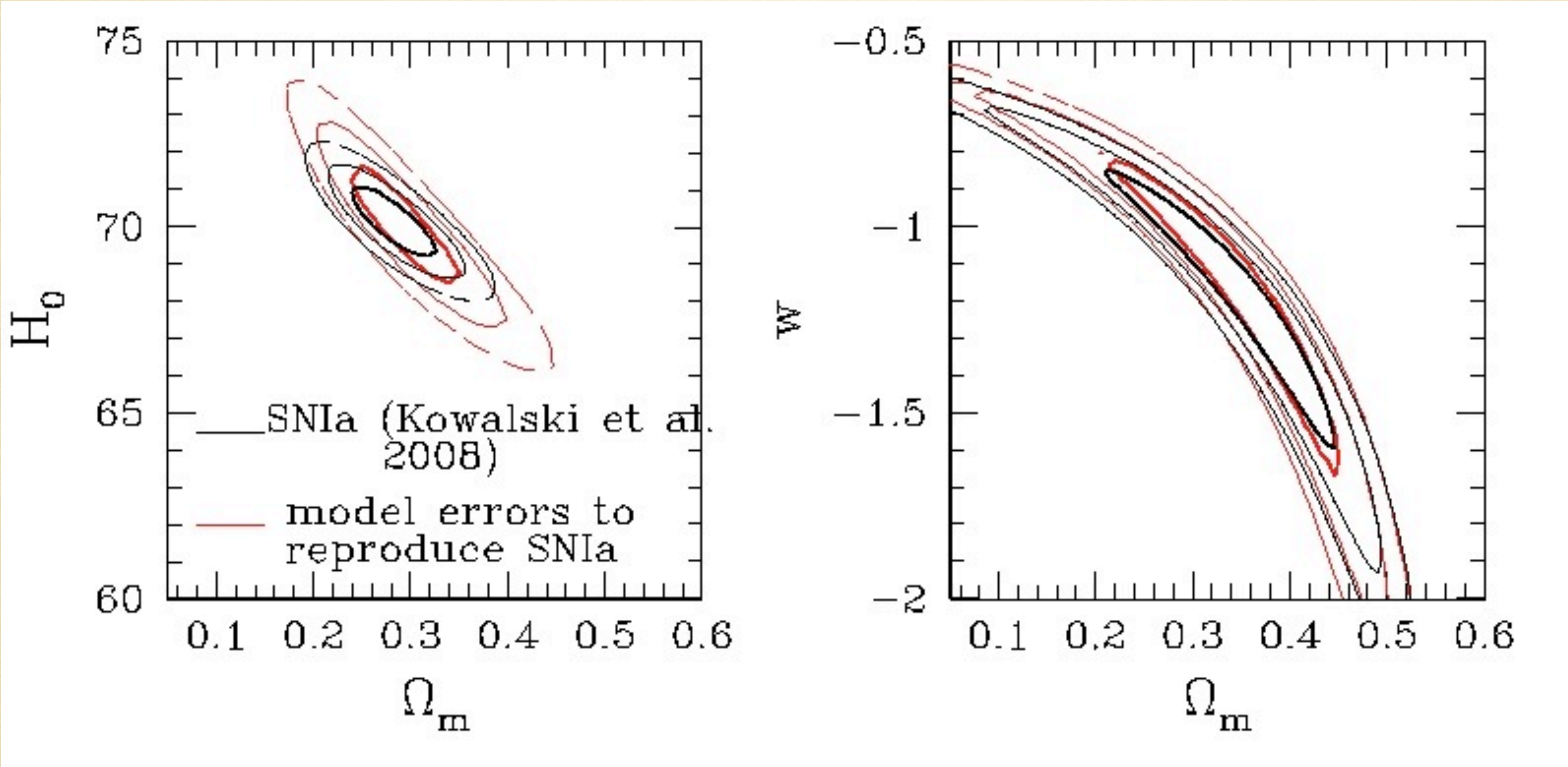


We tested which strategy is more efficient: (1) reduce significantly the random SN Ia distance modulus uncertainty or (2) include a population of higher-z standard candles (tracing the peak of the Δ(m−M) difference) having a similar or larger error budget than lower-z SN Ia?

# *How to proceed to reduce uncertainties in the $w$-$\Omega_m$*

**We model the SNIa distance modulus error distribution so that we obtain the same type of $w$-$\Omega_m$ constraints as with the real data.**

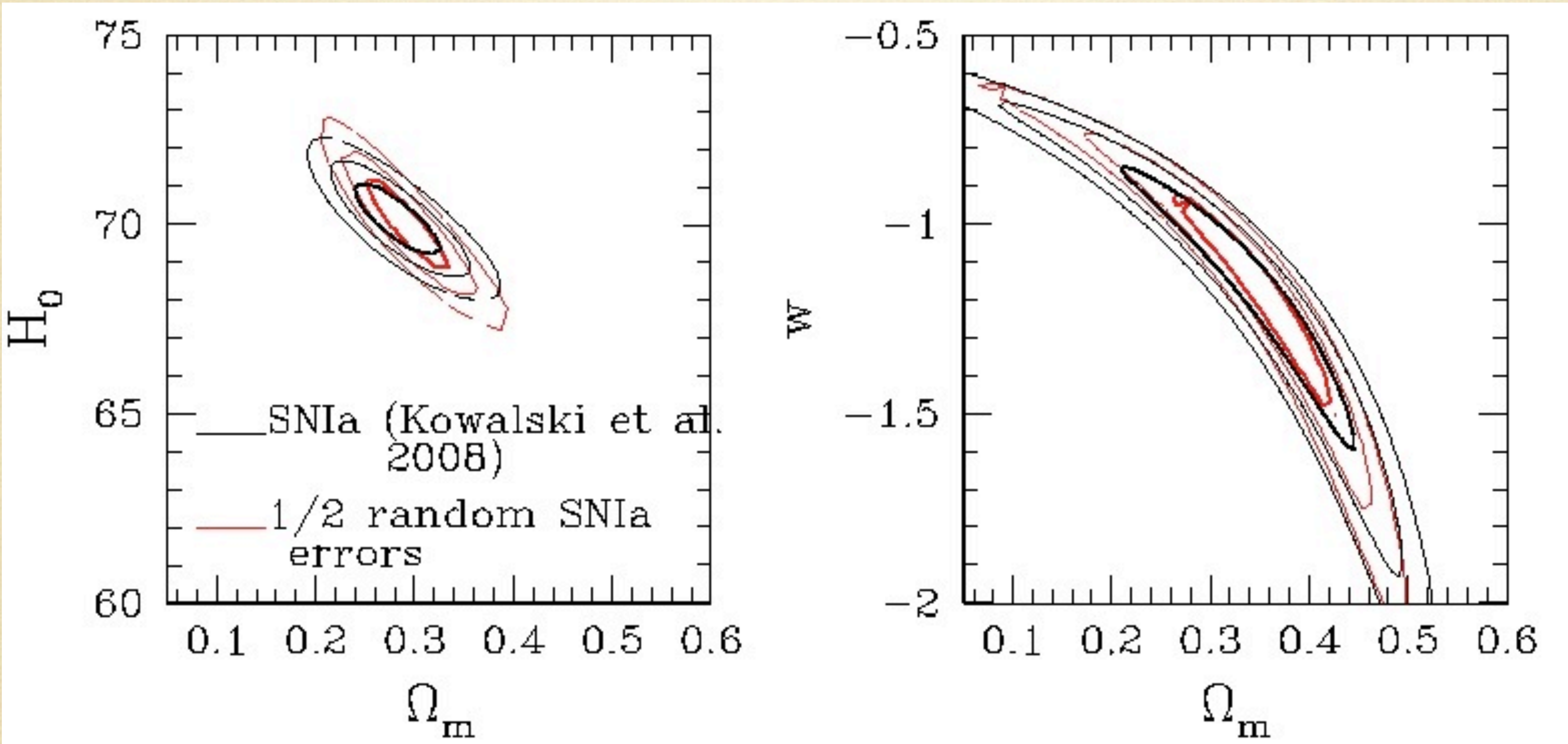


(1) reduce significantly the random SN Ia distance modulus uncertainty (by 1/2). ✗

# *How to proceed to reduce uncertainties in the $w$-$\Omega_m$*

**We model the SNIa distance modulus error distribution so that we obtain the same type of $w$-$\Omega_m$ constraints as with the real data.**

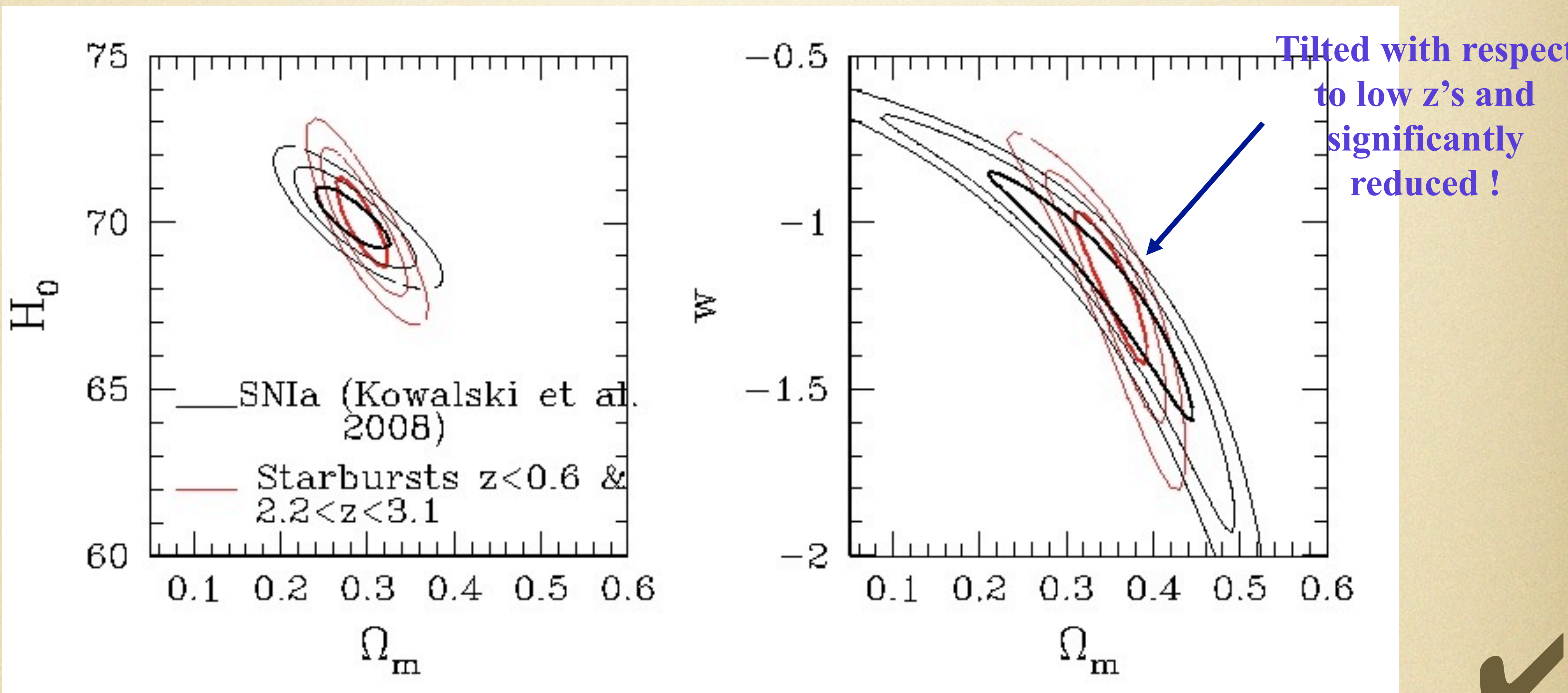


✔

(2a) include a population of higher-z standard candles (tracing the peak of the Δ(m−M) difference) having a **similar** error budget that lower-z SN Ia.

# *How to proceed to reduce uncertainties in the $w$-$\Omega_m$*

**We model the SNIa distance modulus error distribution so that we obtain the same type of $w$-$\Omega_m$ constraints as with the real data.**

**see Plionis etal 2011, MNRAS.416.2981**

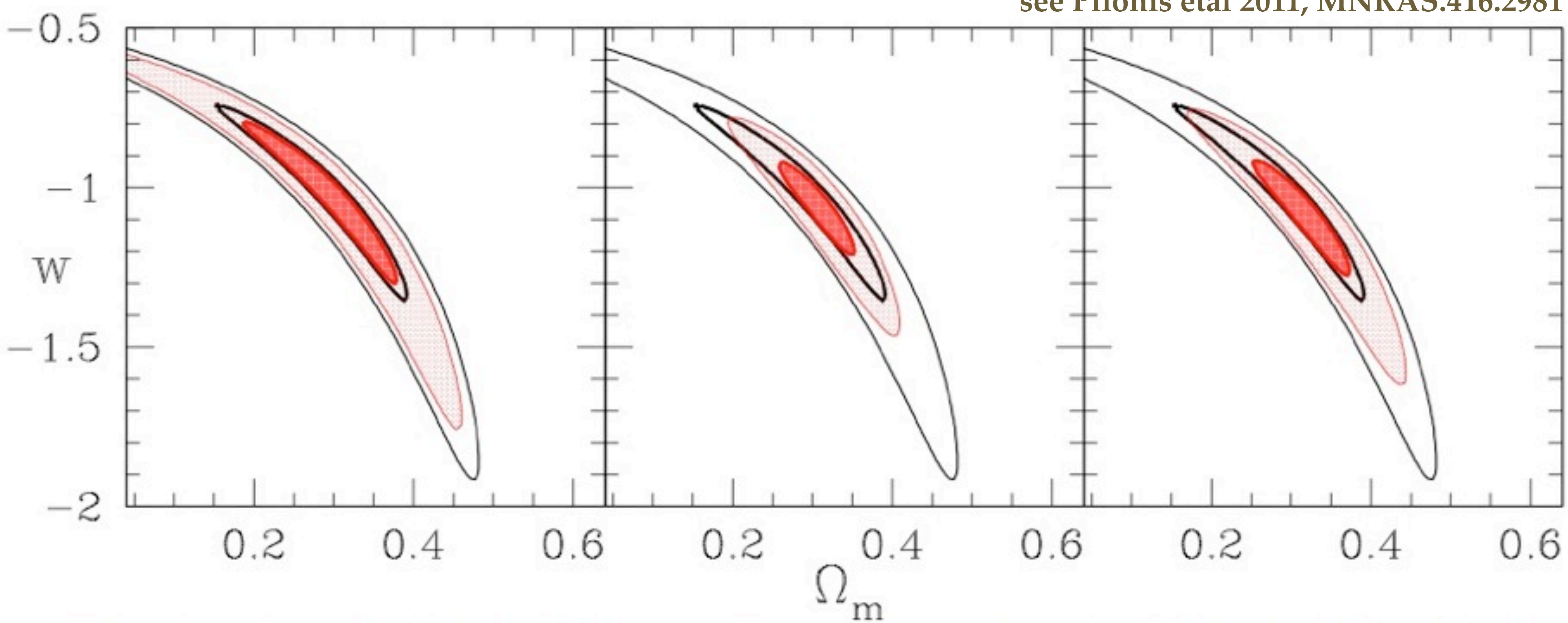


**Figure 7.** Comparison of the model *Constitution* SNIa constraints (black contours) with those (filled contours) derived by reducing to half their uncertainties (*left panel*), with those derived by adding a sample of 76 high $z$ tracers ($2 \lesssim z \lesssim 3.5$) with a distance modulus mean uncertainty of $\langle \sigma_\mu \rangle \simeq 0.5$ and no lensing degradation (*central panel*), and with those by including statistically the expected lensing degradation (*right panel*). For clarity we show only contours corresponding to the 1 and 3 $\sigma$ confidence levels.

✔

(2b) include a numerous population of higher-z standard candles (tracing the peak of the Δ(m−M) difference) having a **larger** error budget than low-z SN Ia.

This is the essence of our project which aims to sample $H_0(z)$ up to z~4

- The paramount importance of the measurement of $H_0$ and the detection and quantification of dark energy implies that alternative methods should be developed and applied.

- The paramount importance of the measurement of $H_0$ and the detection and quantification of dark energy implies that alternative methods should be developed and applied.

- Our aim is to determine $H_0$, and constrain the dark energy equation of state by using HII galaxies and Giant HII regions.

- The paramount importance of the measurement of $H_0$ and the detection and quantification of dark energy implies that alternative methods should be developed and applied.

- Our aim is to determine $H_0$, and constrain the dark energy equation of state by using HII galaxies and Giant HII regions.

- We hope to provide an **independent check** on the experiments that are based on more traditional tracers (SN Ia's and galaxies or clusters of galaxies) and new means to study the systematic errors of the methods.

# *What are H II Galaxies?*

HII galaxies are compact  massive burst of star formation in dwarf galaxies.

The luminosity of HII galaxies is completely overwhelmed by that of the burst. As a consequence they show the spectrum of an HII region (that’s what they are!) and are very compact.

They are discovered mainly in spectroscopic surveys due to their strong narrow emission lines, i.e. very large equivalent width, i.e. EWH$\beta$>50Å or EWH$\alpha$>200Å.

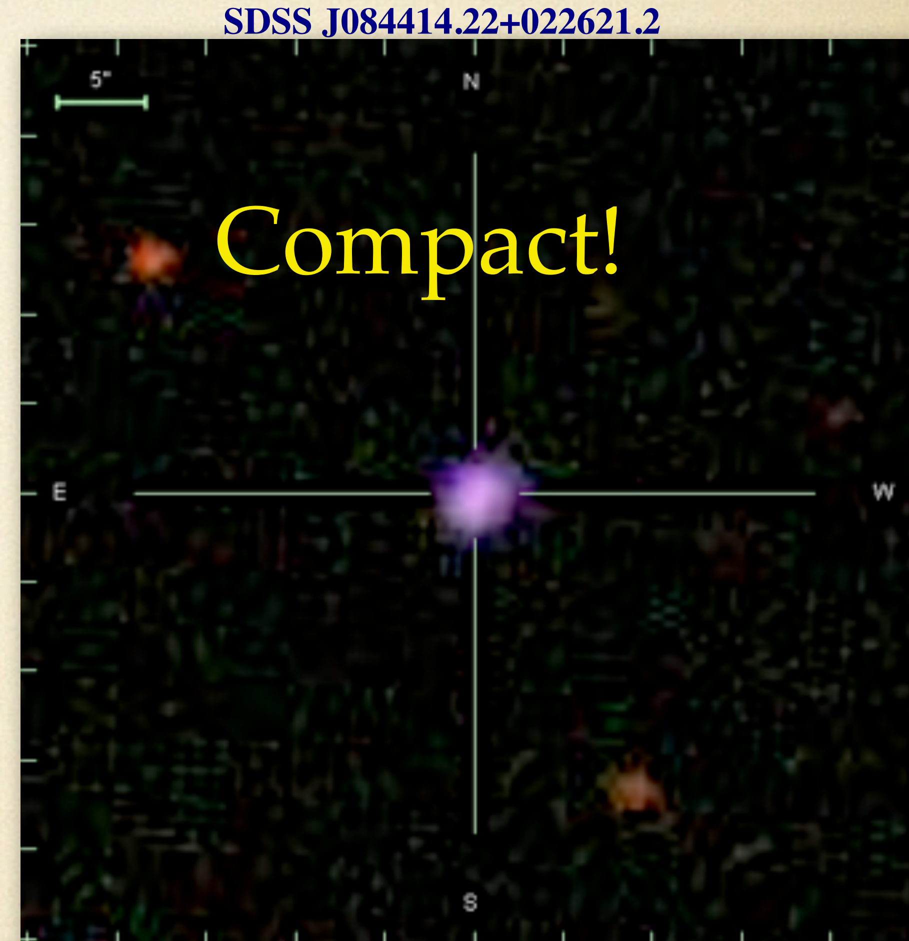


Because the luminosity of HII galaxies is dominated by the starburst component they can be observed at very large redshifts, and this fact makes them cosmologically very interesting objects.

**The observed properties are those of the young burst with almost no information (contamination) from the parent galaxy. This is a consequence of selecting candidates with EqwHα>200Å.**

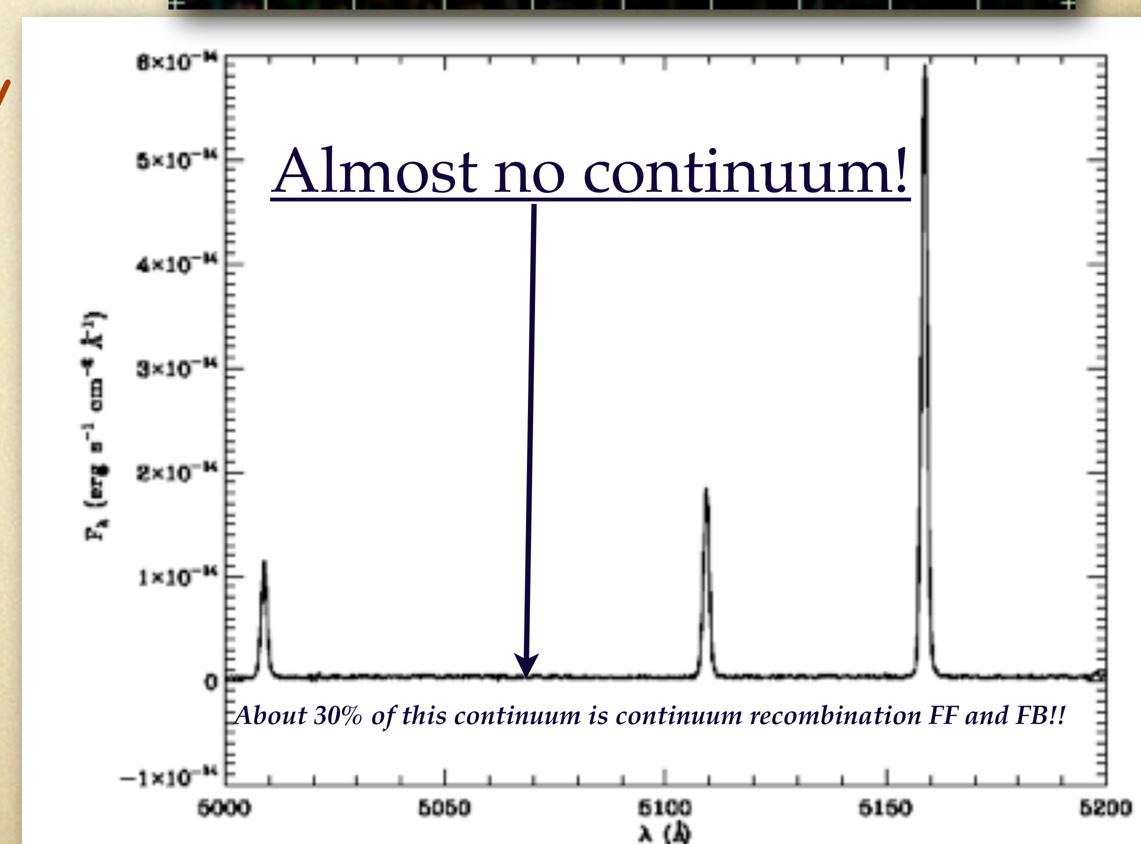

# *Images of H II Galaxies*

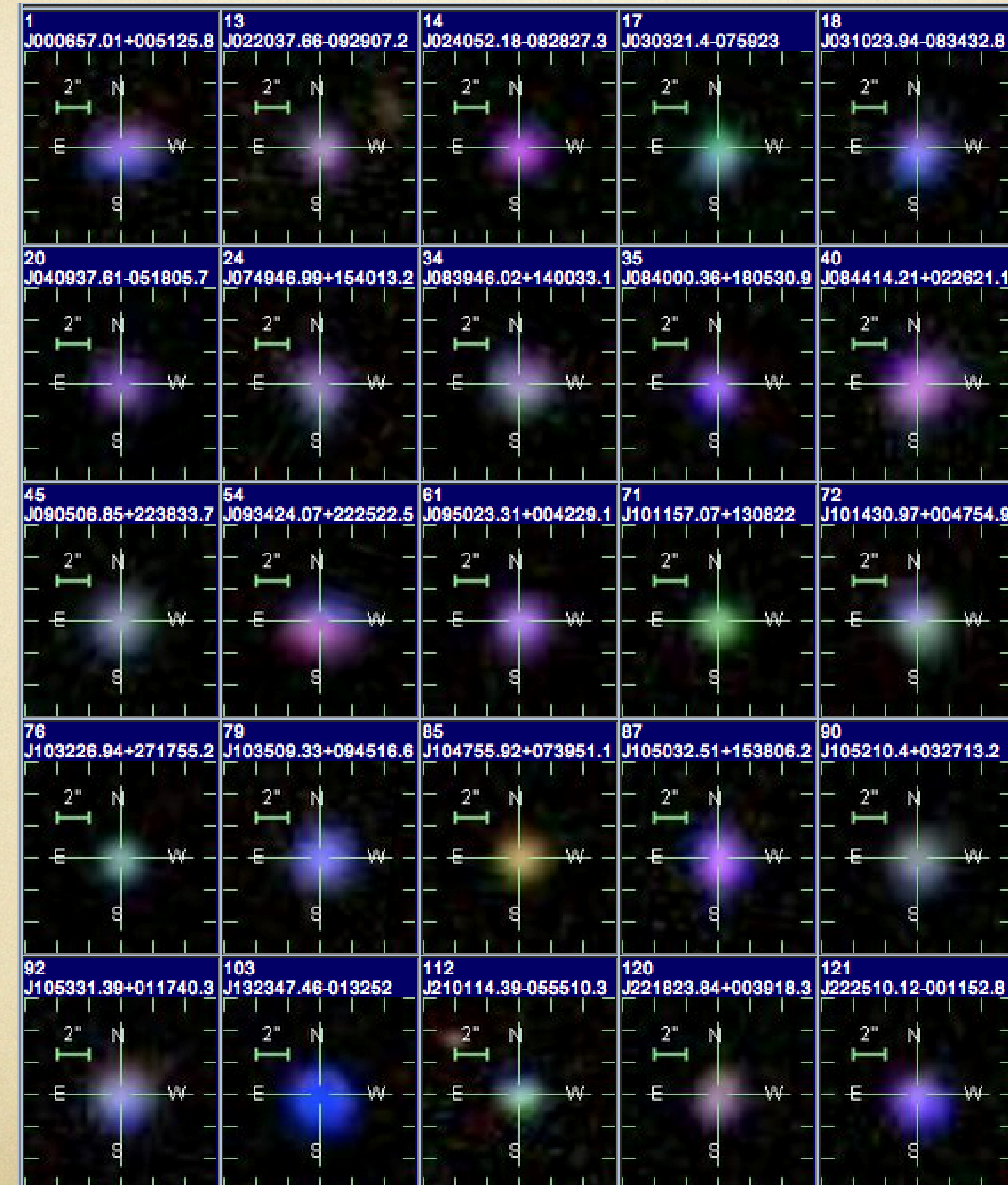

# *Evolution of the Eq. width of Hβ in a burst (SB99)*

*Selecting systems with EW of Hβ > 50Å guarantees that the system is very young and pre-eminent, i.e. minimum contamination from older populations.*

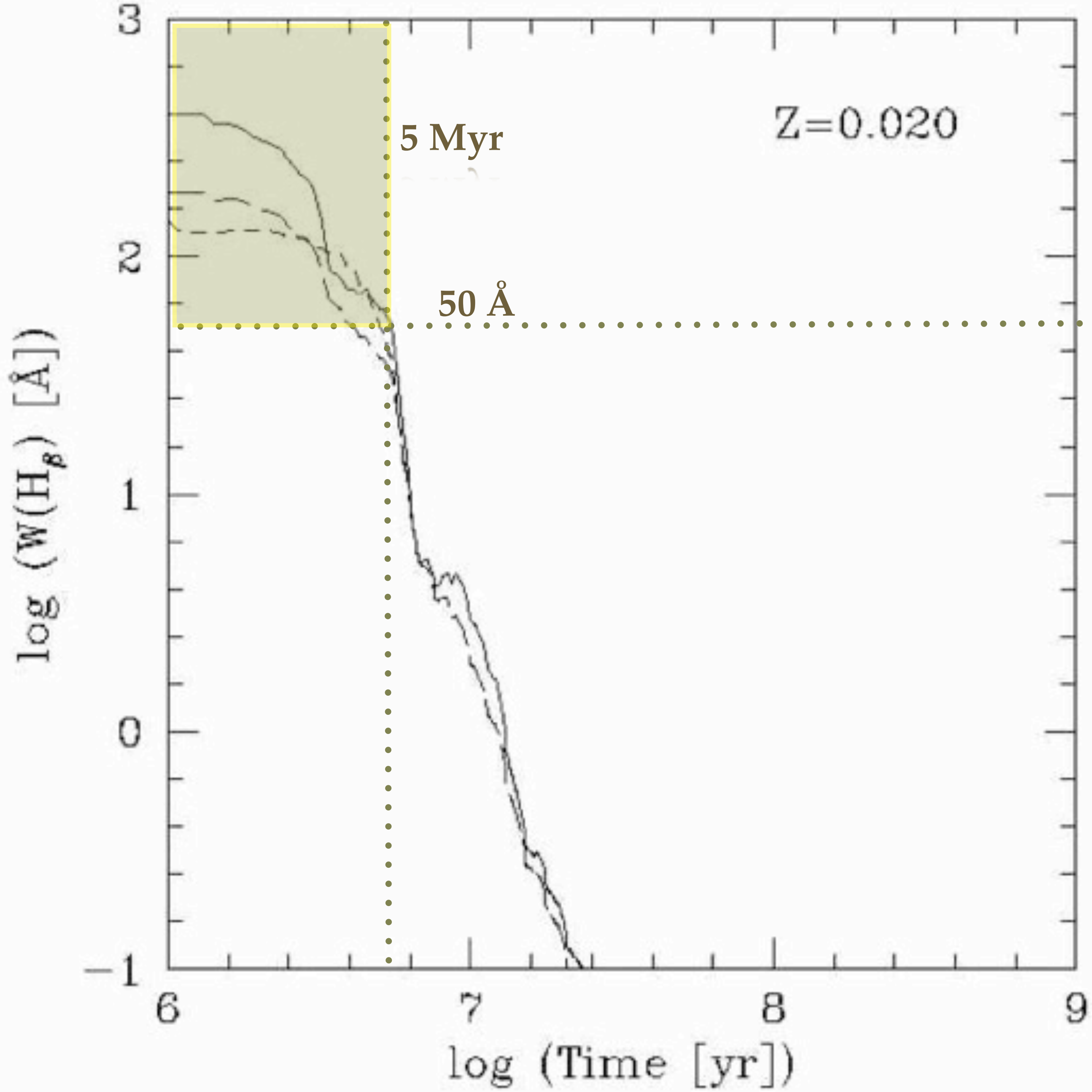


FIG. 85b

FIG. 85.—Hβ equivalent width vs. time. Star formation law: instantaneous; *solid line*, $\alpha = 2.35$, $M_{up} = 100\ M_\odot$; *long-dashed line*, $\alpha = 3.30$, $M_{up} = 100\ M_\odot$; *short-dashed line*, $\alpha = 2.35$, $M_{up} = 30\ M_\odot$; (*a*) $Z = 0.040$; (*b*) $Z = 0.020$; (*c*) $Z = 0.008$; (*d*) $Z = 0.004$; (*e*) $Z = 0.001$.

# *Are BCD HII Galaxies?*

**The answer is: generally no.**
BCDs are selected by colour and compactness and this provides samples of galaxies with a young population but in contrast with HII galaxies, the underlying galaxy is clearly visible in the images and the spectrum. Only those BCD that satisfy the criteria EW:Hα>200Å are HII galaxies.
**Thus HII galaxies can be considered as the youngest BCDs.**

BCD

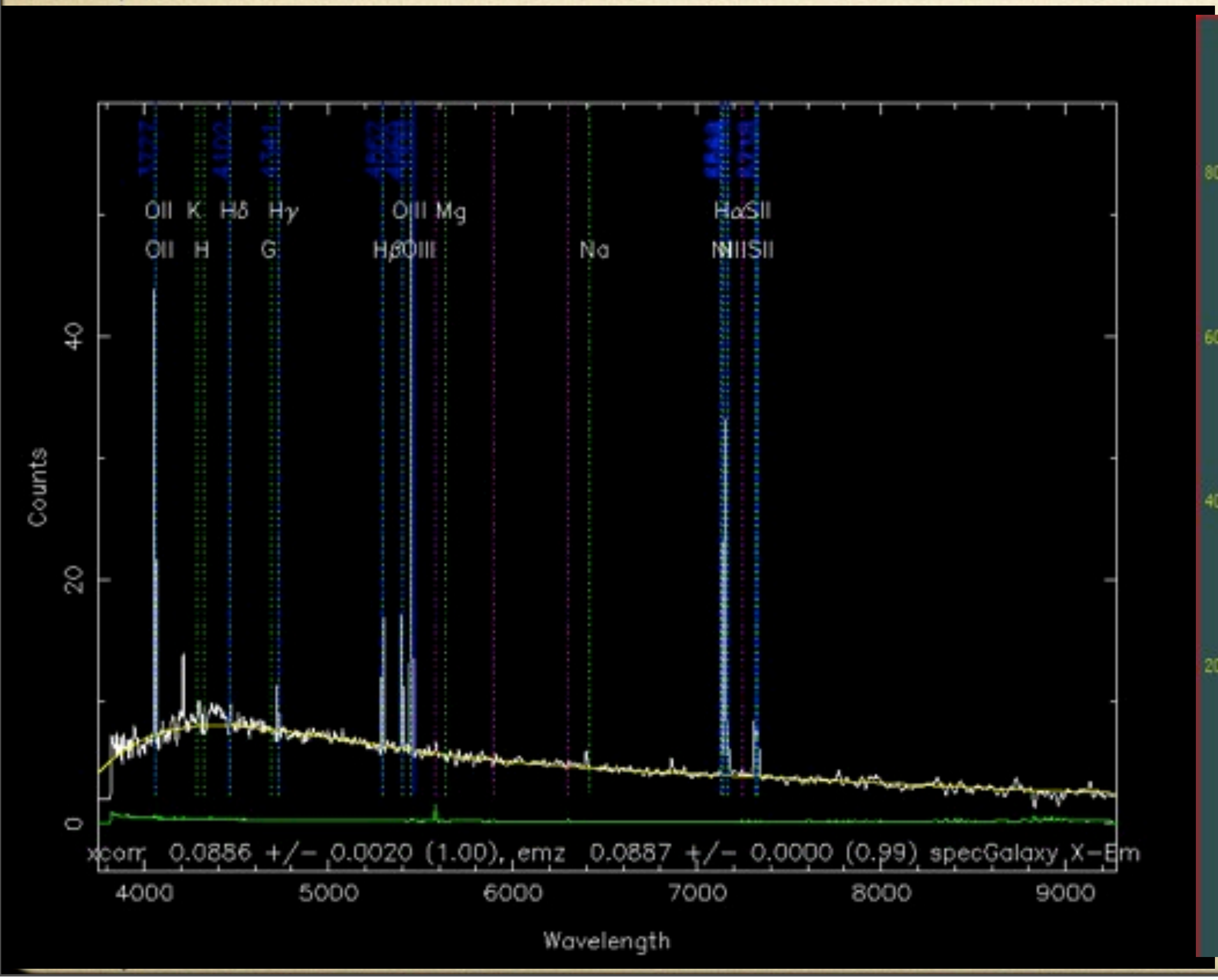


HIIGx

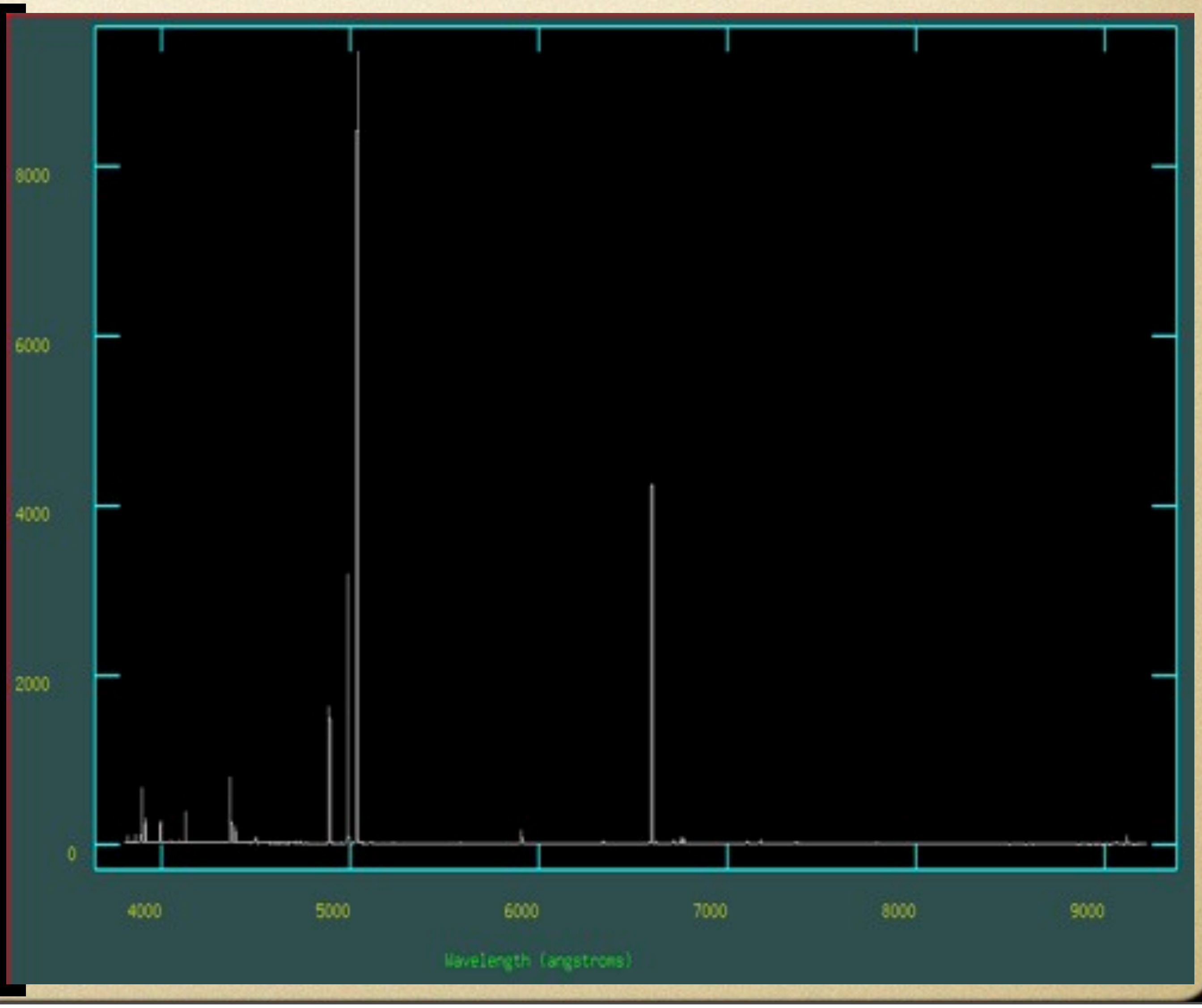

# Are BCD HII Galaxies?

## Can HII galaxies evolve into BCD?

Possibly. As the burst evolves, its luminosity rapidly diminishes and after few million years it becomes less luminous than the parent galaxy.
A problem though is that in general BCDs have higher O/H than HIIGx.

BCD

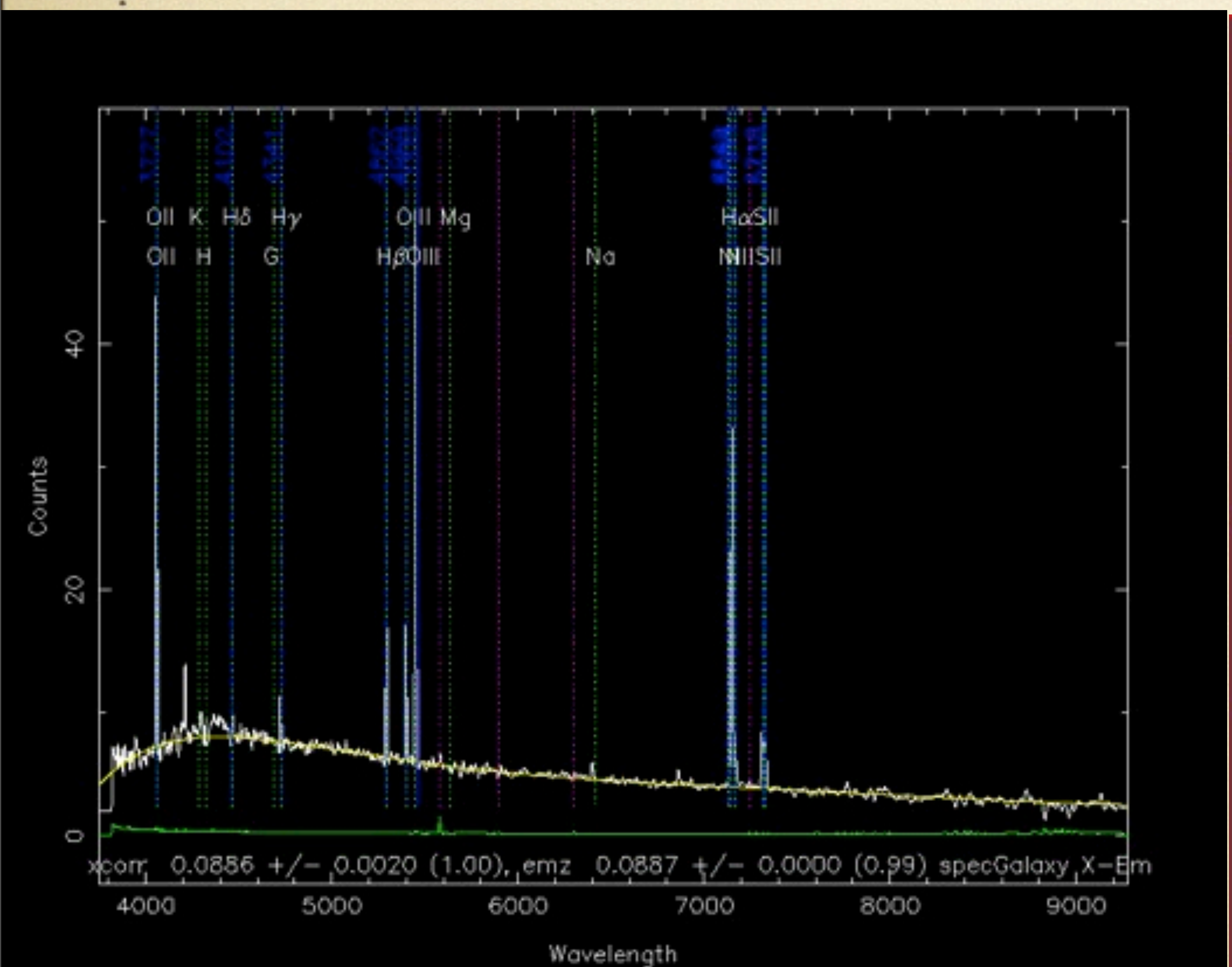


HIIGx

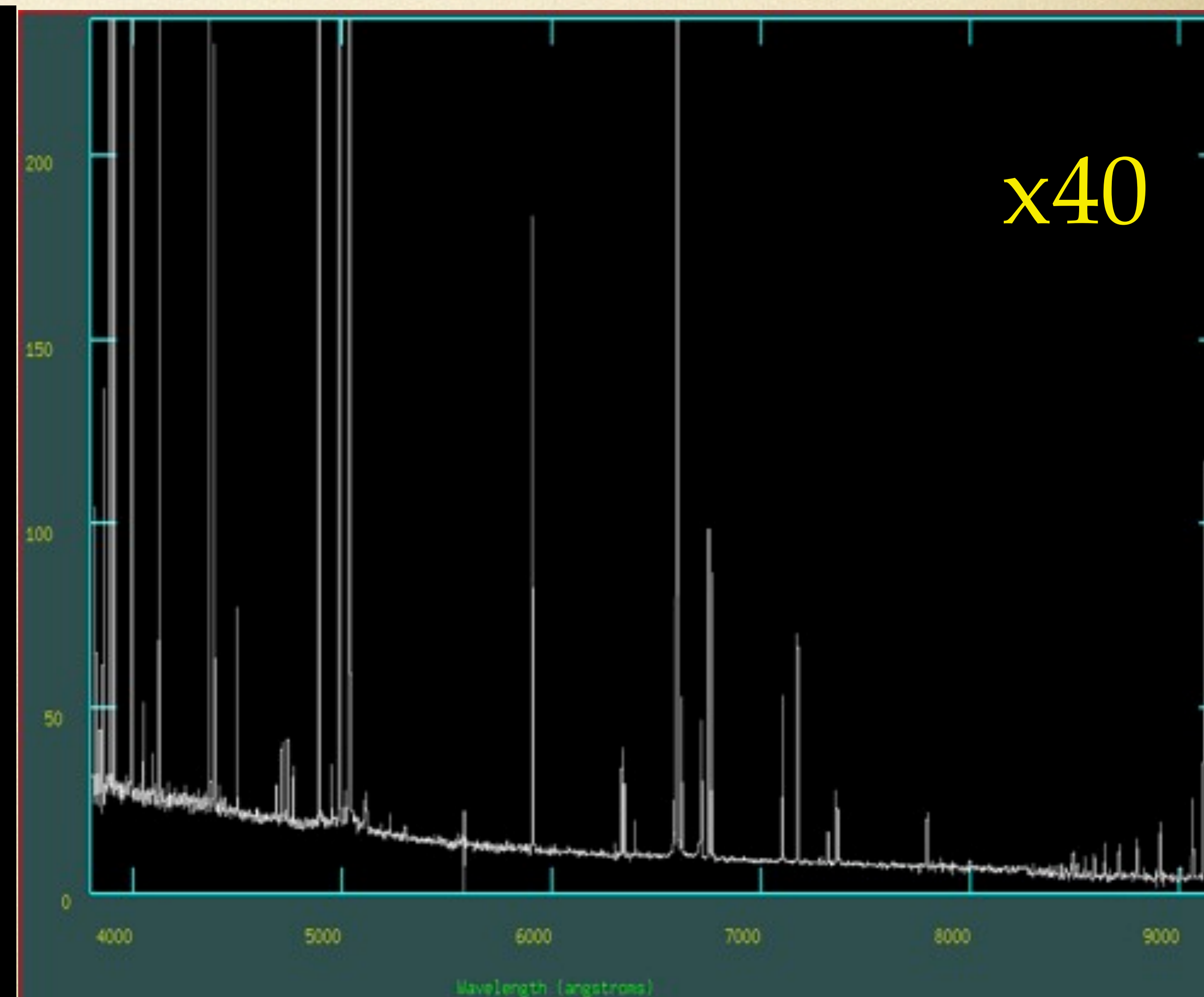

# *HIIGx and BCD Diagnostic Diagrams*

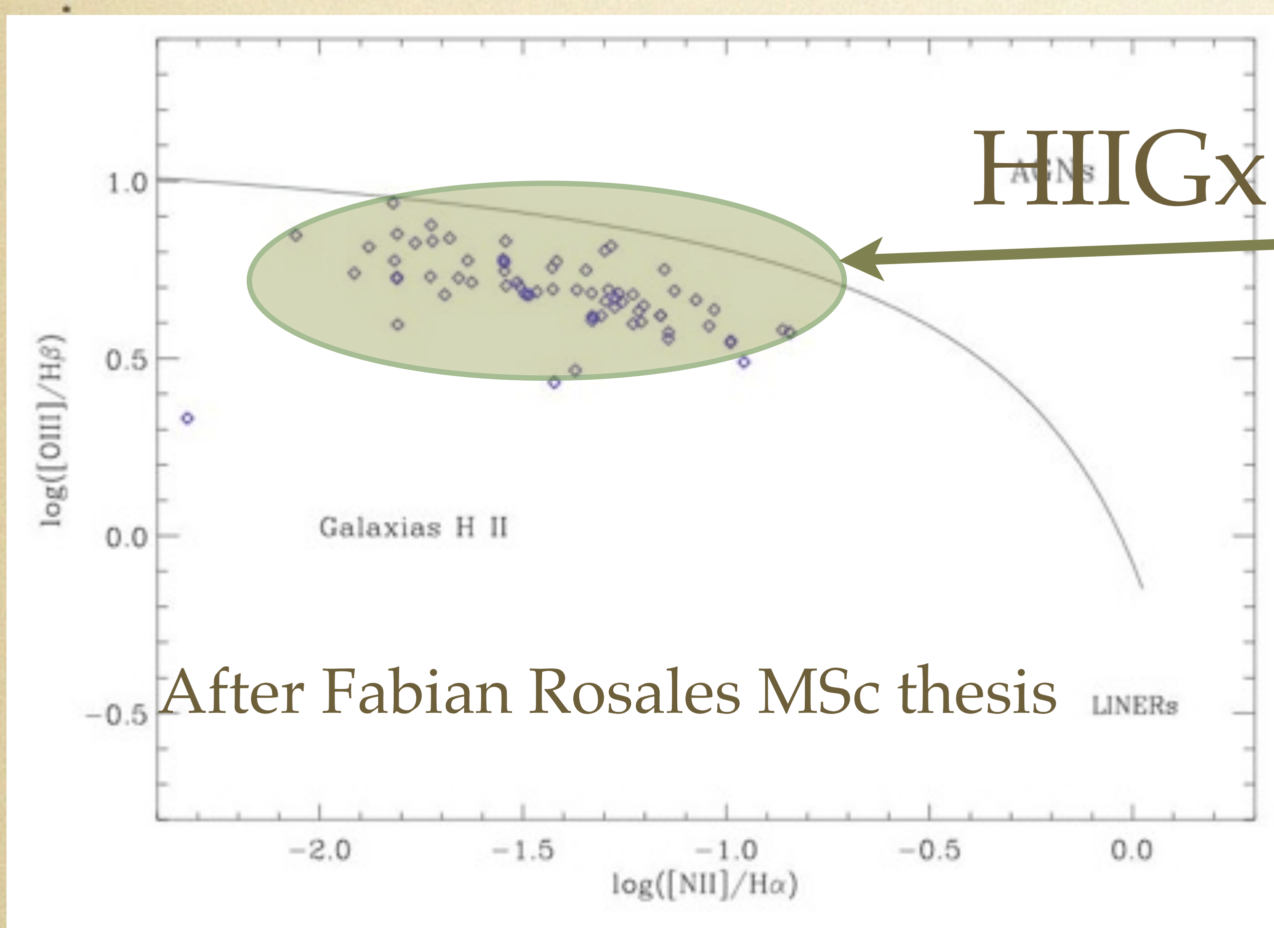


HIIGx

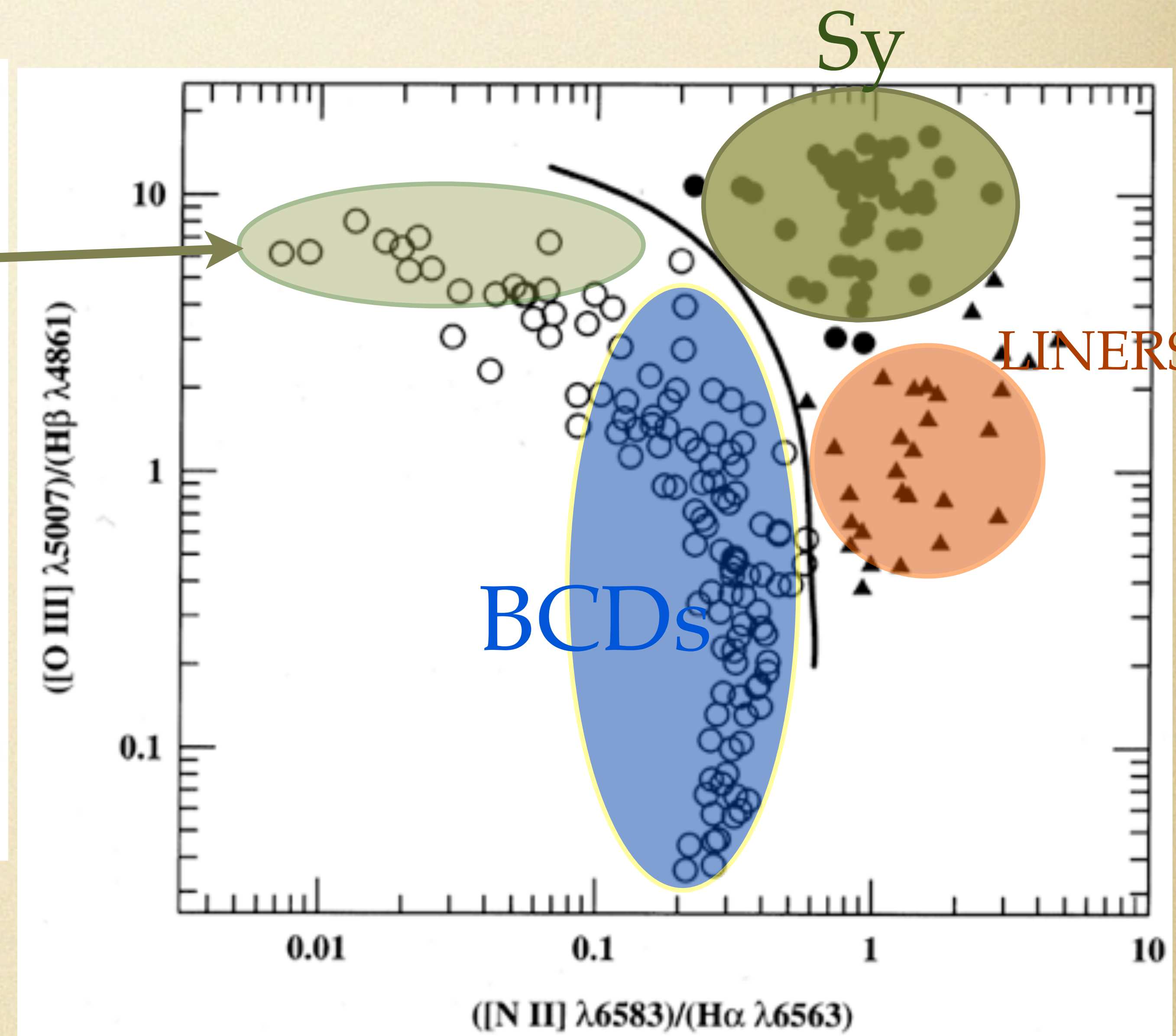

# *Range of properties of the starbursts in HII Galaxies*

$10^{40}$ ergs/s < **L(H$\beta$)** < $10^{43}$ ergs/s

$3\times10^{42}$ ergs/s < **$L_{BOL}$** < $3\times10^{45}$ ergs/s

$10^{9}$ $L_{O}$ < **$L_{BOL}$** < $10^{12}$ $L_{O}$

3 $M_{O}$/yr < **SFR** < 3000 $M_{O}$/yr

20 km/s < $\sigma$ < 70 km/s

50 km/s < **FWHM** < 150 km/s

$10^{7}$ $M_{O}$ < **Mass** < $10^{10}$ $M_{O}$

50 pc < **Size** < 5 kpc

1/50th Solar < **O/H** < 1/5th Solar

# The Distance Indicator

**Correlation between Hβ line luminosity and stellar velocity dispersion,** measured from the line-widths of local HII regions (eg., Terlevich & Melnick 1981, Melnick, Terlevich & Moles 1988, Bordalo & Telles 2011).

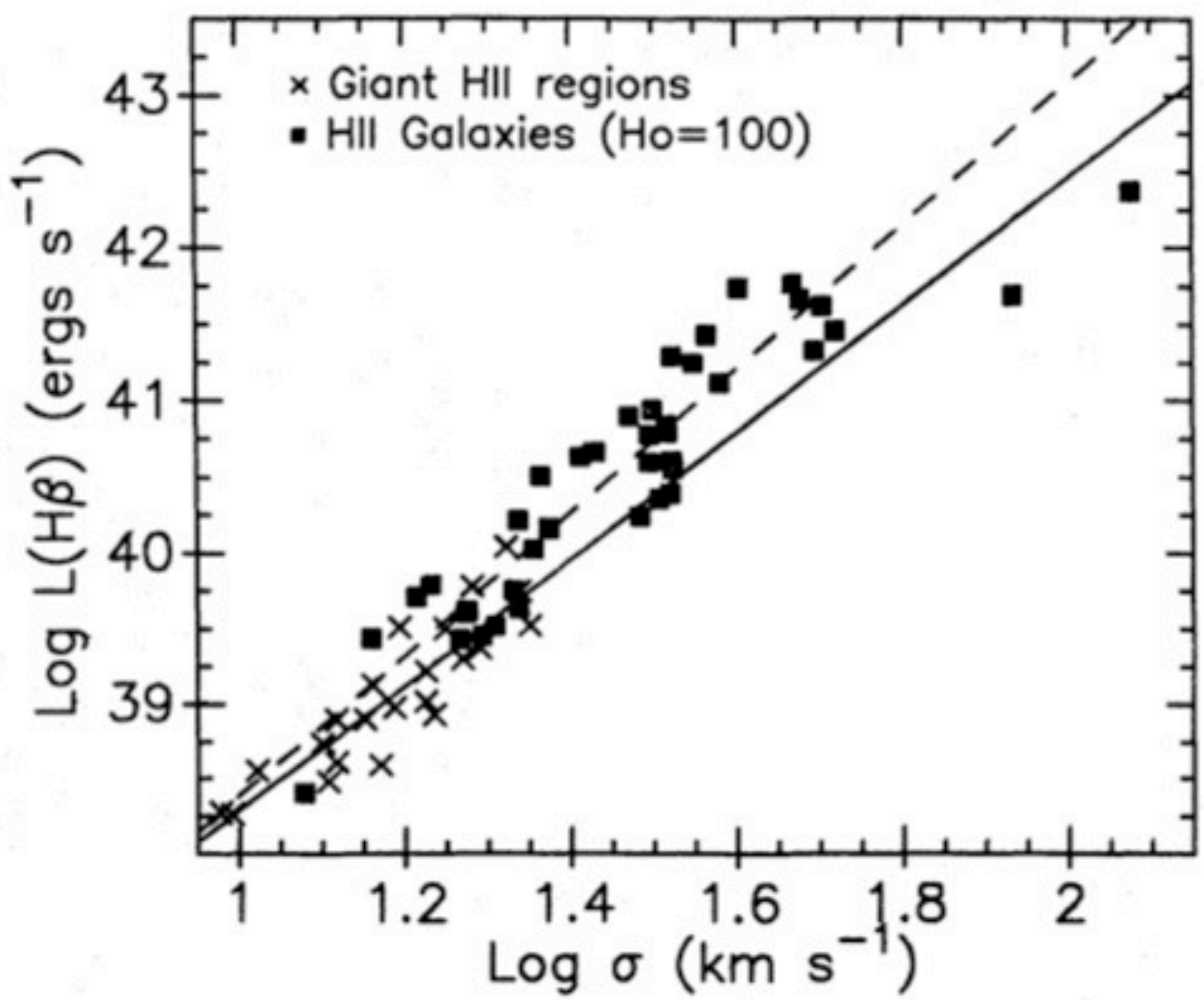


**Figure 3.** Logarithmic plot of the integrated Hβ luminosities of giant HII regions and HII galaxies versus the rms widths of their emission line profiles. The solid line shows a least squares fit to the giant HII regions data and the dashed line the corresponding fit to the HII galaxies. A Hubble constant of $H_0=100\,\mathrm{km\,s^{-1}\,Mpc^{-1}}$ was used to compute the HII galaxies' luminosities.

# Giant HII regions and HII galaxias (TM81)

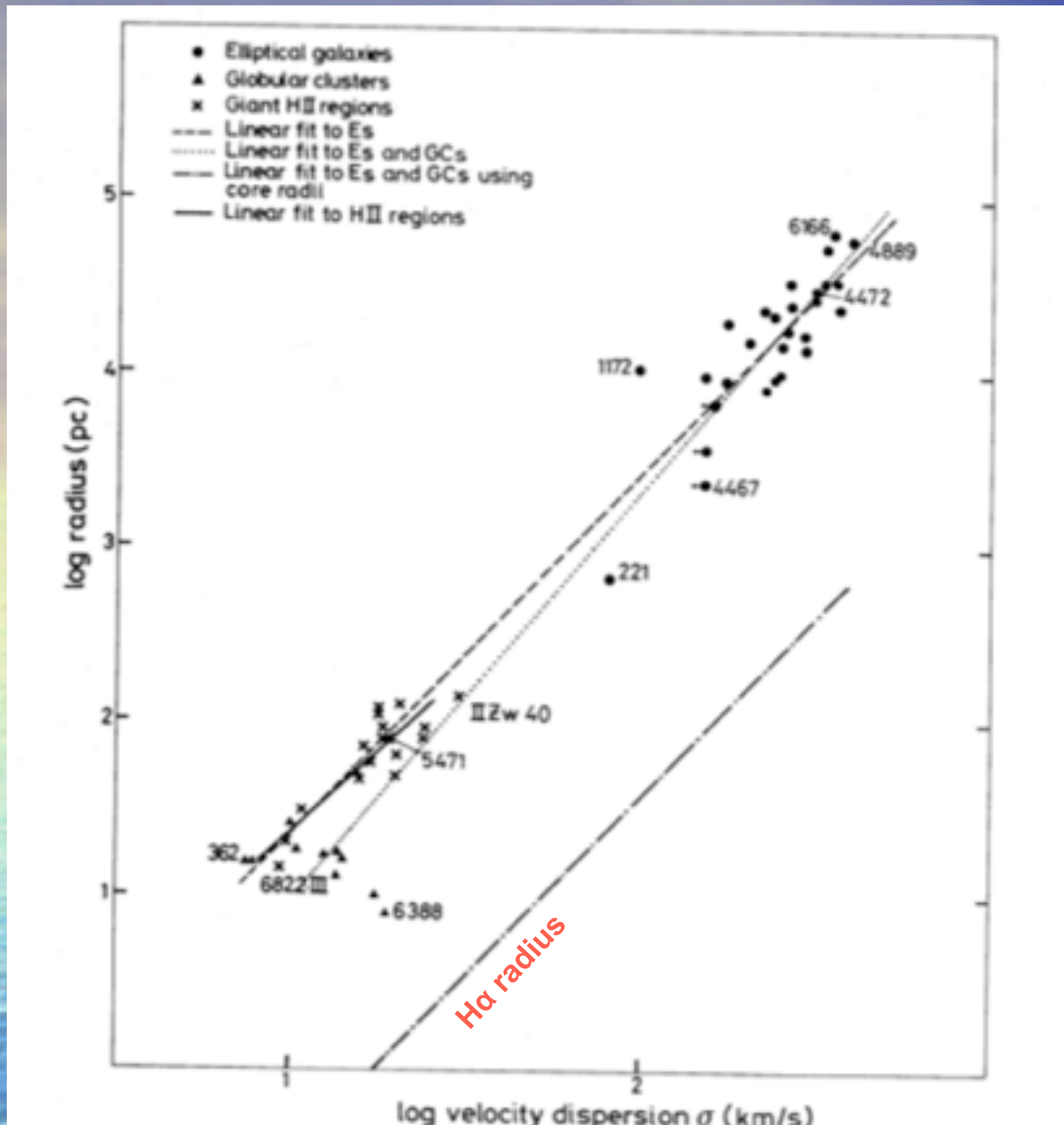


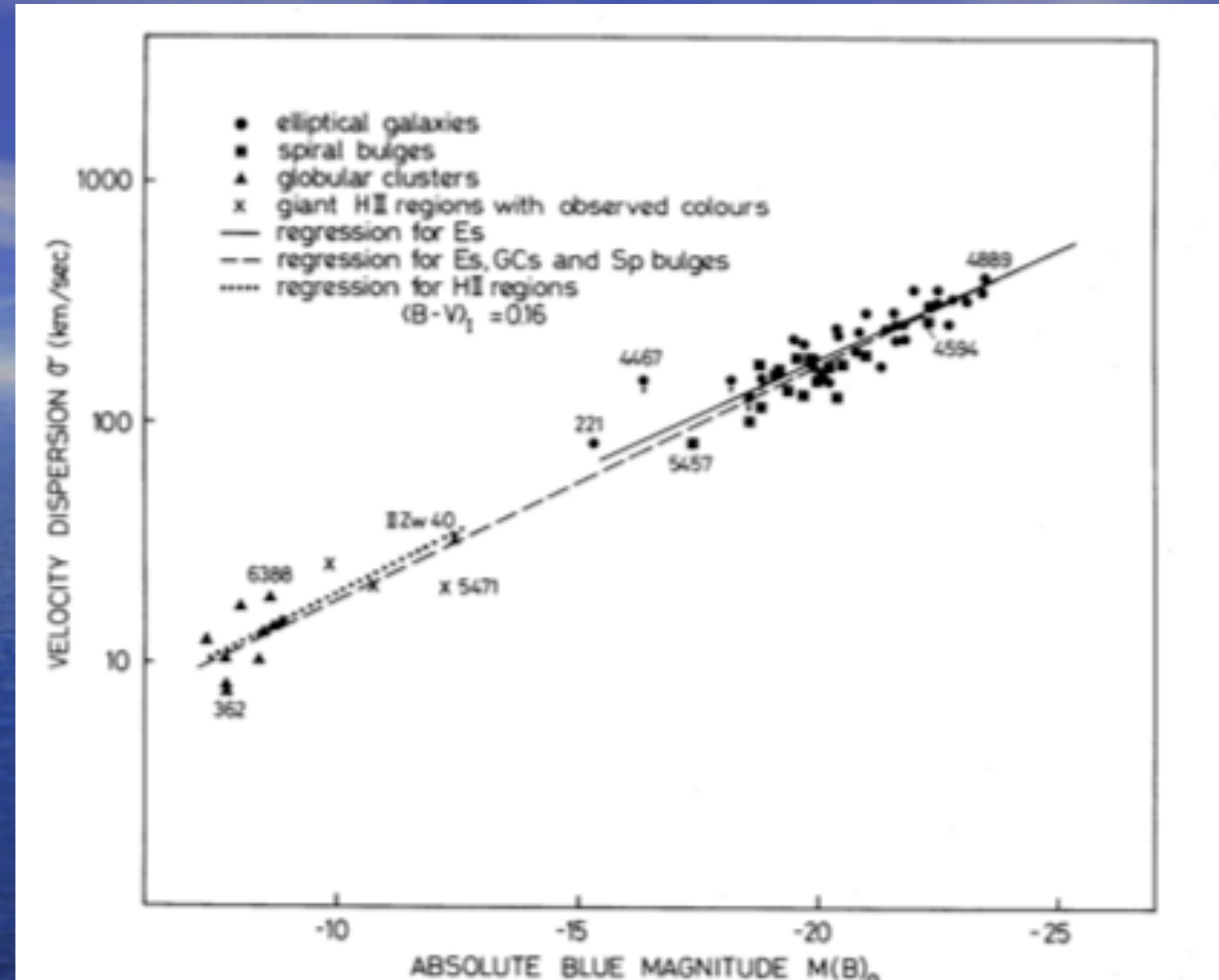


It is straightforward to verify that systems satisfying relations of the form $L \propto \sigma^4$ and $R \propto \sigma^2$ must have constant surface brightnesses and $M/L$ ratios (Sargent *et al.* 1977). We have shown that globular clusters, elliptical galaxies and spiral bulges define narrow $(L, \sigma)$ and $(R, \sigma)$ relations. This implies that these systems must have similar surface brightness and $M/L$ ratios. In fact for globular clusters $1 \lesssim M/L \lesssim 3$ (Illingworth 1976) while for elliptical galaxies the $M/L$ ratios lie in the range 4 to 10 (Faber & Jackson 1976; Schechter & Gunn 1979), on the average only a factor of 3 larger than globular clusters over a range of $10^8$ in mass. Similarly, the average mean surface brightness of globular clusters is less than 1 mag brighter than the corresponding value for elliptical galaxies over a range of nearly 14 mag in luminosity.

# The Fundamental Plane of HII Galaxies

There is a tight L-σ relation for HII galaxies,

Allowing for a Hubble time of evolution in luminosity, the FP of HII galaxies looks as an extension of the FP of Elliptical galaxies shifted towards luminosities and velocity dispersions that are typical of GC and dwarf spheroidals.

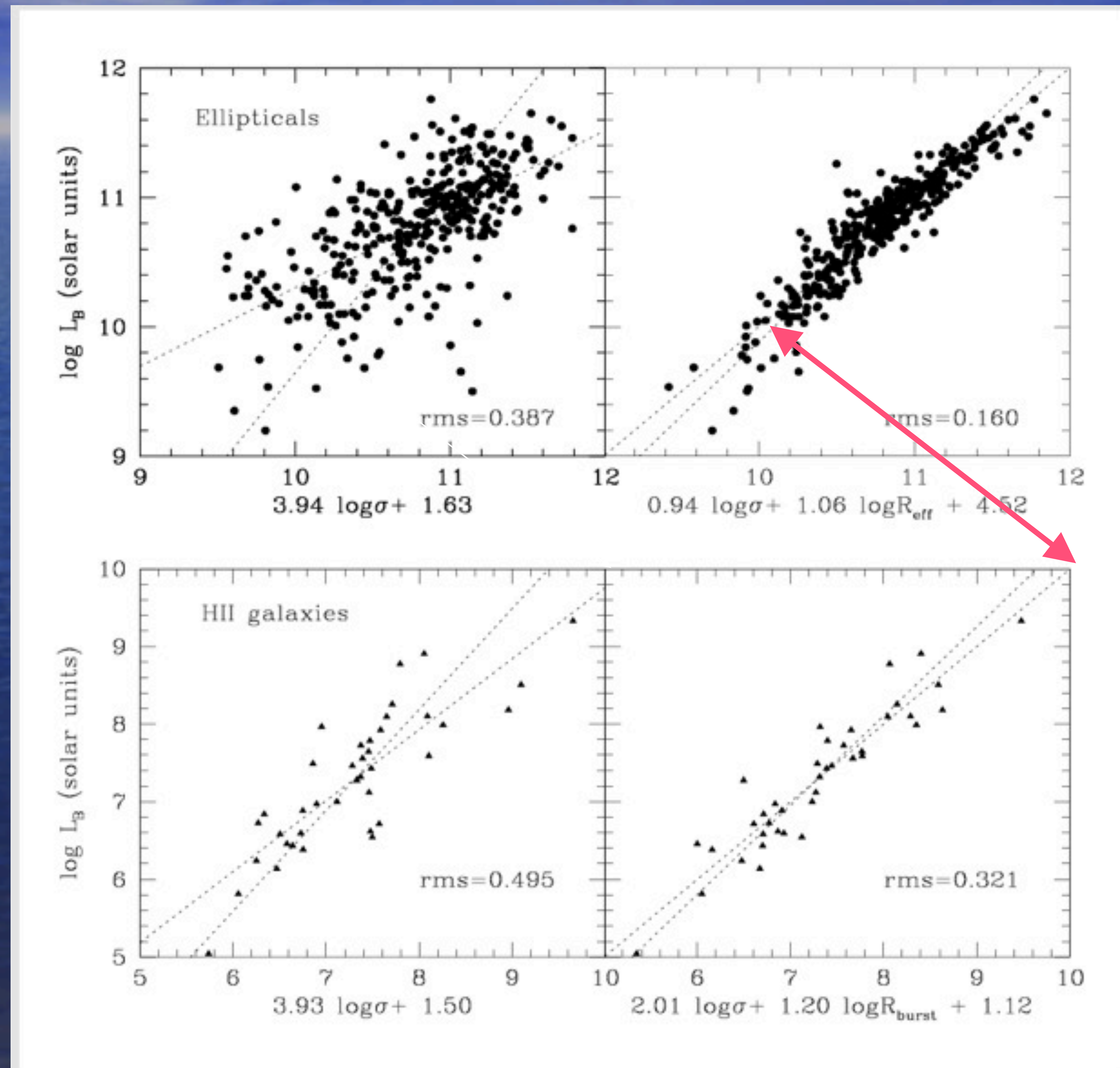


Telles 1998, Telles etal 1998,1999

# The Fundamental Plane of  Ellipticals & HII Galaxies

There is a tight L-σ relation for HII galaxies,

Allowing for a Hubble time of evolution in luminosity,  the FP of HII galaxies looks as an extension of  the FP of  Elliptical galaxies shifted towards luminosities and velocity dispersions that are typical of GC and dwarf spheroidals.

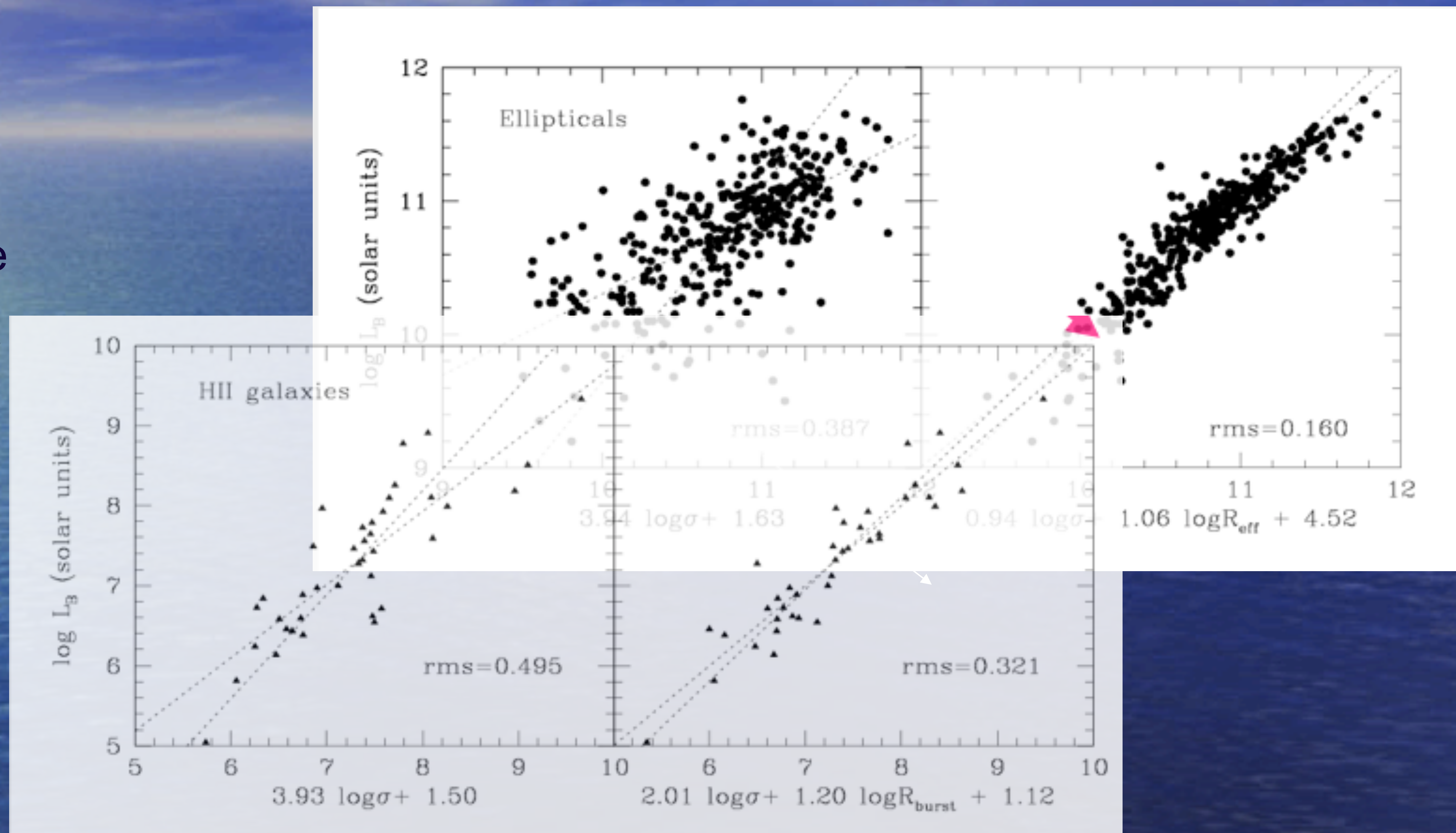


Telles 1998, Telles etal 1998,1999

# *The L-σ Distance Indicator*

**Correlation between** **Hβ line luminosity** **and** **stellar velocity dispersion,** measured from the line-widths of local HII regions (eg., Terlevich & Melnick 1981, Melnick, Terlevich & Moles 1988, Bordalo & Telles 2011).

THE ASTROPHYSICAL JOURNAL, 735:52 (26pp), 2011 July 1 BORDALO & TELLES

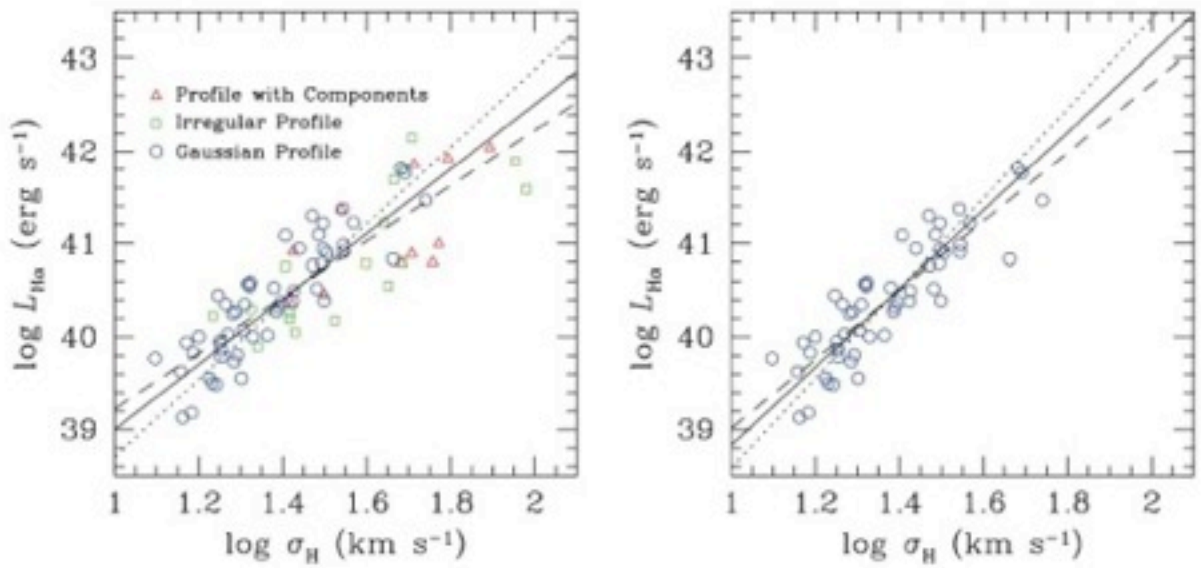


**Figure 7.** $L_{H\alpha}$–$\sigma_H$ relation for all galaxies with homogeneous spectrophotometry (81 objects G, I, and C, left) and for only those showing regular Gaussian profiles (53 objects G, right). The dashed line represents OLS(Y|X), the dotted line represents OLS(X|Y), and the solid line represents the bisector fit. All regression coefficients are presented in Table 6.

(A color version of this figure is available in the online journal.)

**Table 6**
Regressions for log $L_{H\alpha}$ Versus log $\sigma_H$

| Linear Regression | Intercept (A) | Slope (B) | rms |
|---|---|---|---|
| | All galaxies (81 objects) Pearson correlation coefficient ($r$) = 0.85, log $L$ = A + B × log $\sigma$ | | |
| OLS(Y\|X) | 36.21 ± 0.32 | 3.01 ± 0.23 | 0.37 |
| OLS(X\|Y) | 34.52 ± 0.38 | 4.18 ± 0.27 | |
| OLS Bisector | 35.49 ± 0.32 | 3.51 ± 0.23 | |
| | Galaxies with Gaussian profiles (53 objects), $r$ = 0.88 | | |
| OLS(Y\|X) | 35.29 ± 0.42 | 3.72 ± 0.31 | 0.31 |
| OLS(X\|Y) | 33.73 ± 0.47 | 4.85 ± 0.34 | |
| OLS Bisector | 34.61 ± 0.41 | 4.22 ± 0.30 | |
| | More restrictive subsample (37 objects), $r$ = 0.90 | | |
| OLS(Y\|X) | 34.80 ± 0.41 | 4.14 ± 0.29 | 0.29 |
| OLS(X\|Y) | 33.45 ± 0.53 | 5.13 ± 0.38 | |
| OLS Bisector | 34.19 ± 0.43 | 4.58 ± 0.30 | |

# The L-σ relation

The observed correlations between **$H_\beta$ line luminosity, size** and **stellar velocity dispersion in HII galaxies and Giant HII** :

$$L(H\beta) \propto \sigma^4$$

and

$$Size \propto \sigma^2$$

Suggesting that these systems are gravitationally bound and that the M/L (IMF) does not change across the sample (Terlevich & Melnick 81).

**REMEMBER: These are properties of the massive region of star formation not of the host galaxy.**

# *An Alternative high-z Distance Indicator*

## The L(H$\beta$)- $\sigma$ correlation holds at least up to z~3

Melnick, Terlevich & Terlevich 2000

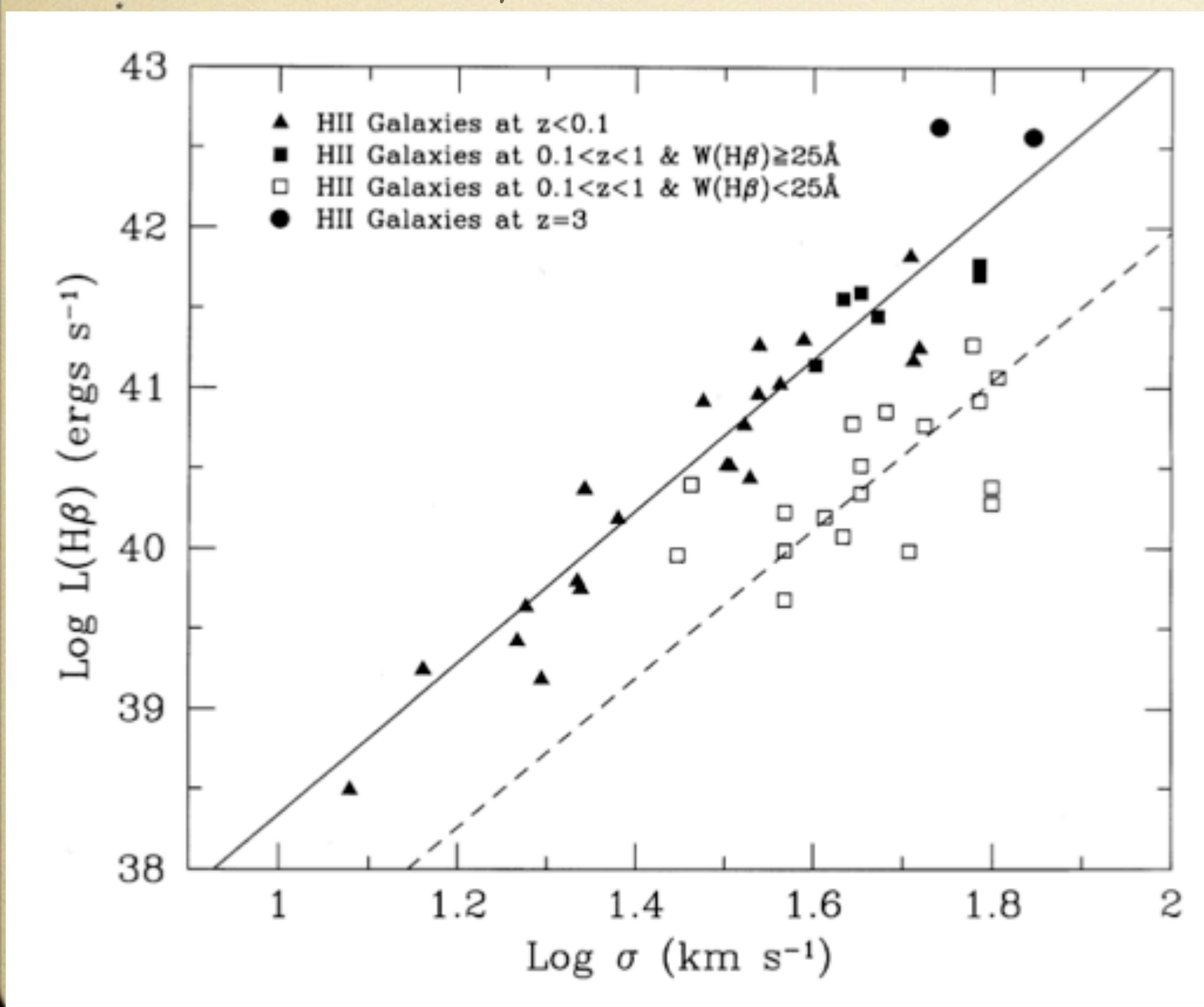


Siegel et al. 2005

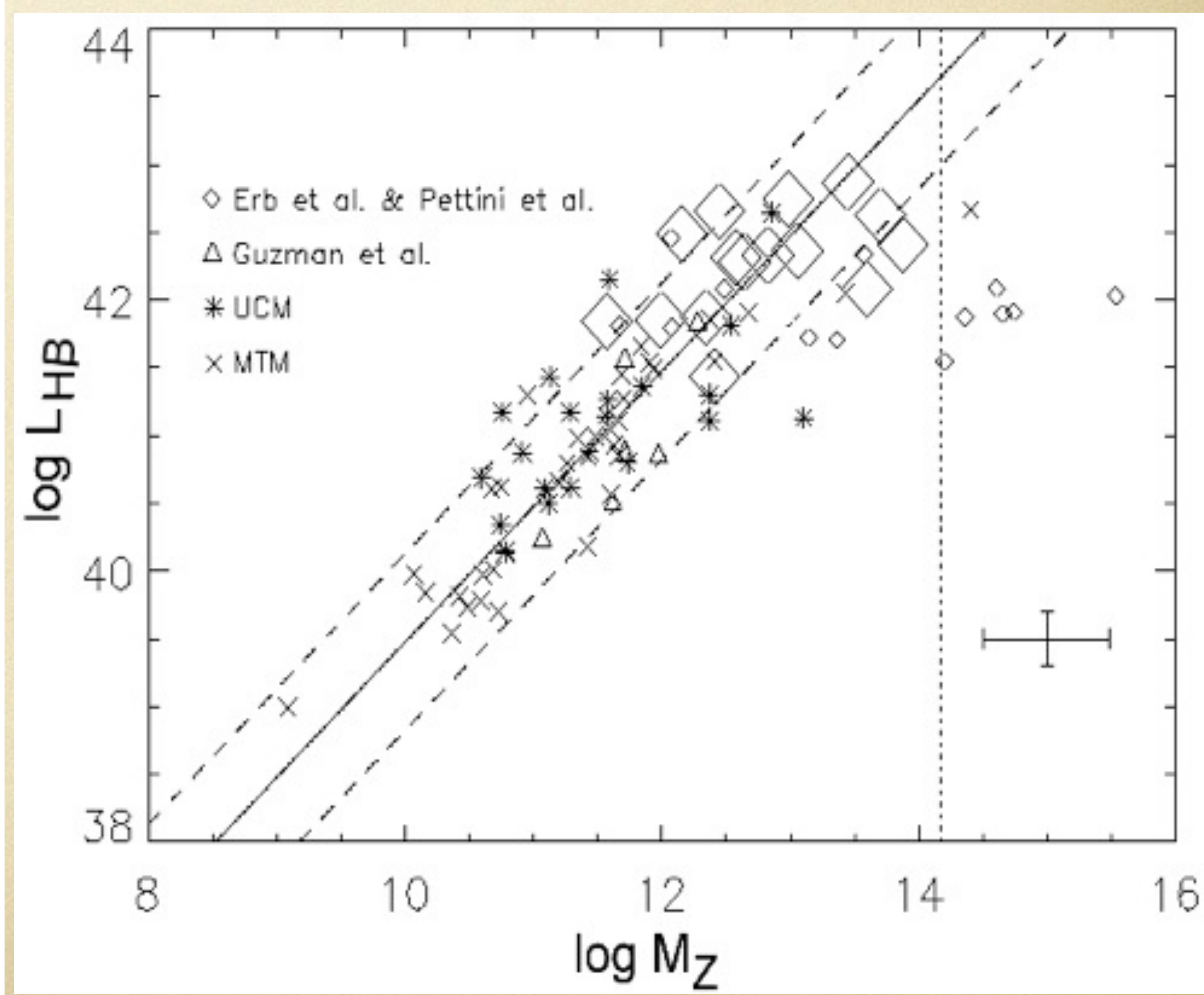

# *Early indications on how to reduce the uncertainties in the $\Omega_\Lambda$ - $\Omega_m$ plane.*

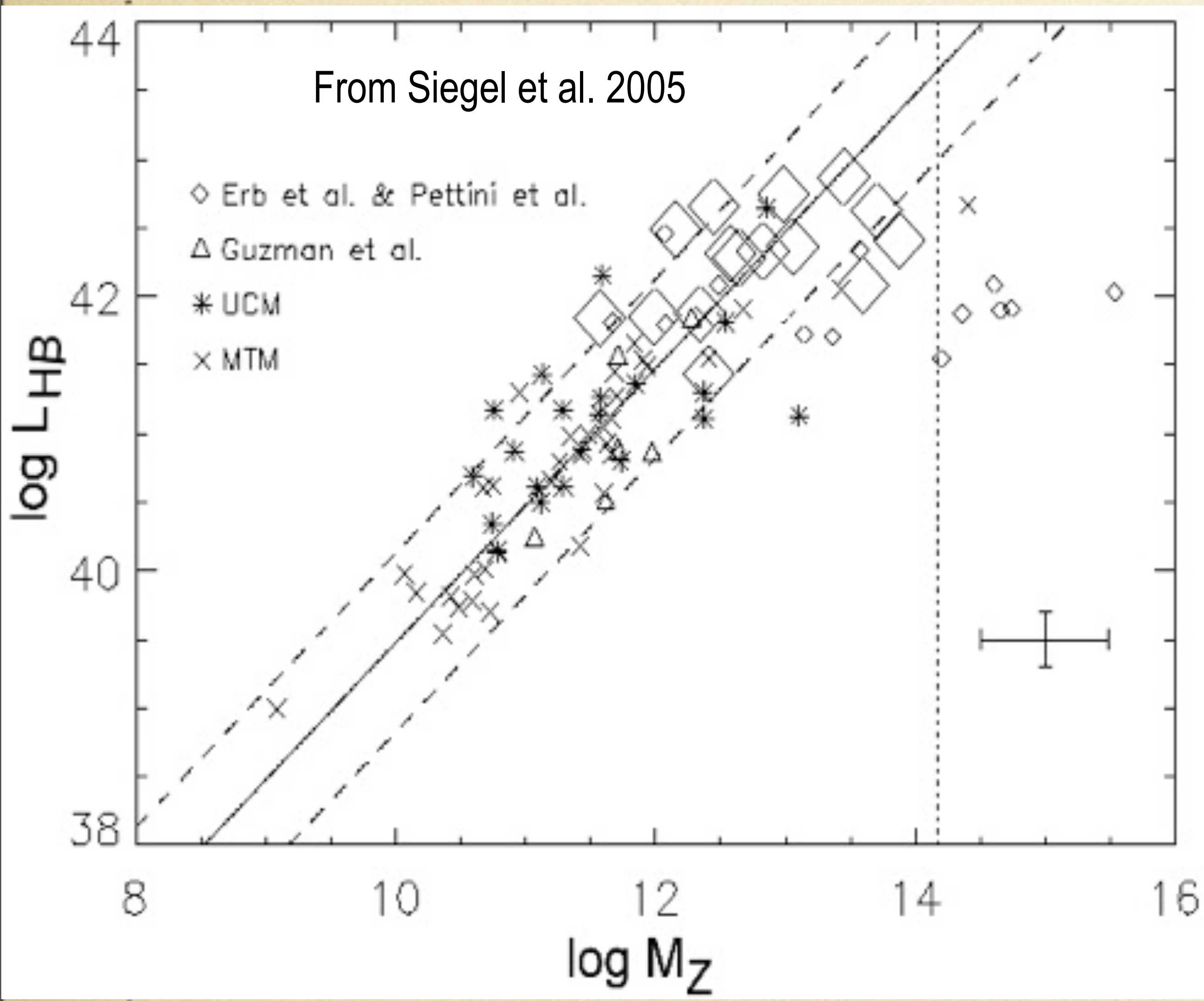


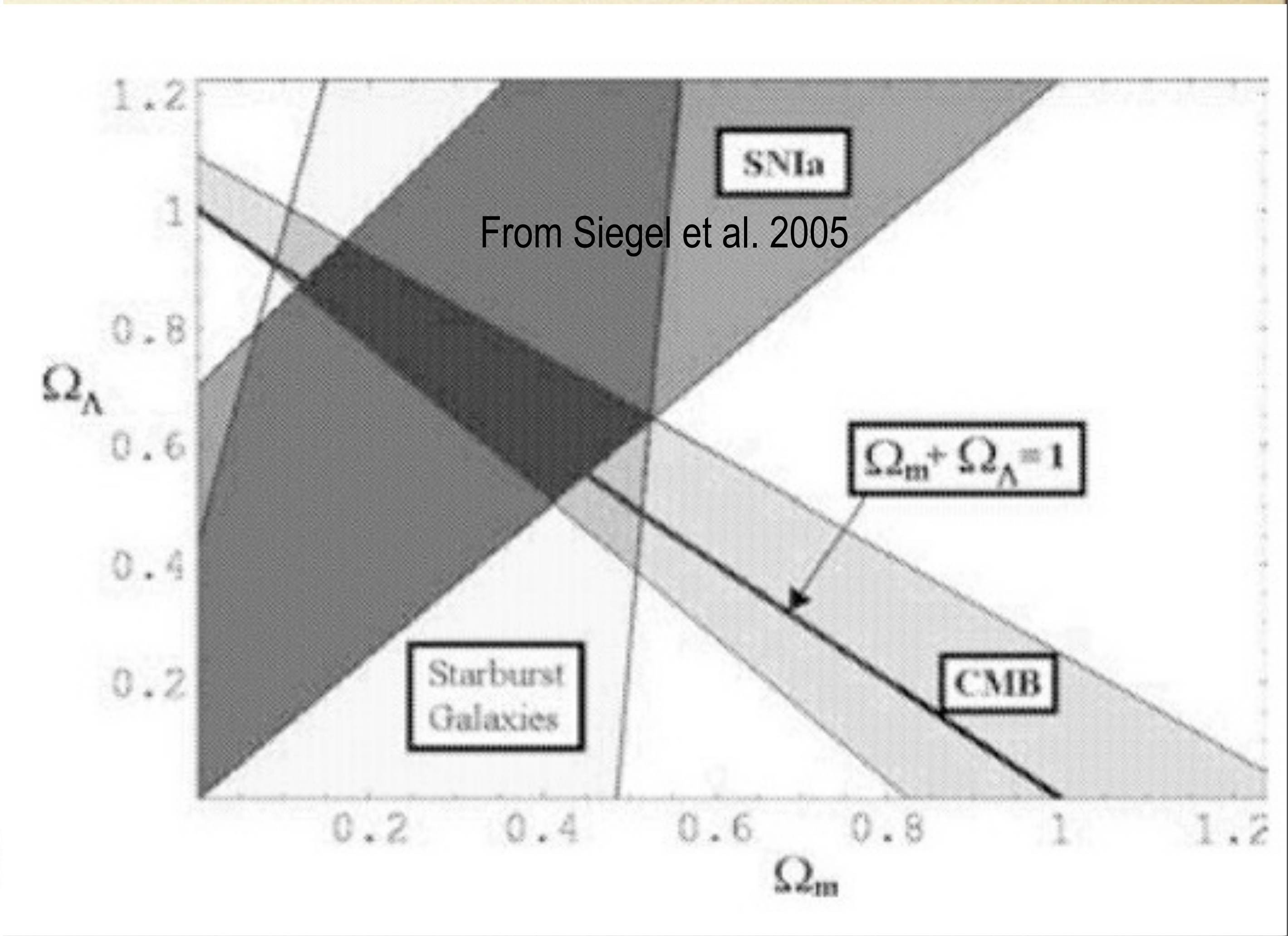


Preliminary indications from Siegel et al. (2005).
**Slope of degeneracy is different between SNIa and HIIGx**

# *Preliminary results on our approach to reduce the uncertainties in the w-$\Omega_m$ plane.*

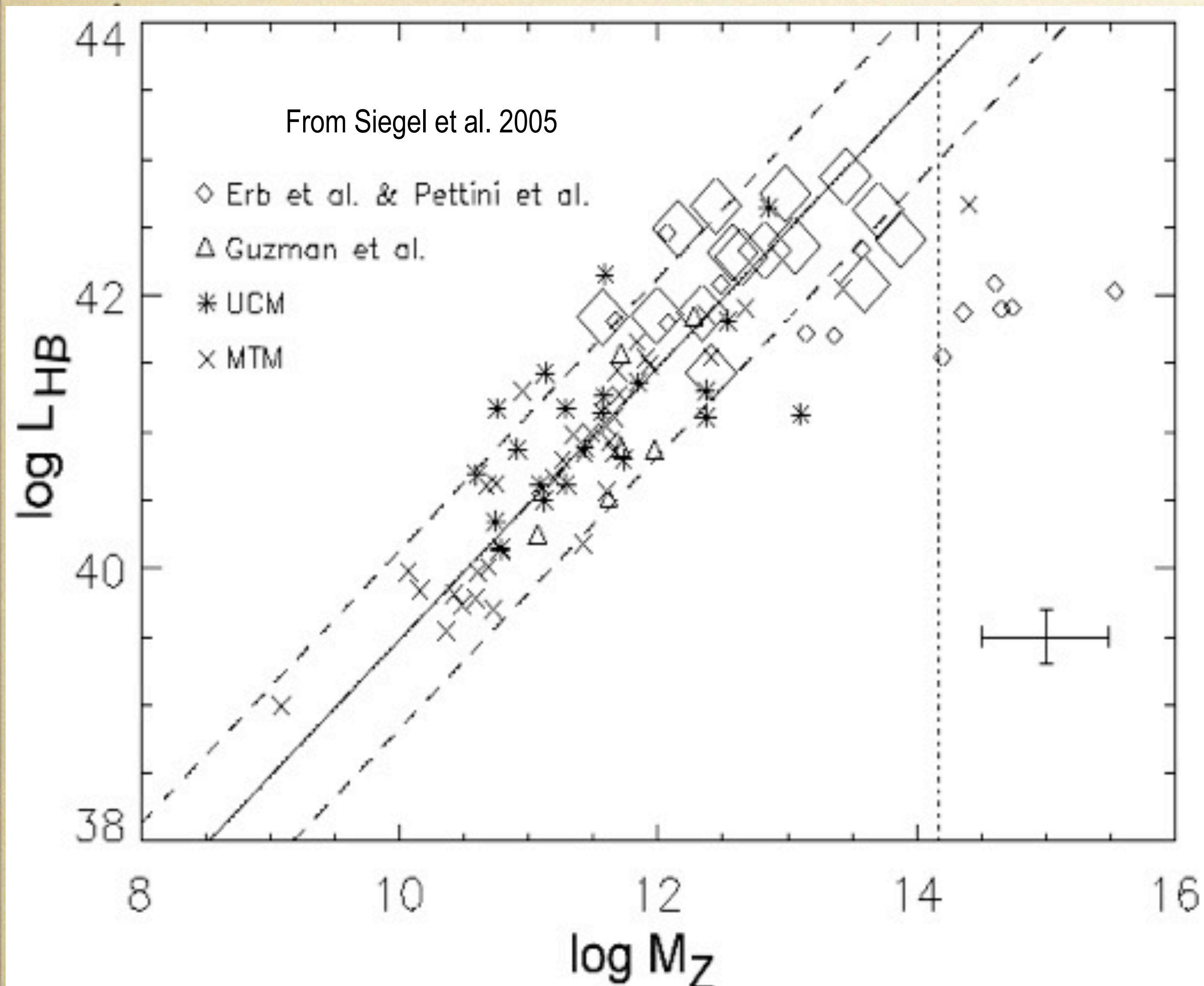


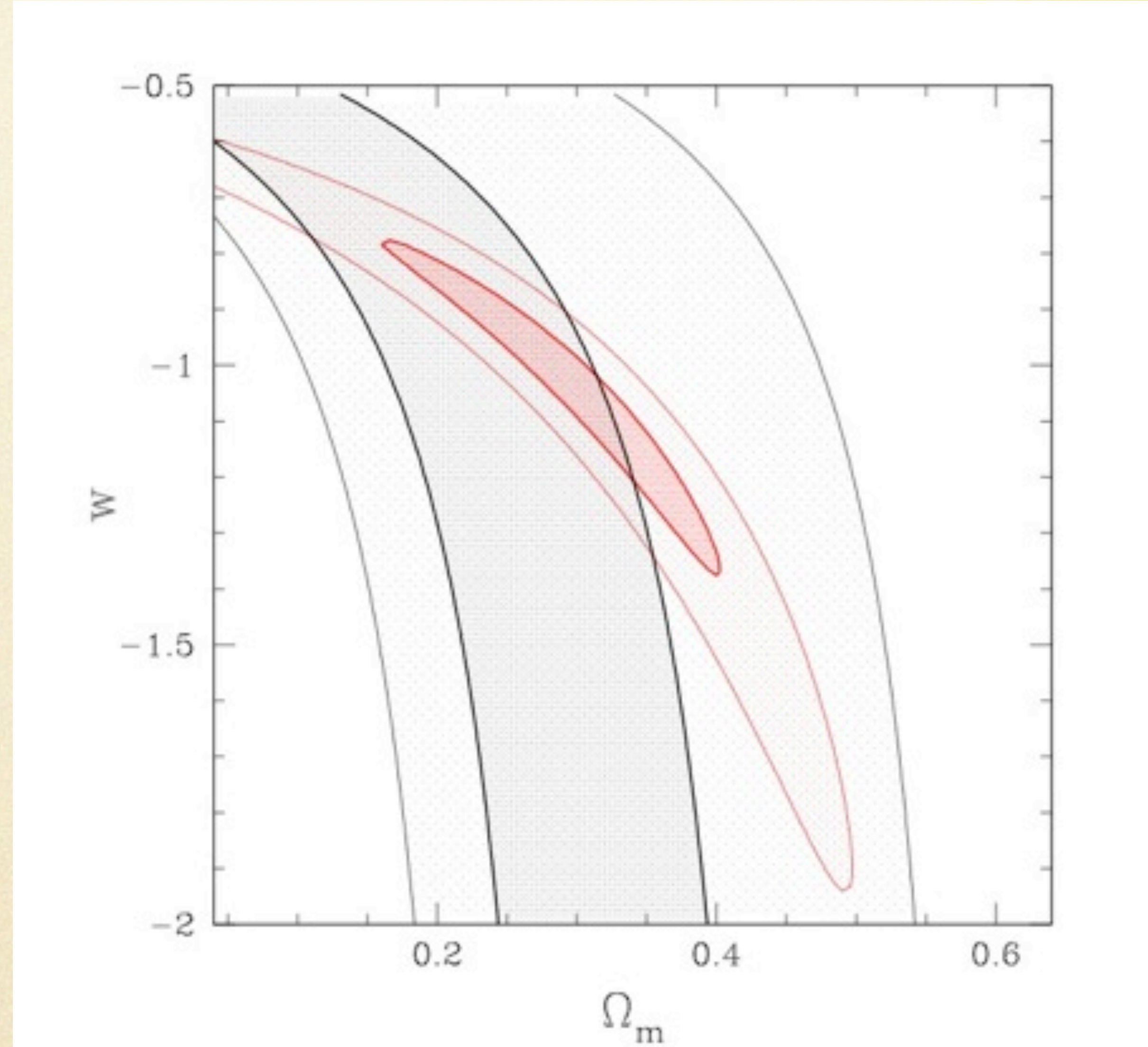


**Figure 10.** The HII-galaxy QDE constraints (in the $\Omega_m$, w plane), based on the Siegel et al. sample after excluding two HII galaxies showing strong indications for a rotational velocity component. Although the constraints are weak, leaving completely unconstrained the value of w, they are consistent at a $\sim 1\sigma$ level with the SNIa results (thin red contours).

2b) include a numerous population of ( higher-z standard candles (tracing the peak of the $\Delta(m-M)$ difference) having a **larger** error budget than low-z SN Ia.
The plot shows the solution for the Siegel et al 2005 sample of 15 high z HII galaxies.

# H II Galaxies - The Local Sample

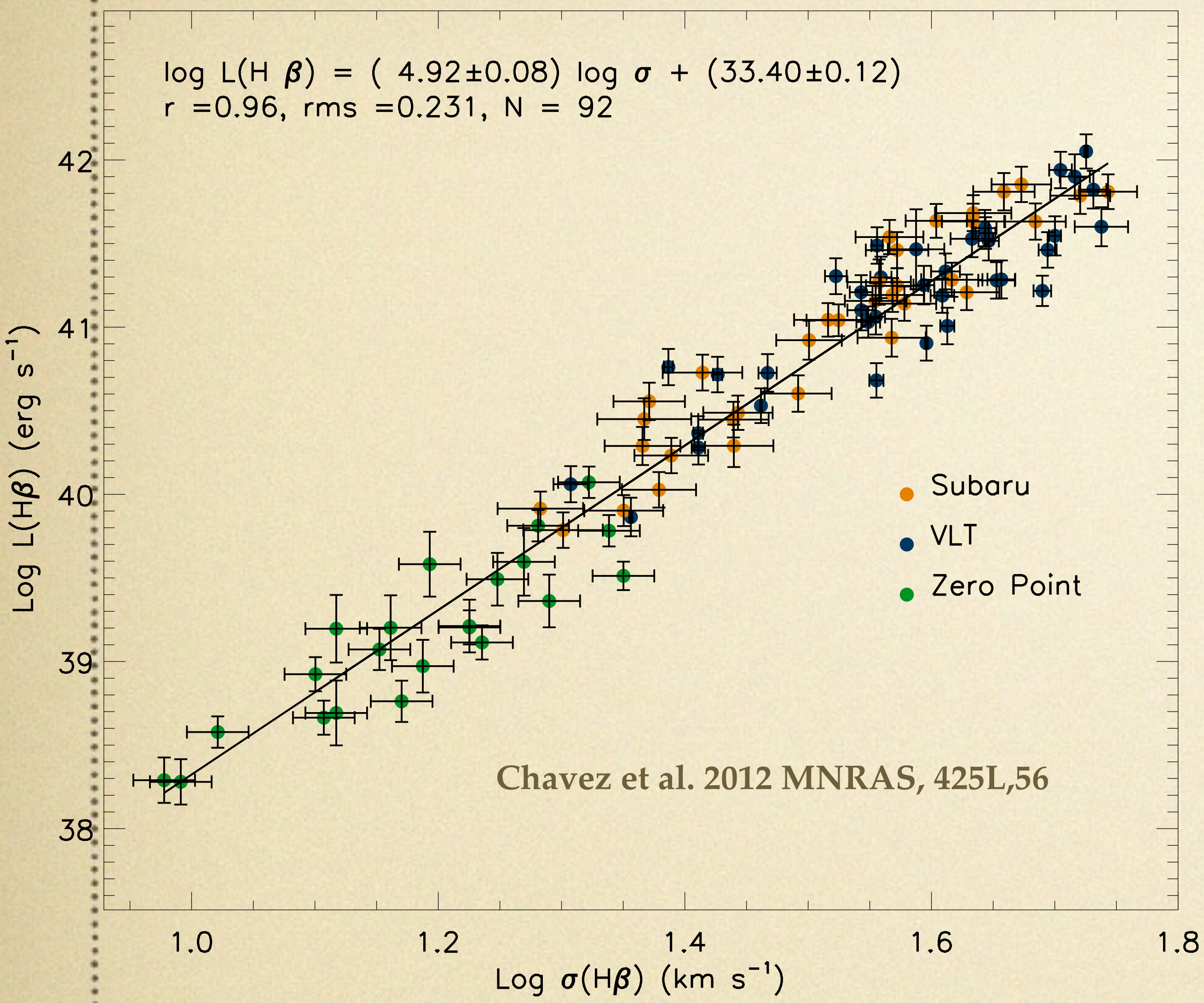


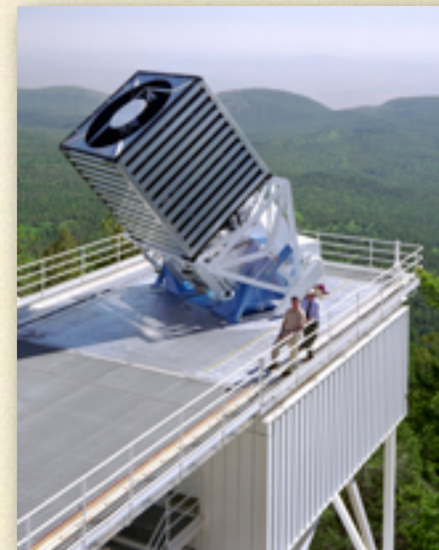

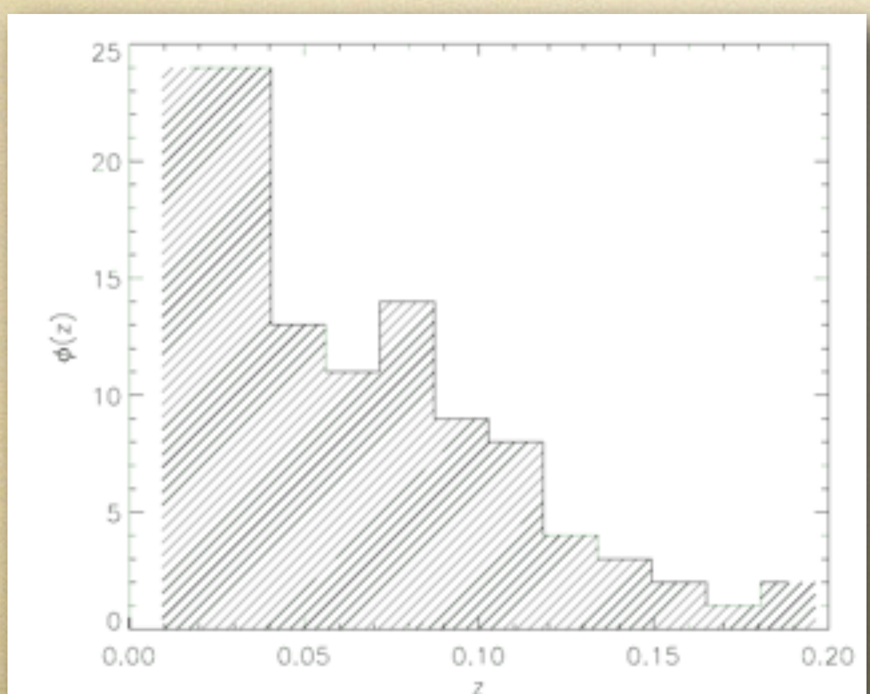


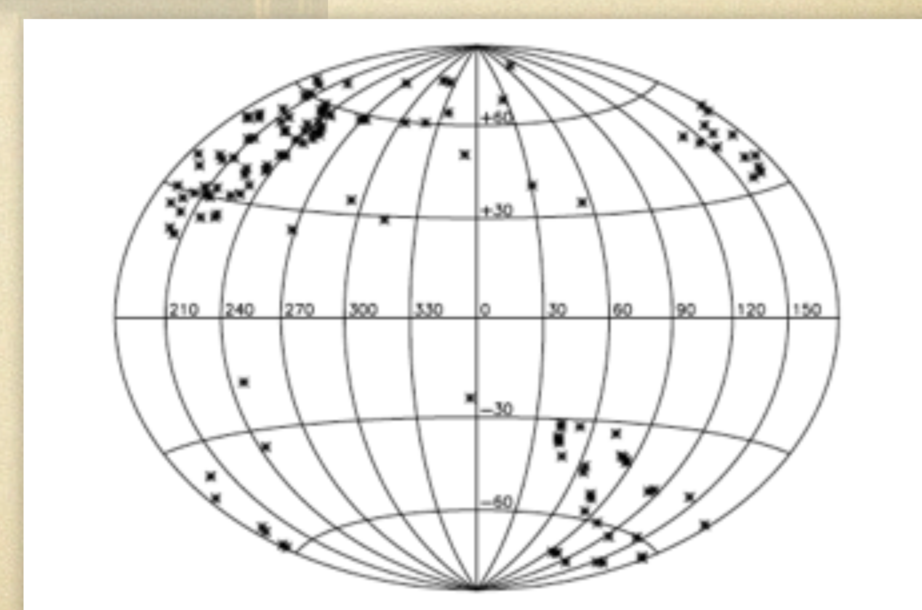

# *The Sample selection*

HIIGx selected from SDSS and SCHIIGx having:

(1) Emission line ratios corresponding to SB

(2) EW of H$\beta$ > 50Å or EW of H$\alpha$ > 200Å

(3) Petrosian radius < 3 arcsec

And after high dispersion observations:

(4) Gaussian emission line profiles

# Observations and data reduction

| Dates | Telescope | Instrument | Detector | Slit-width |
|---|---|---|---|---|
| 5 & 16 Nov 2008 | NOAJ-Subaru | HDS | EEV $(2 \times 2K \times 4K)^a$ | 4″ |
| 16 & 17 Apr 2009 | ESO-VLT | UVES-Red | EEV $(2 \times 2K \times 4K)$ | 2″ |
| 15 - 17 Mar 2010 | OAN - 2.12m | B&C | SITe3 $(1K \times 1K)$ | 10″ |
| 10 - 13 Apr 2010 | OAGH - 2.12m | B&C | VersArray $(1300 \times 660)$ | 8.14″ |
| 8 -10 Oct 2010 | OAN - 2.12m | B&C | Thompson 2K | 13.03″ |
| 7 - 11 Dic 2010 | OAGH - 2.12m | B&C | VersArray $(1300 \times 660)$ | 8.14″ |
| 4 - 6 Mar 2011 | OAN - 2.12m | B&C | Thompson 2K | 13.03″ |
| 1 - 4 Apr 2011 | OAGH - 2.12m | B&C | VersArray $(1300 \times 660)$ | 8.14″ |

- UVES data was reduced using pipeline V4.7.4 on GASGANO V2.4.0.
- HDS data was reduced using IRAF and a script for overscan removal and detector linearity corrections provided by the NOAJ-Subaru telescope team.
- Long Slit data was reduced using IRAF.

# Hβ Photometry Comparison

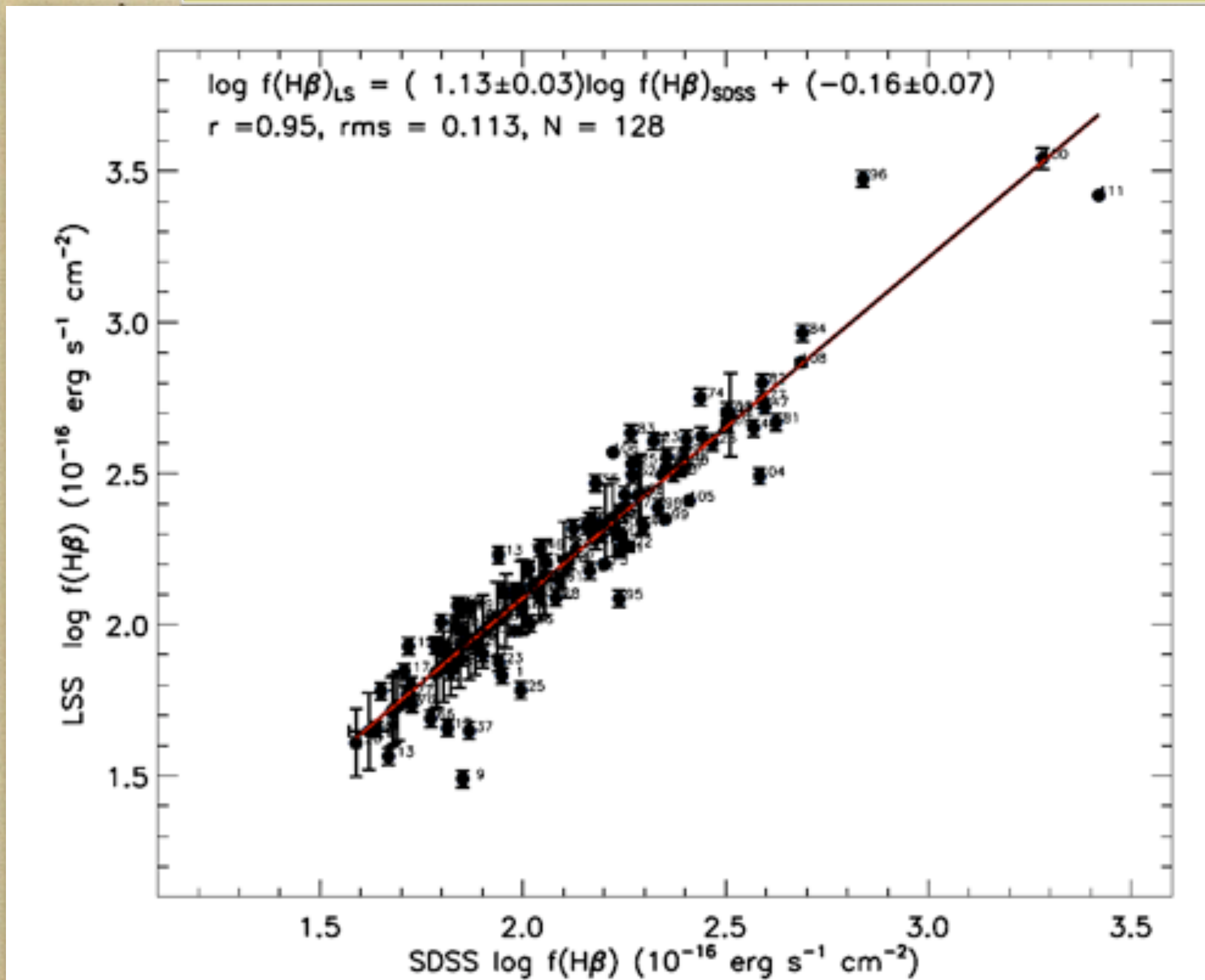


Long Slit vs SDSS Hβ fluxes after correcting the SDSS data for aperture effects

SPM Long Slit Spectrum

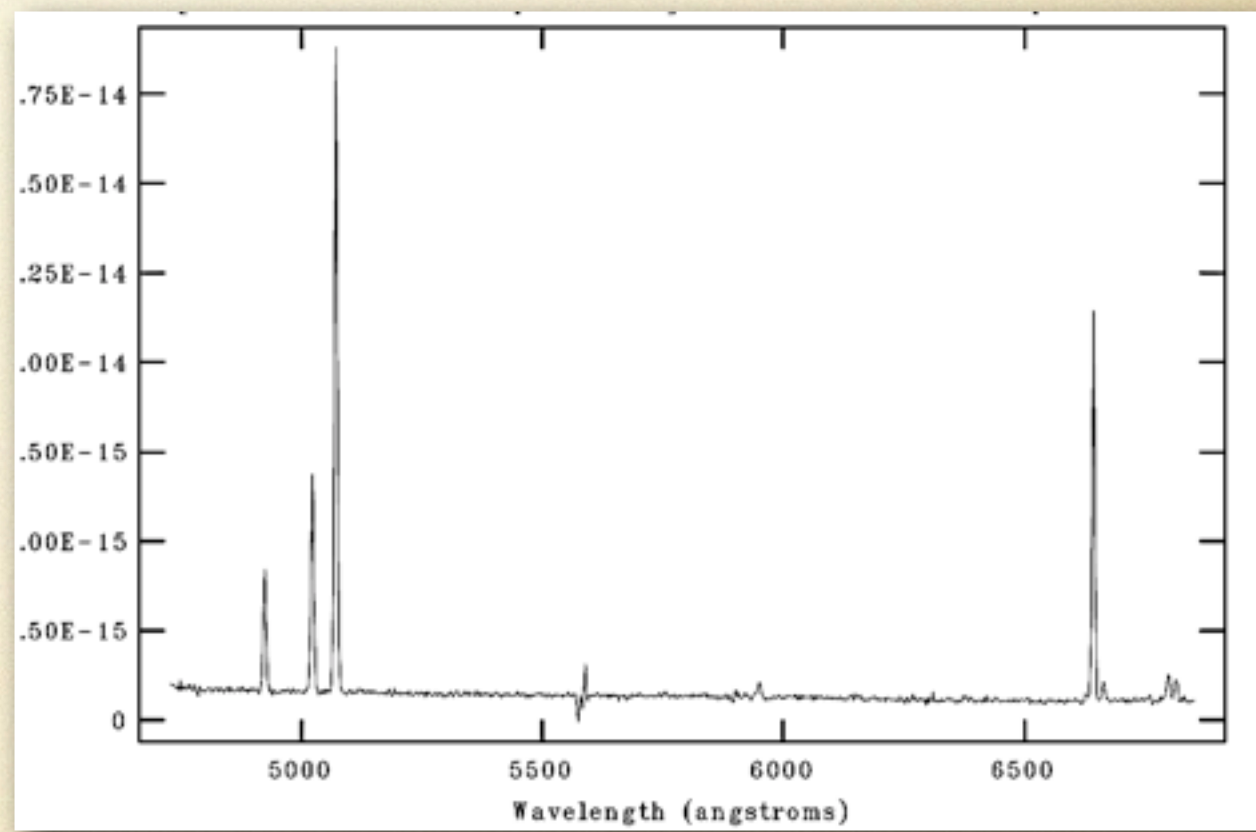


SDSS Spectrum

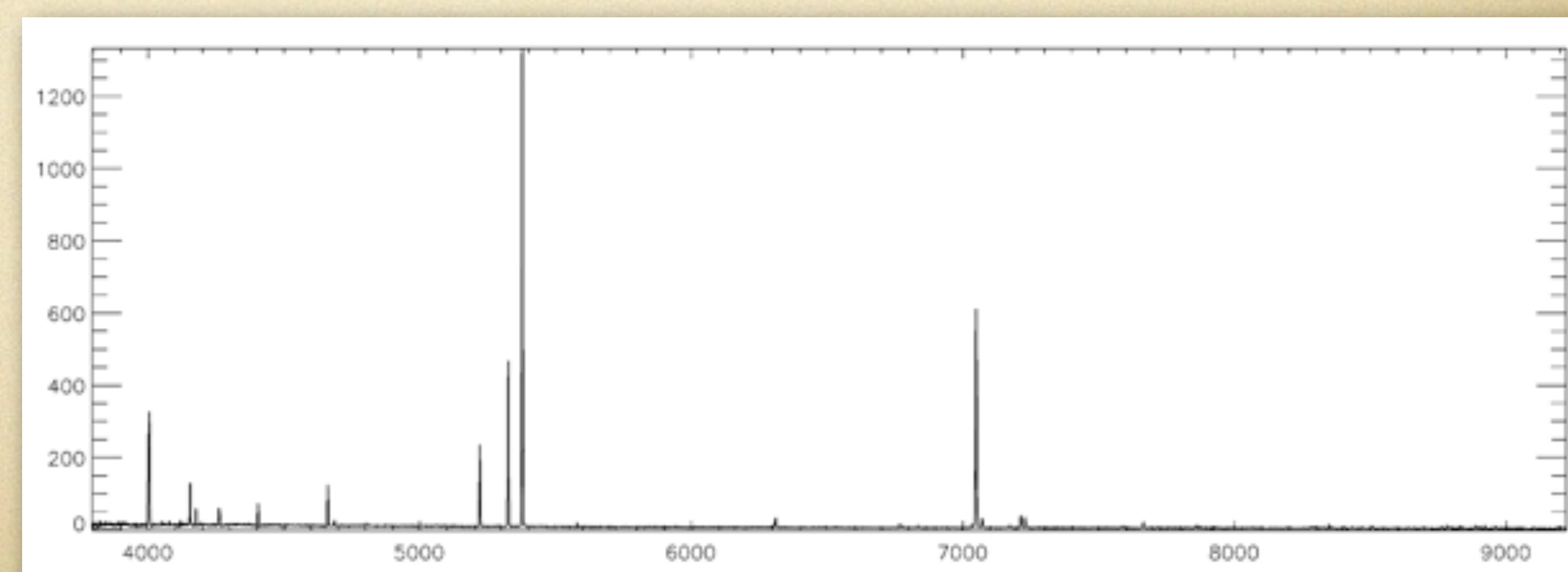

# Velocity dispersions: HDS Data aperture corrections.

J031023-083432

SDSS r band photometry

$$\sigma_0^2 = \sigma_{obs}^2 - \sigma_{th}^2 - \sigma_{inst}^2$$

$$\sigma_{th} = \sqrt{\frac{kT}{mc^2}}\lambda_0$$

$$g(\lambda) = \int f(\lambda - x)h(x)dx$$

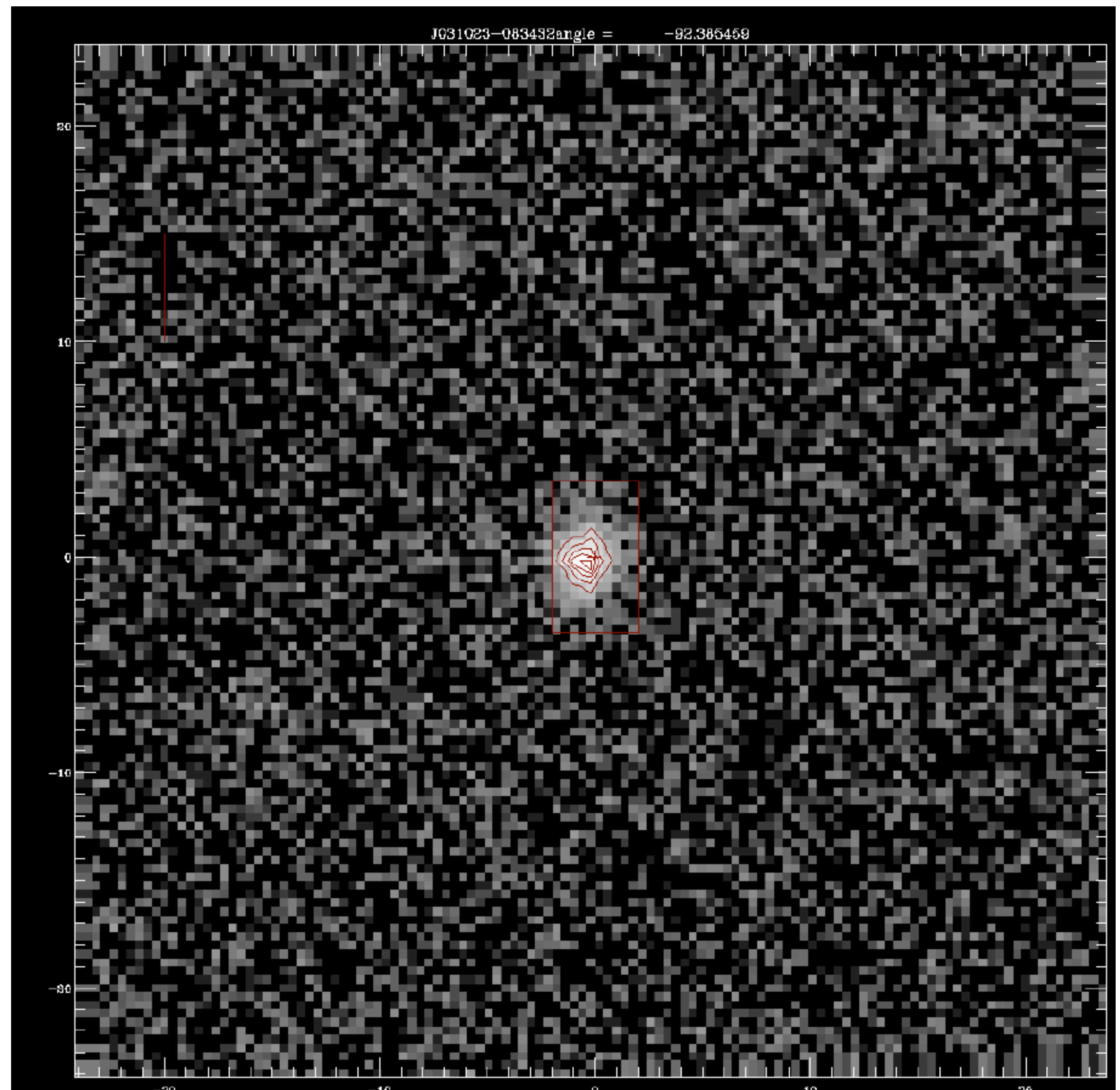

# Velocity dispersions: UVES Data

[O III] λ 4959

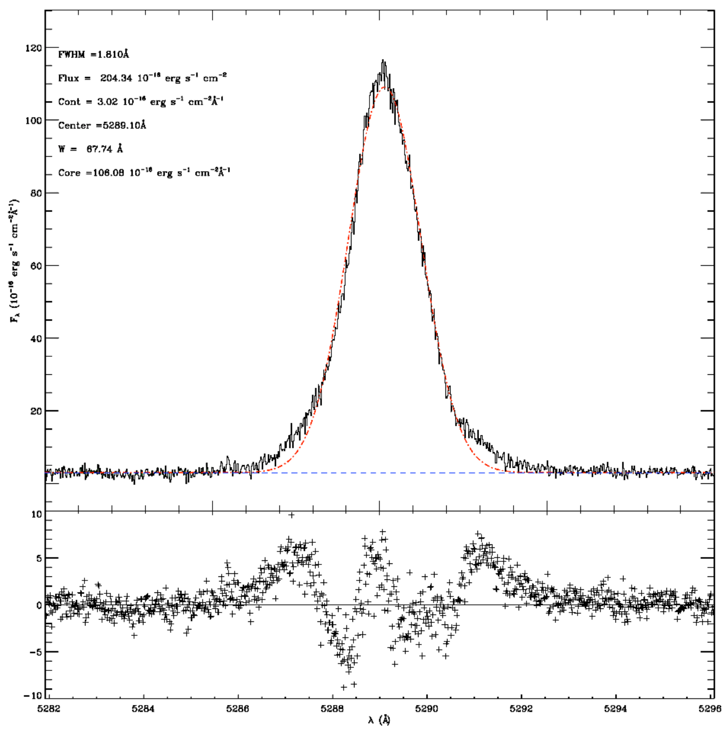


[O III] λ 5007

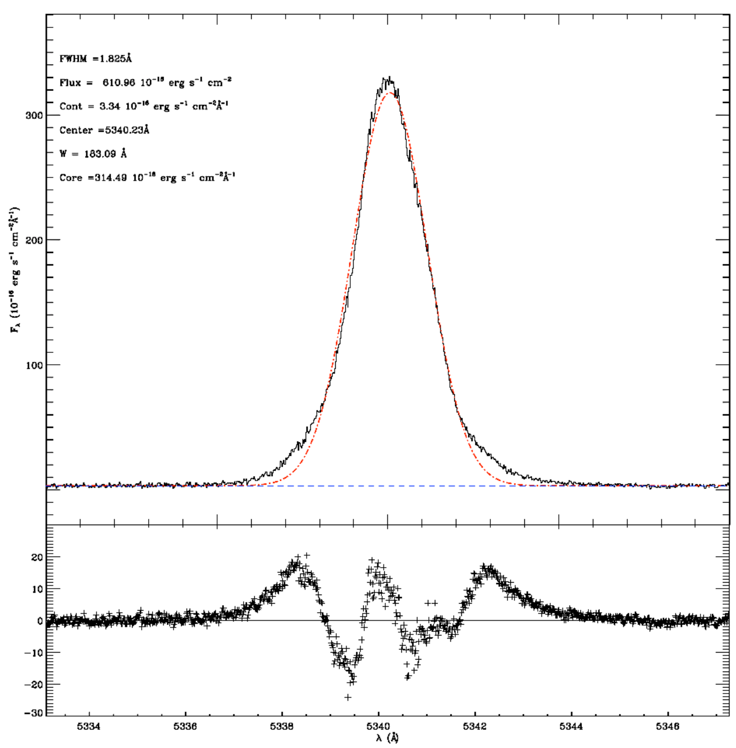


J222510-001152 Hβ

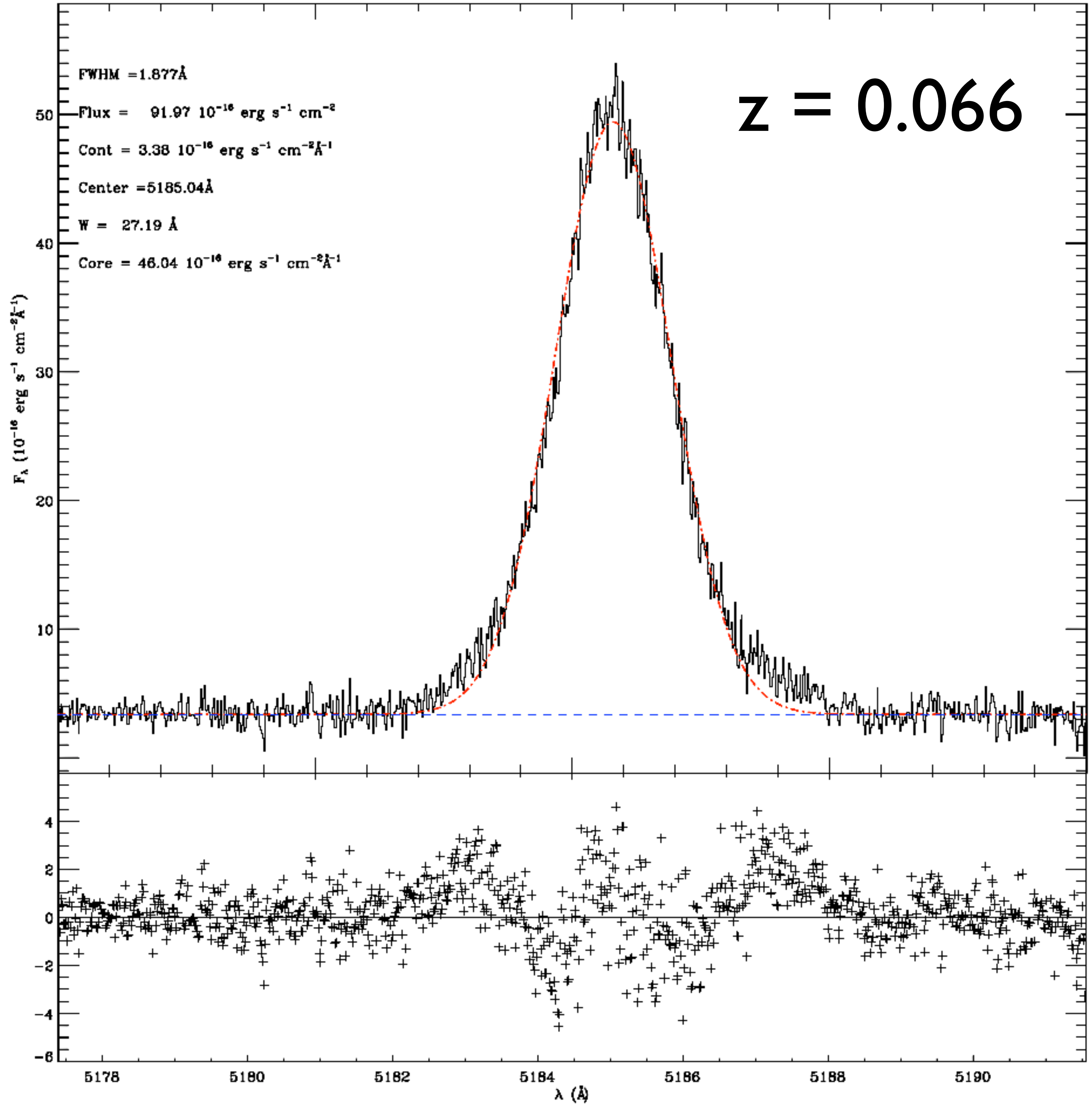

# Velocity dispersions: HDS Data

[O III] λ 4959

J005602-101009 Hβ

z = 0.058

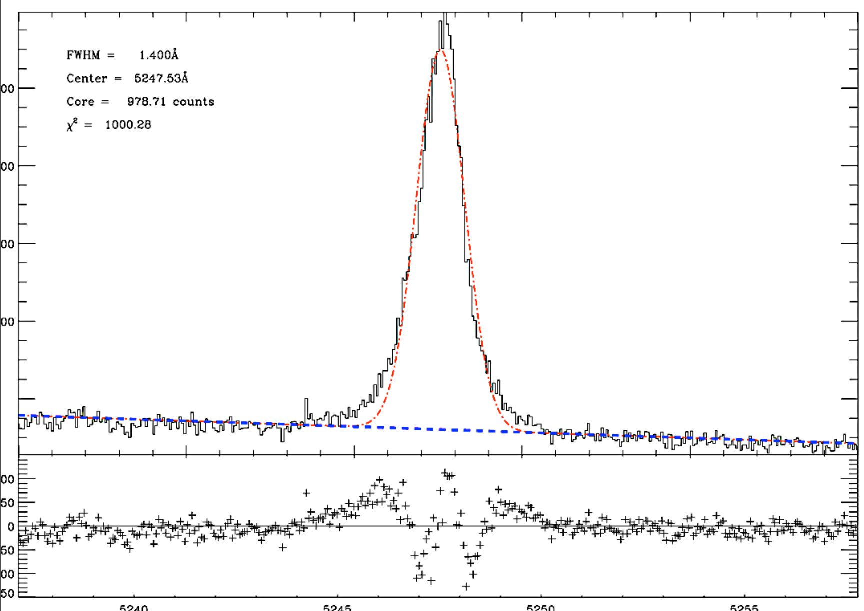


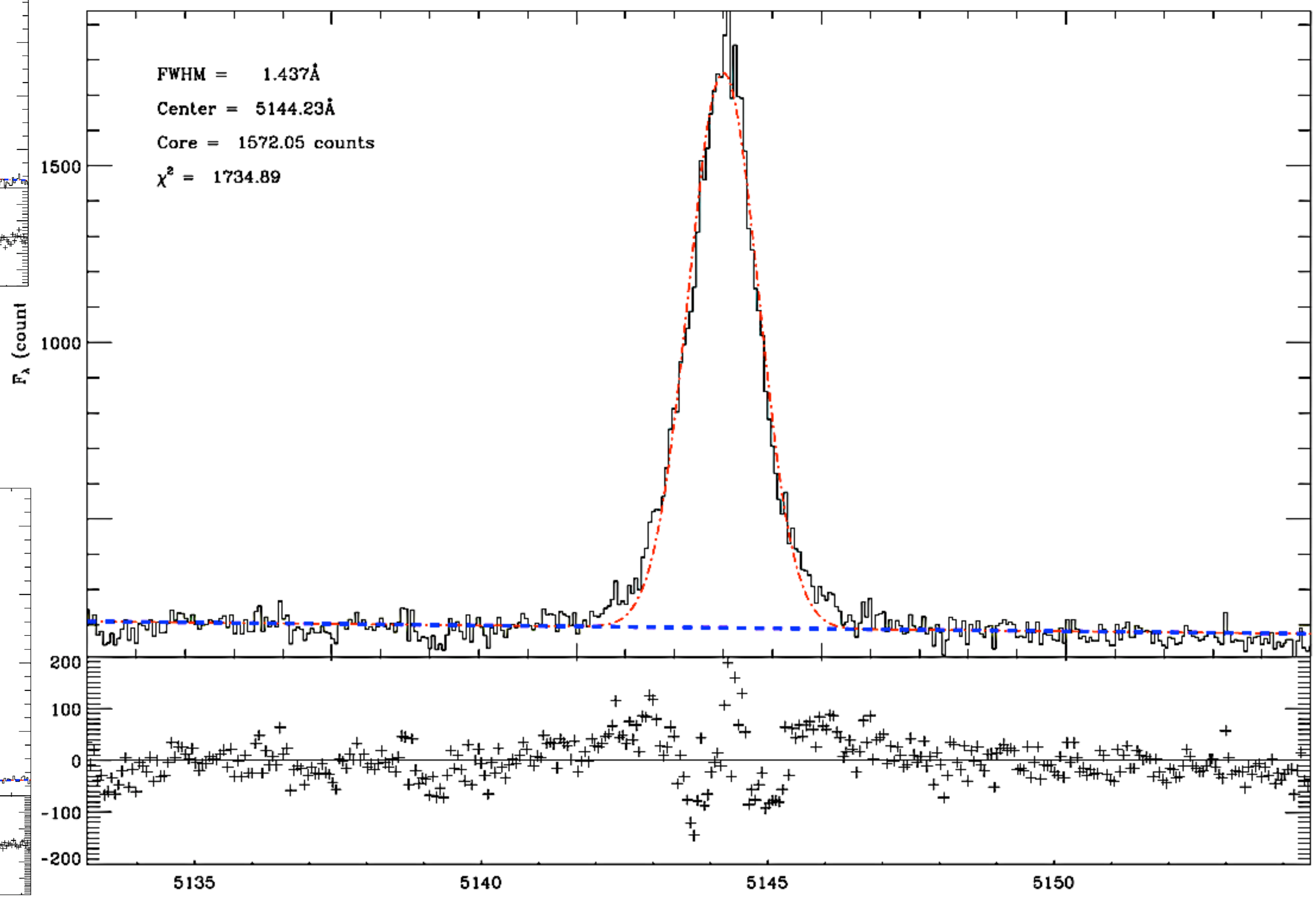


[O III] λ 5007

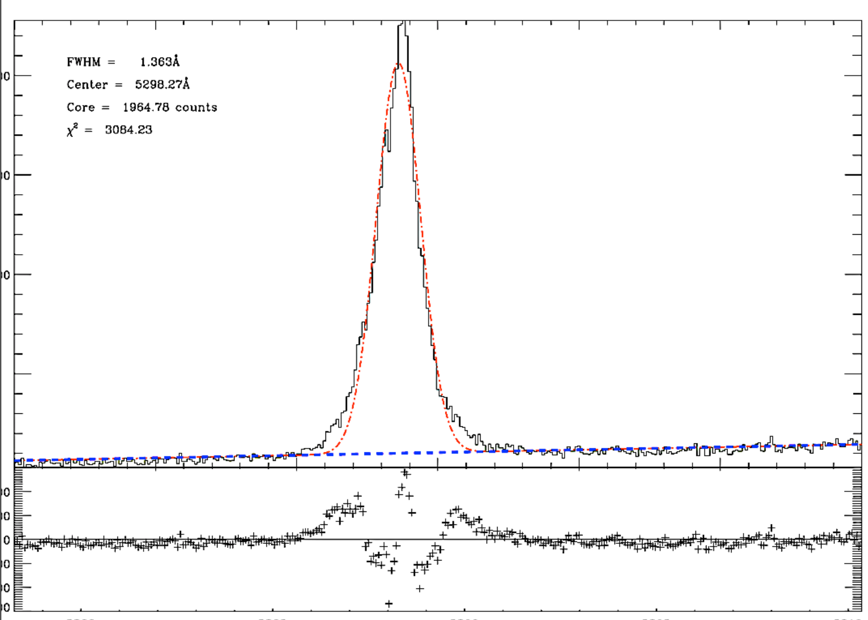

# Rotation

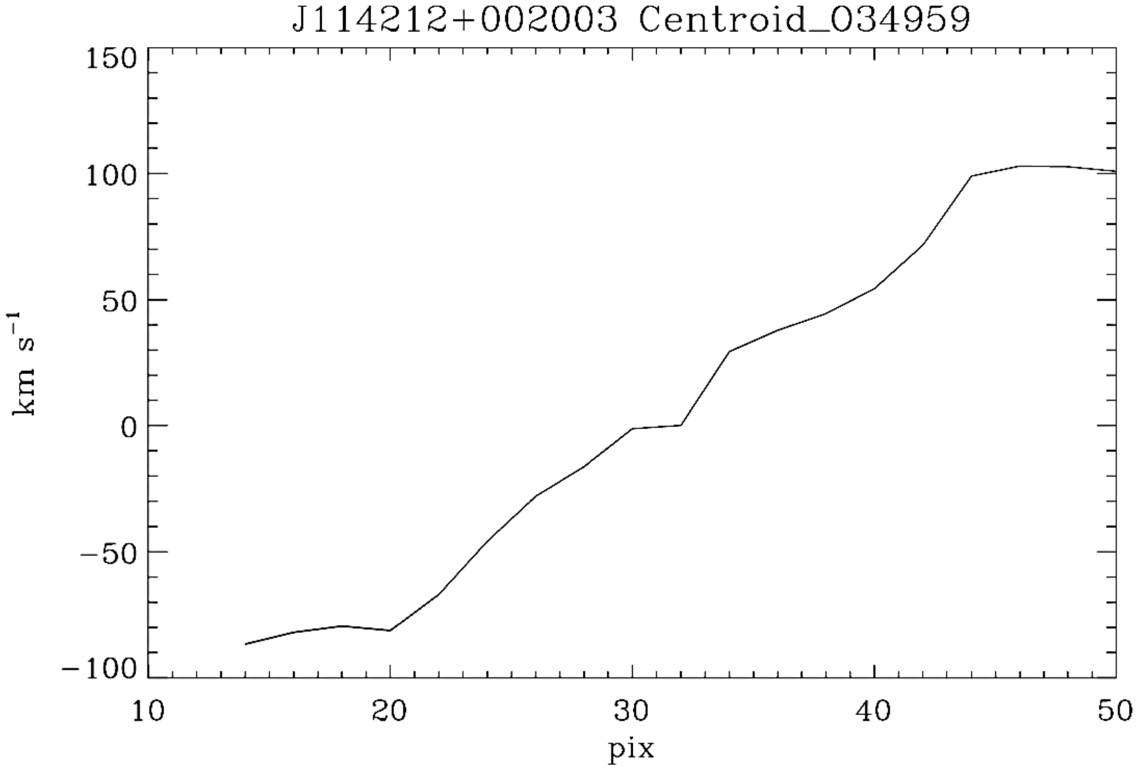


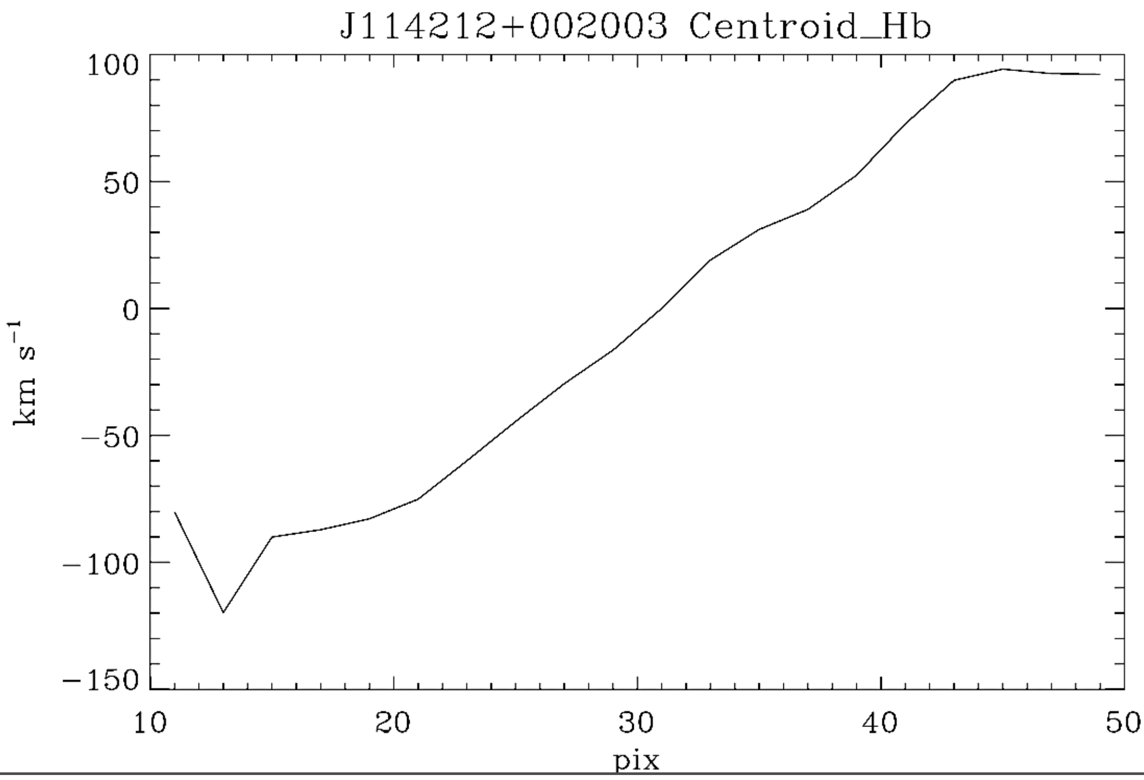


## J114212+002003 [O III] λ 4959

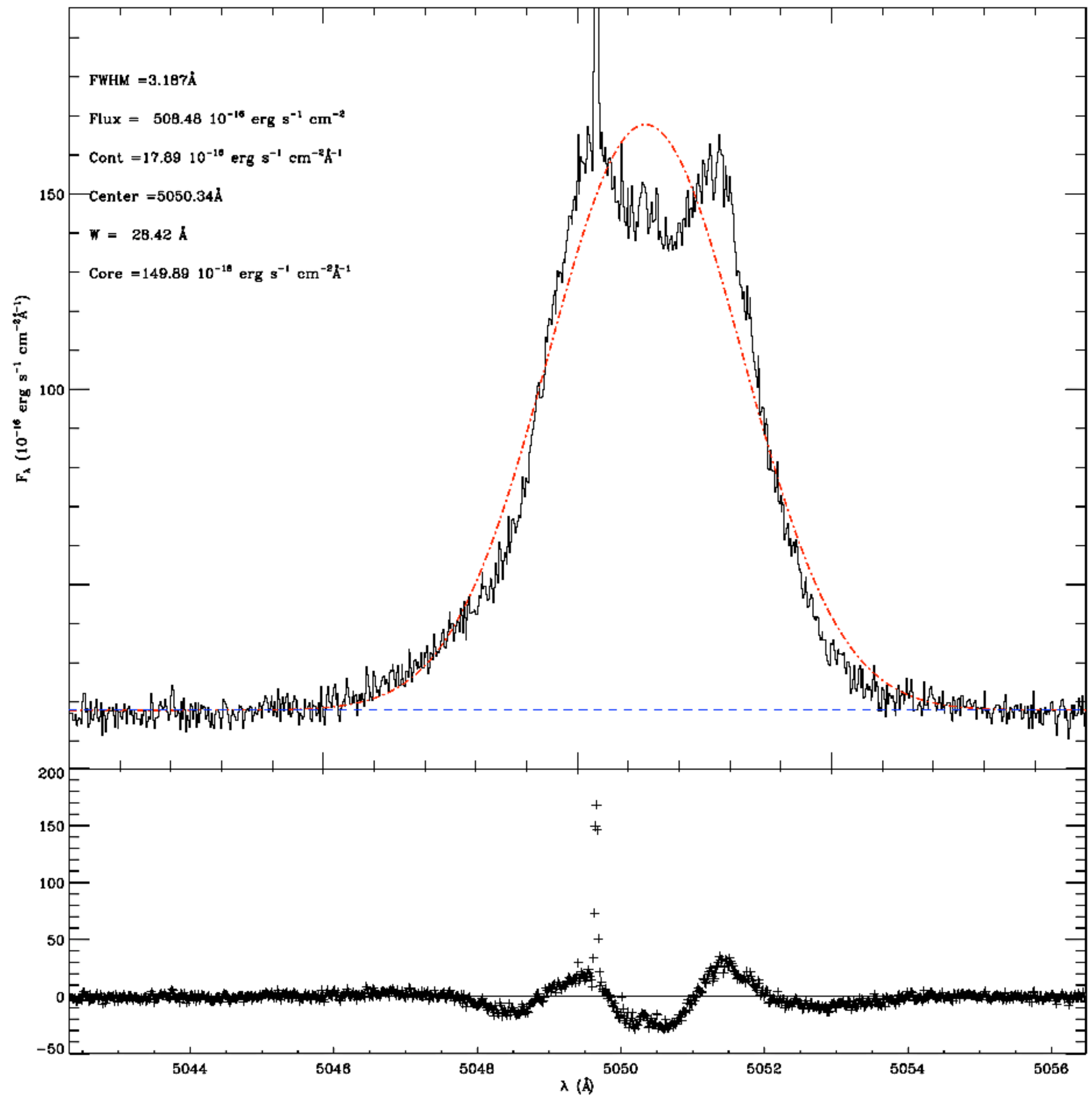


Wed, 24 Jul 2013

# Double Lines

## J142342+225728 Hβ

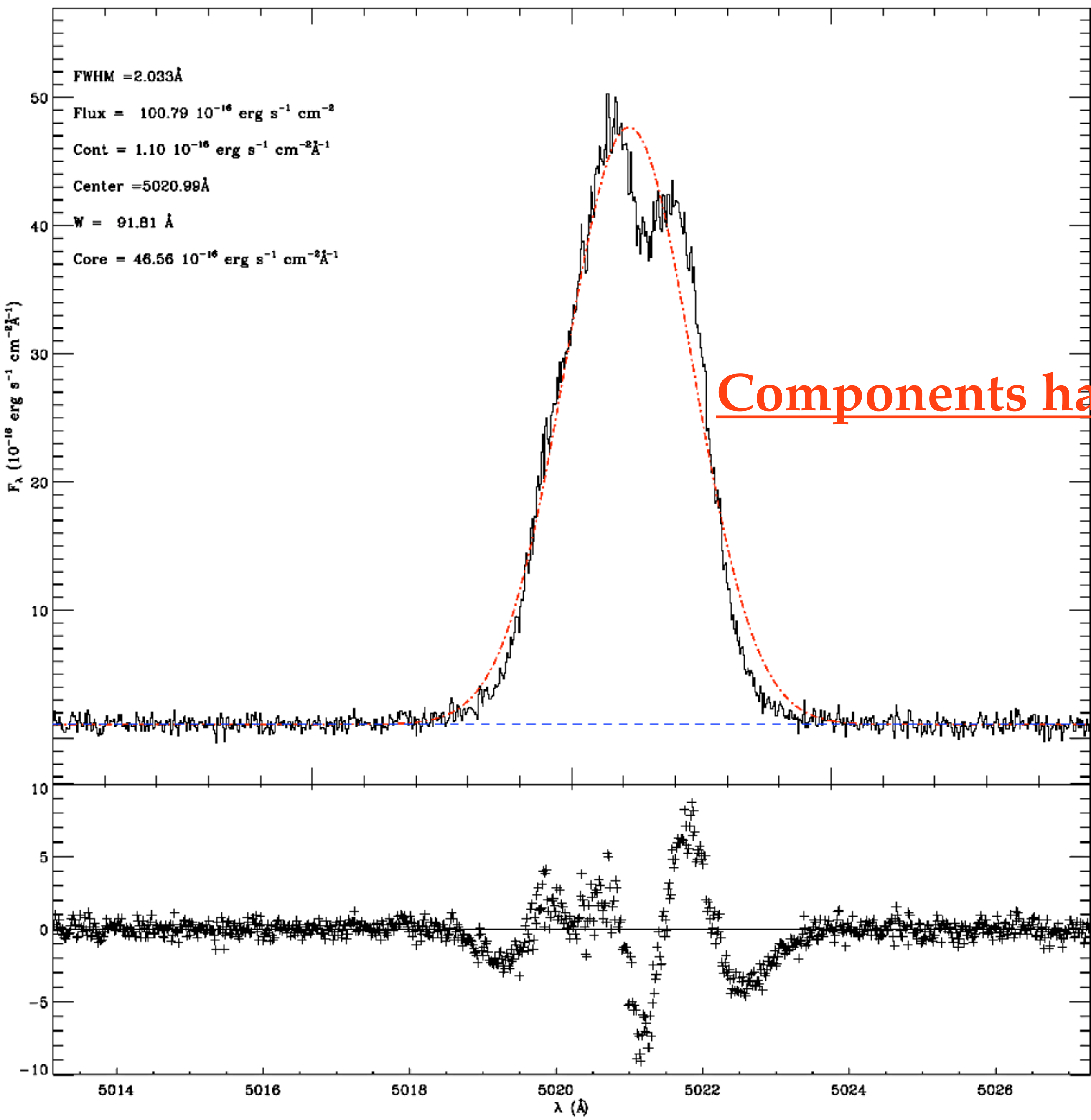


## J142342+225728 [O III] λ 5007

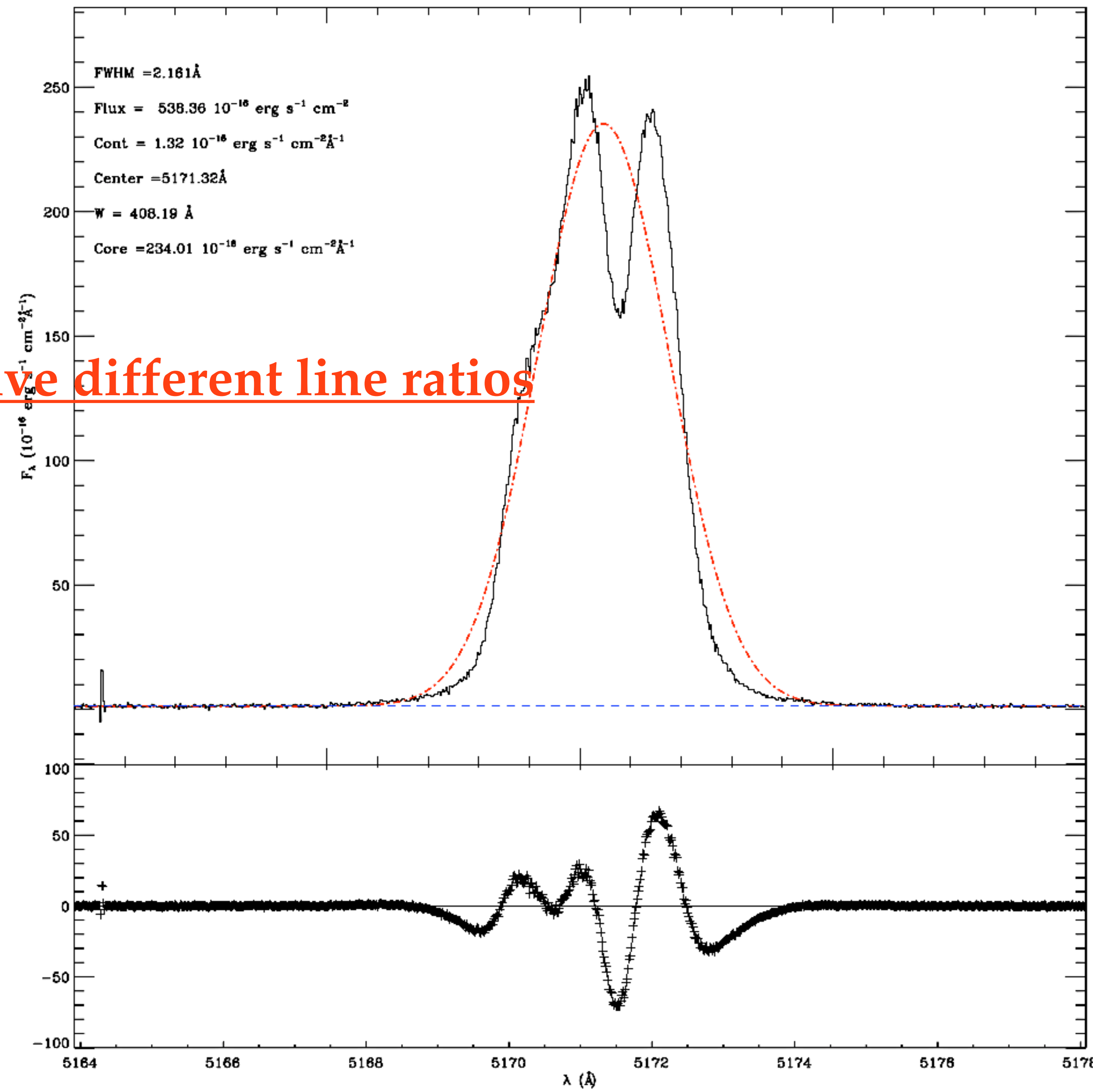


Components have different line ratios

# H II Galaxies - The L-σ relation for all systems

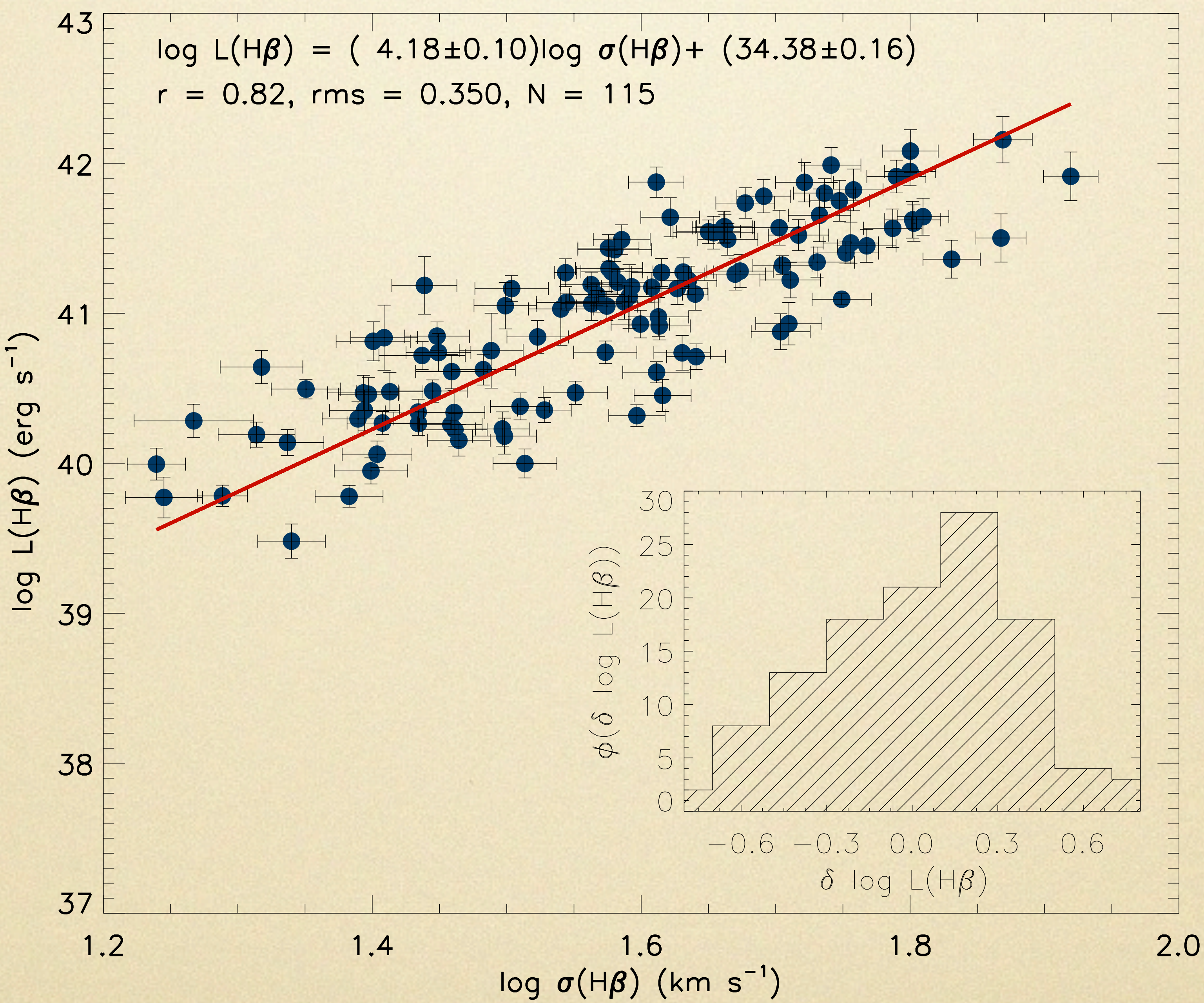

# *H II Galaxies - The L-σ relation for Gaussian profiles*

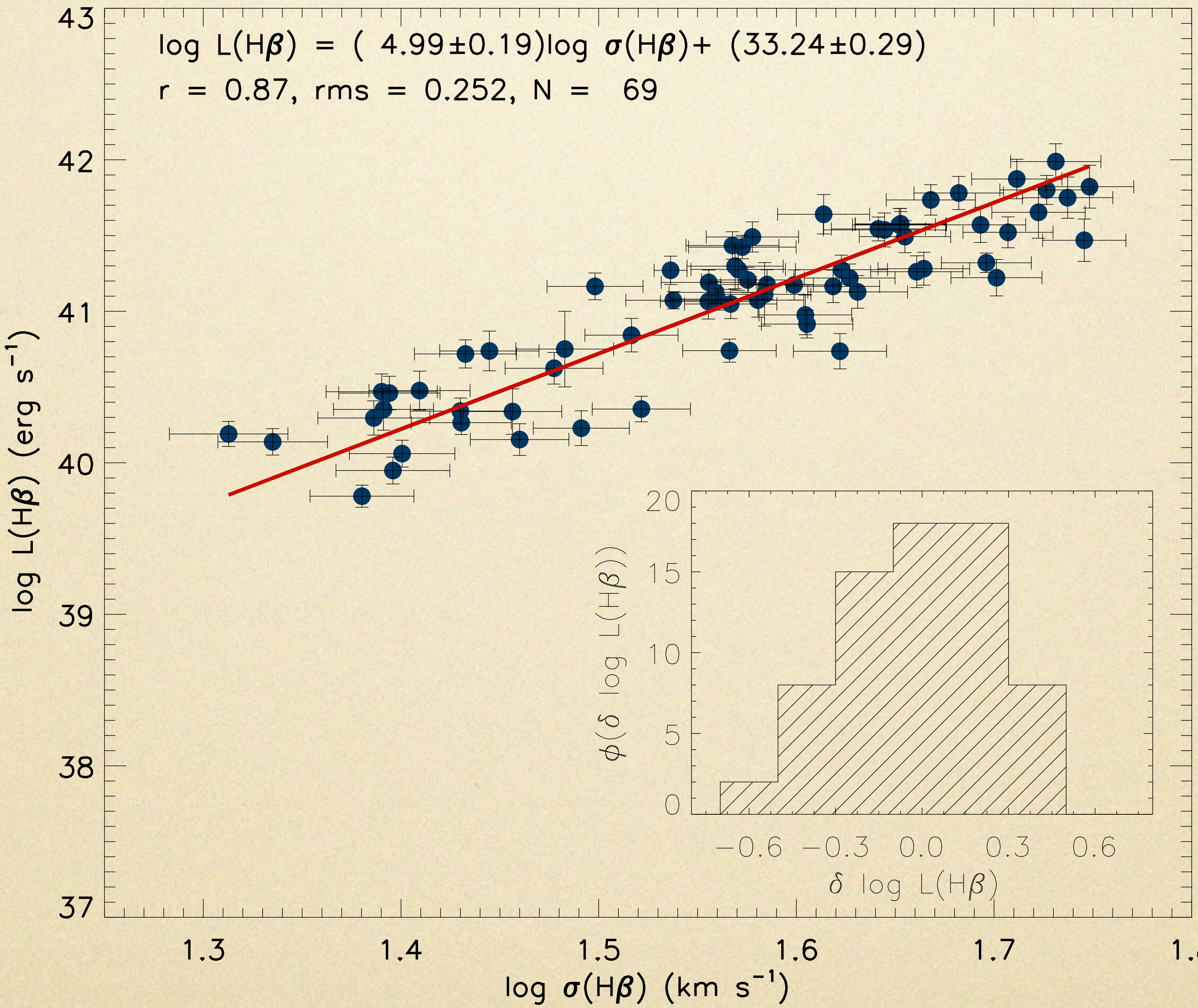

# *Giant H II Regions - The L-σ relation*

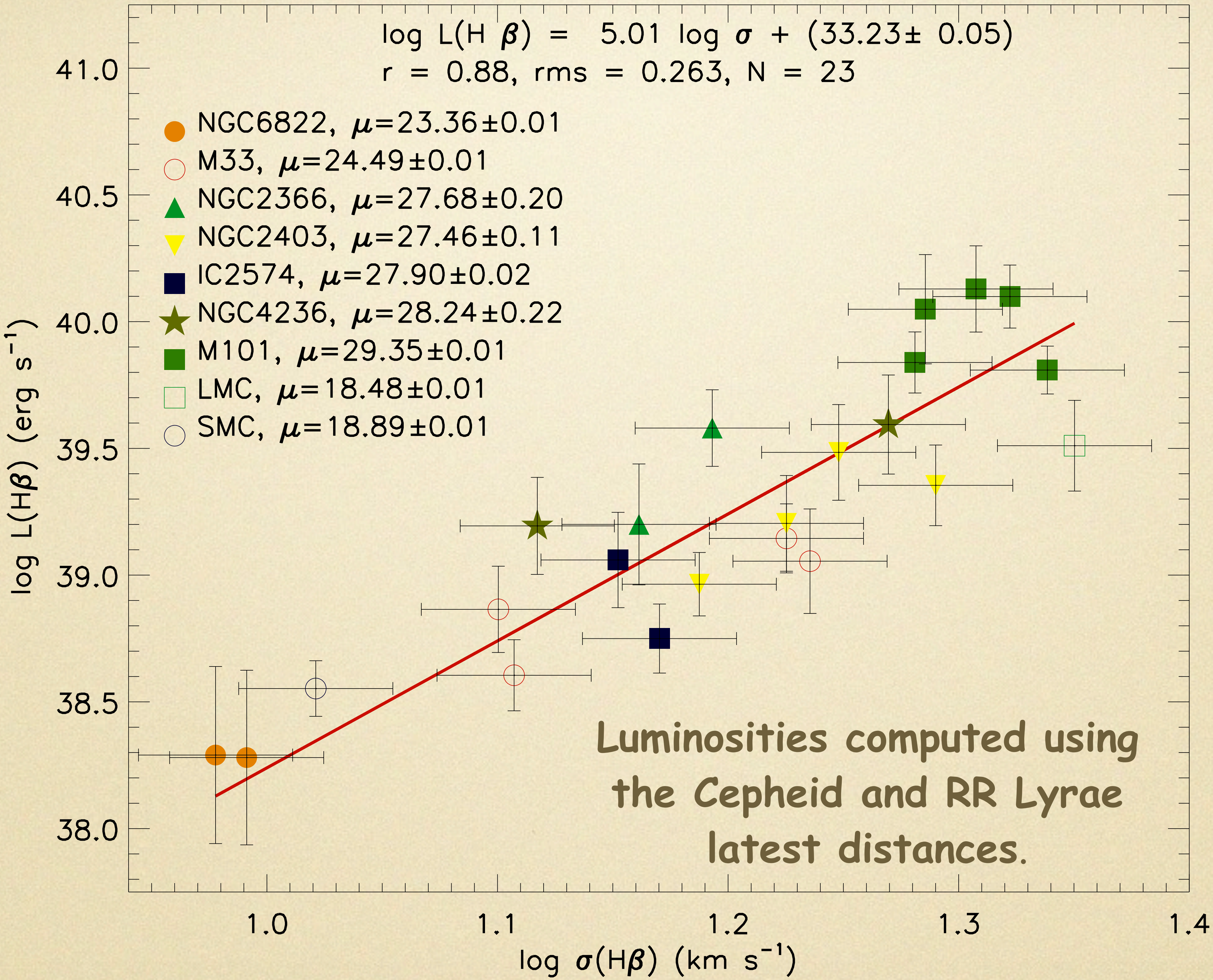


Wed, 24 Jul 2013

# *The new L-σ relation*

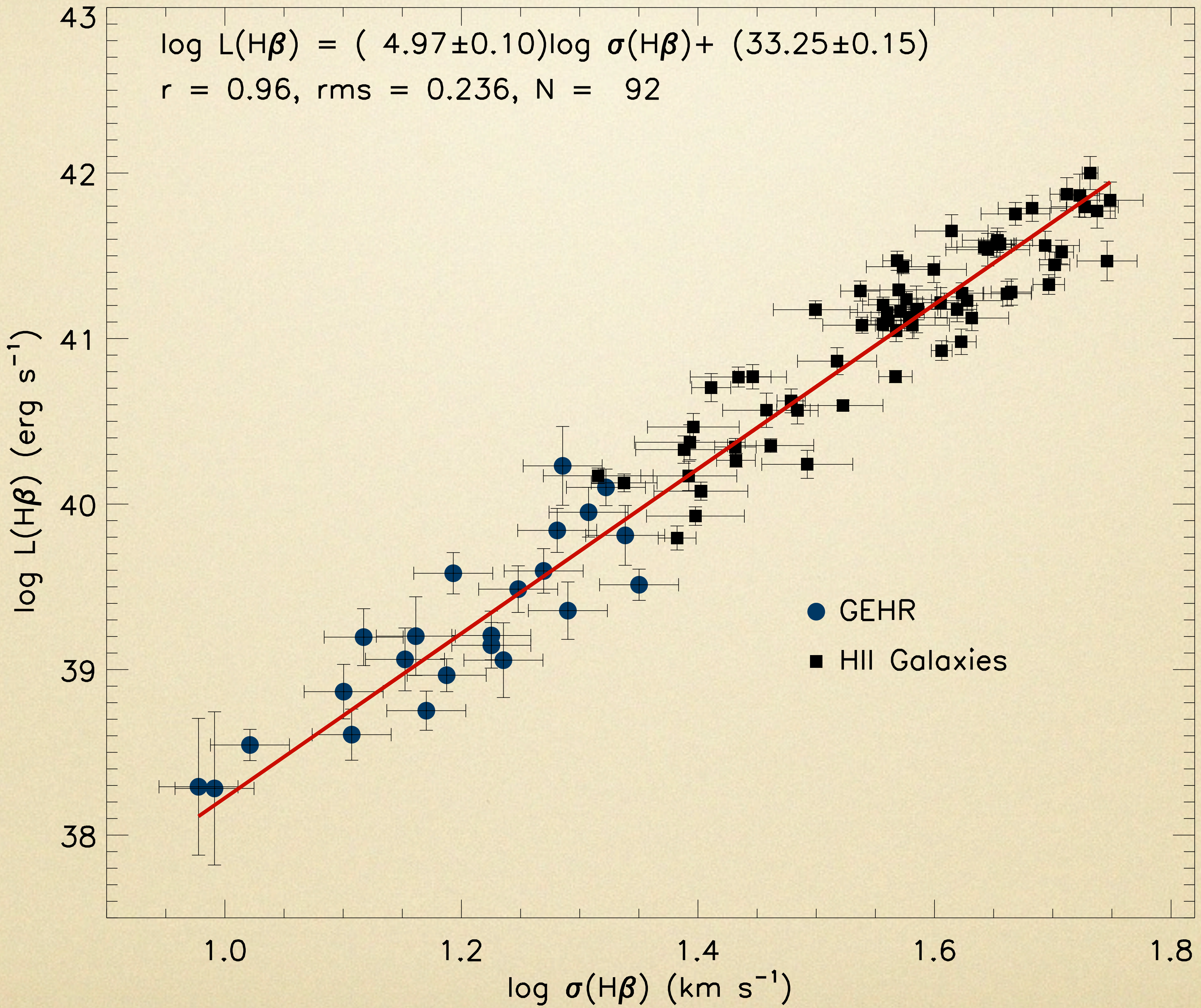


Chavez et al. 2012 MNRAS, 425L,56

# *Measuring $H_0$*

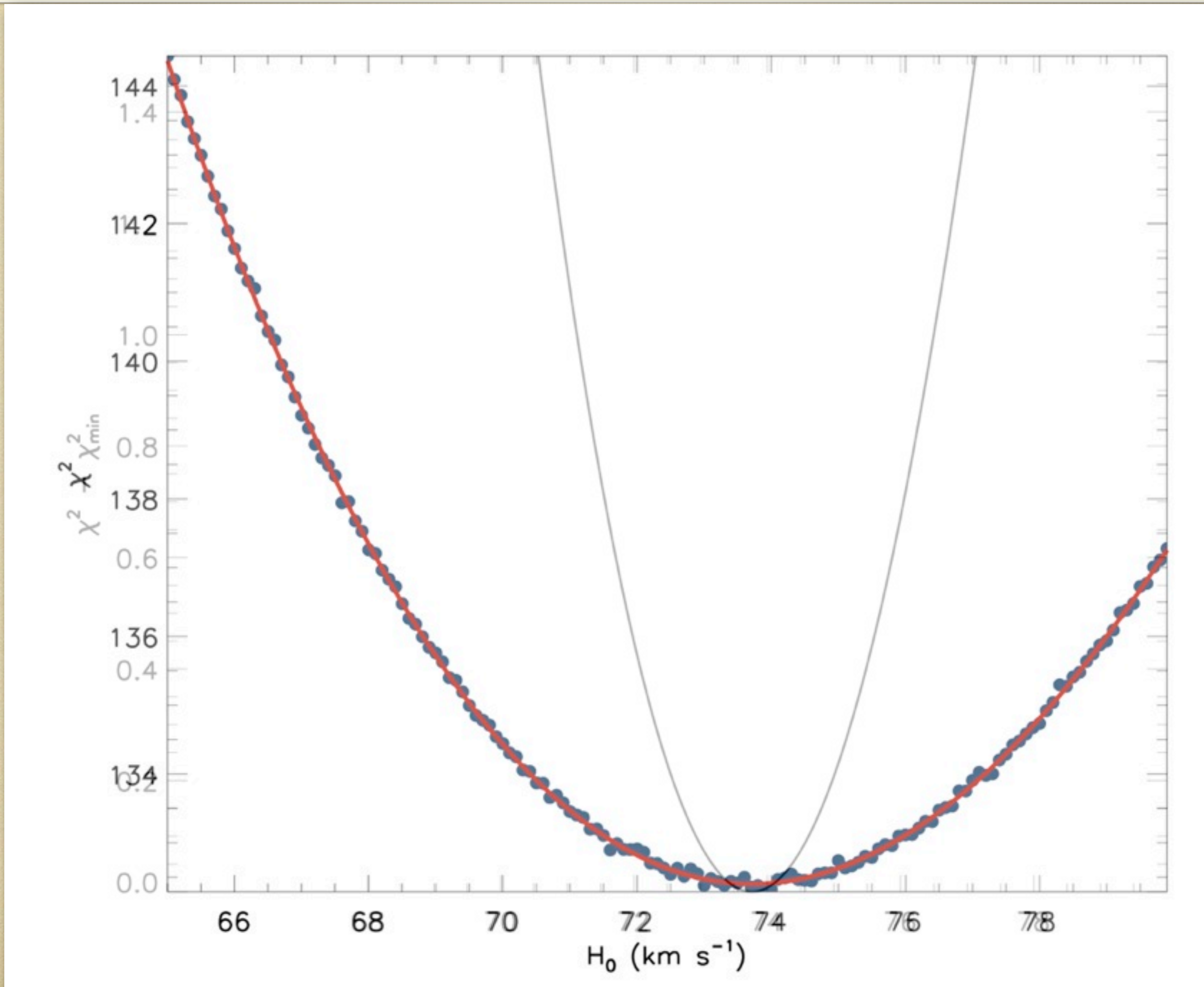

# *Measuring $H_0$*

*Hubble diagram*

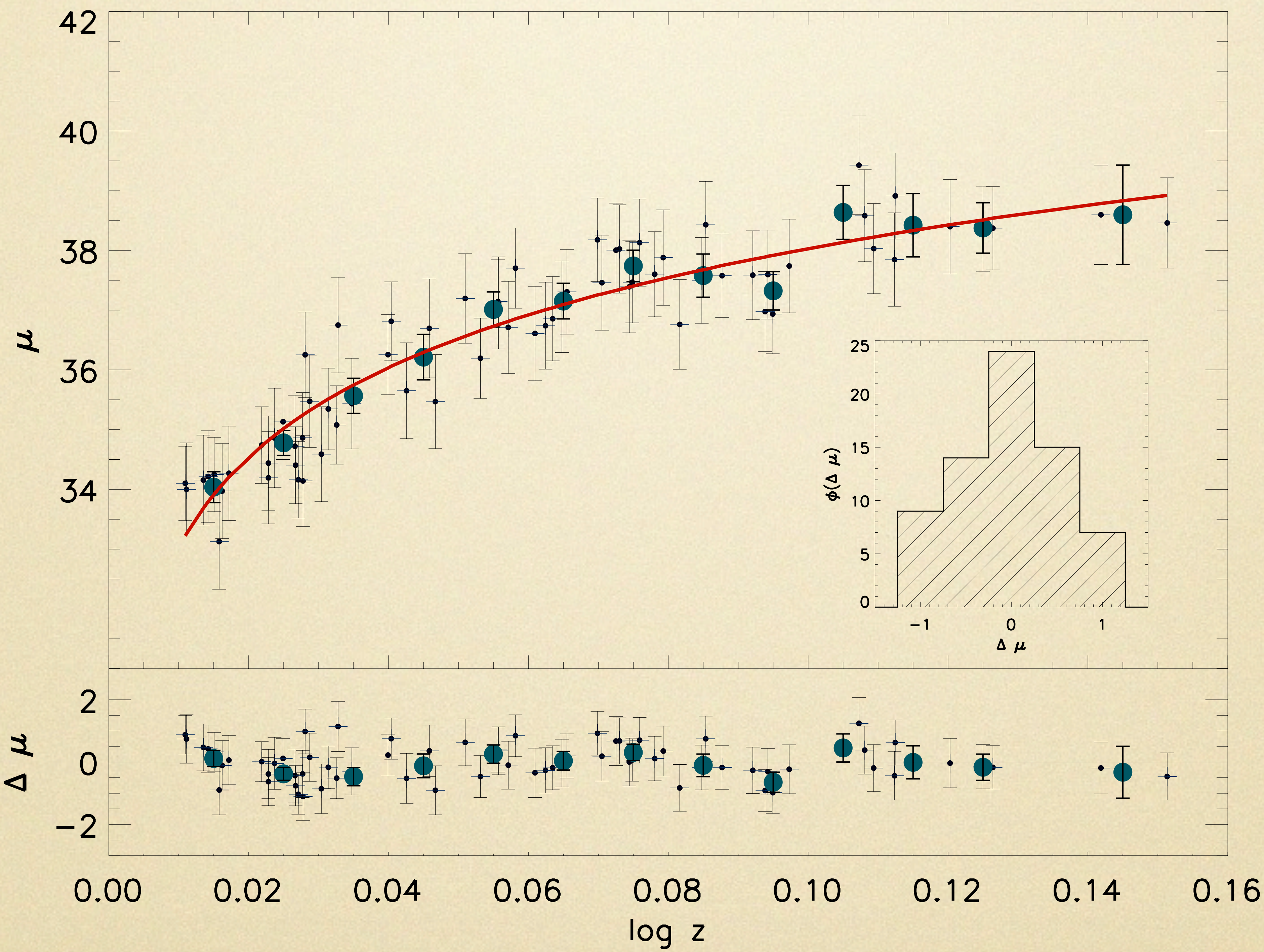


[Chavez et al. 2012 arXiv1203.6222C]

# Measuring $H_0$

We obtained:

Chavez etal 2012 $H_0 = 74.3 \pm 3.0$ (random)$\pm$ 2.9 (systematic)

That should be compared with:

Freedman etal 2001: $H_0 = 72 \pm 8$ (random+systematic)

Sandage etal 2006: $H_0 = 62.3 \pm 5.0$ (random+systematic)

Riess etal 2009: $H_0 = 74.2 \pm 3.6$ (random+systematic)

Riess etal 2012: $H_0 = 73.8 \pm 2.4$ (random+systematic)

and since Chavez etal 2012,

Freedman etal 2012: $H_0 = 74.3 \pm 1.5$ (random)$\pm$ 2.1 (systematic)

The historic improvement in the error budget is mostly due to the better distances to the "anchor" sample of nearby galaxies.

# *Measuring $H_0$*

While the error in distance for a Giant HII region or HII galaxy is about 0.12 dex, i.e. about 2.5 times larger than of the SNIa, the fact that there are more than one HII region per galaxy (typically 2-3) and furthermore there are more nearby galaxies with Cepheid determination and HII regions than with SNIa, makes our method a strong competitor capable of reaching random error < 1 km/s in the determination of $H_0$ .

# Main Points and Conclusions

1. We use HII galaxies as **Tracers** for the **Hubble Relation** and for the **Large Scale Structure** in order to improve constraints on the DE Equation of State

2. We plan to break the known degeneracy between DE and DM content of the universe using **HII Galaxies**.

3. Our analysis shows that to reduce the cosmological parameter solution space, it is by far more important to increase the number of high-z (z>2) tracers than to reduce the low-z tracer individual uncertainties.

# Conclusions

4. We have determined $H_0$ with the new L-σ distance estimator obtaining: $H_0 = 74.3 \pm 4.5$ (random+systematic)

5. The similarity of our result with that of Riess etal (2009,2012) and Freedman etal (2012) implies:

a - We have reasonable good control of the systematic errors, and

b - We have what is probably the best indication of the universality of the IMF, at least inside a volume of 600Mpc in radius. Note that 30Dor is part of the reference sample.

# Future Work (2013-2014)

- **Towards 1% error budget in $H_0$:** Improve the data quality for the present anchor sample and add further 60 GHIIR in 16 additional galaxies with Cepheid distances plus NGC4258 (with "MASER" distance) that has 3 GHIIR. This makes a total of 87 GHIIR in 26 galaxies. Augment the sample of nearby HIIGx to 300.

- **$w - \Omega_m$:** Start the observations of the high z sample of HIIGx.

- The kinematics of massive star forming regions.
- HII galaxies and Giant HII regions
- Circumstellar regions
- 30 Dor: The Giant HII region prototype

Monthly Notices
of the
ROYAL ASTRONOMICAL SOCIETY

MNRAS 432, 810–821 (2013)
Advance Access publication 2013 April 19

doi:10.1093/mnras/stt491

# Implications of the kinematical structure of circumnuclear star-forming regions on their derived properties

Guillermo F. Hägele,[1,2,3★] Ángeles I. Díaz,[3] Roberto Terlevich,[4,5] Elena Terlevich,[4†]
Guillermo L. Bosch[2] and Mónica V. Cardaci[1,2,3]

NGC 3351

F606W

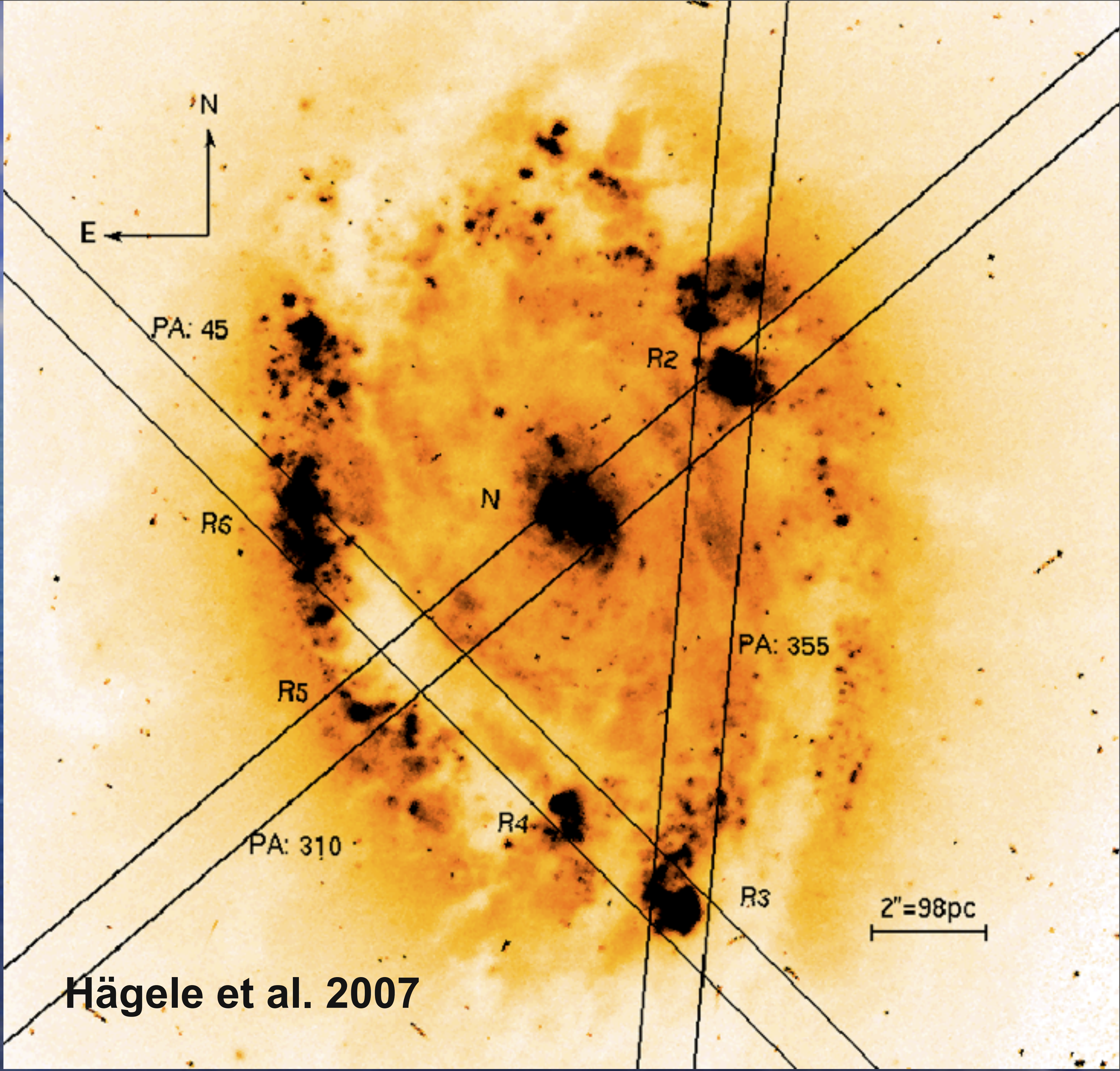

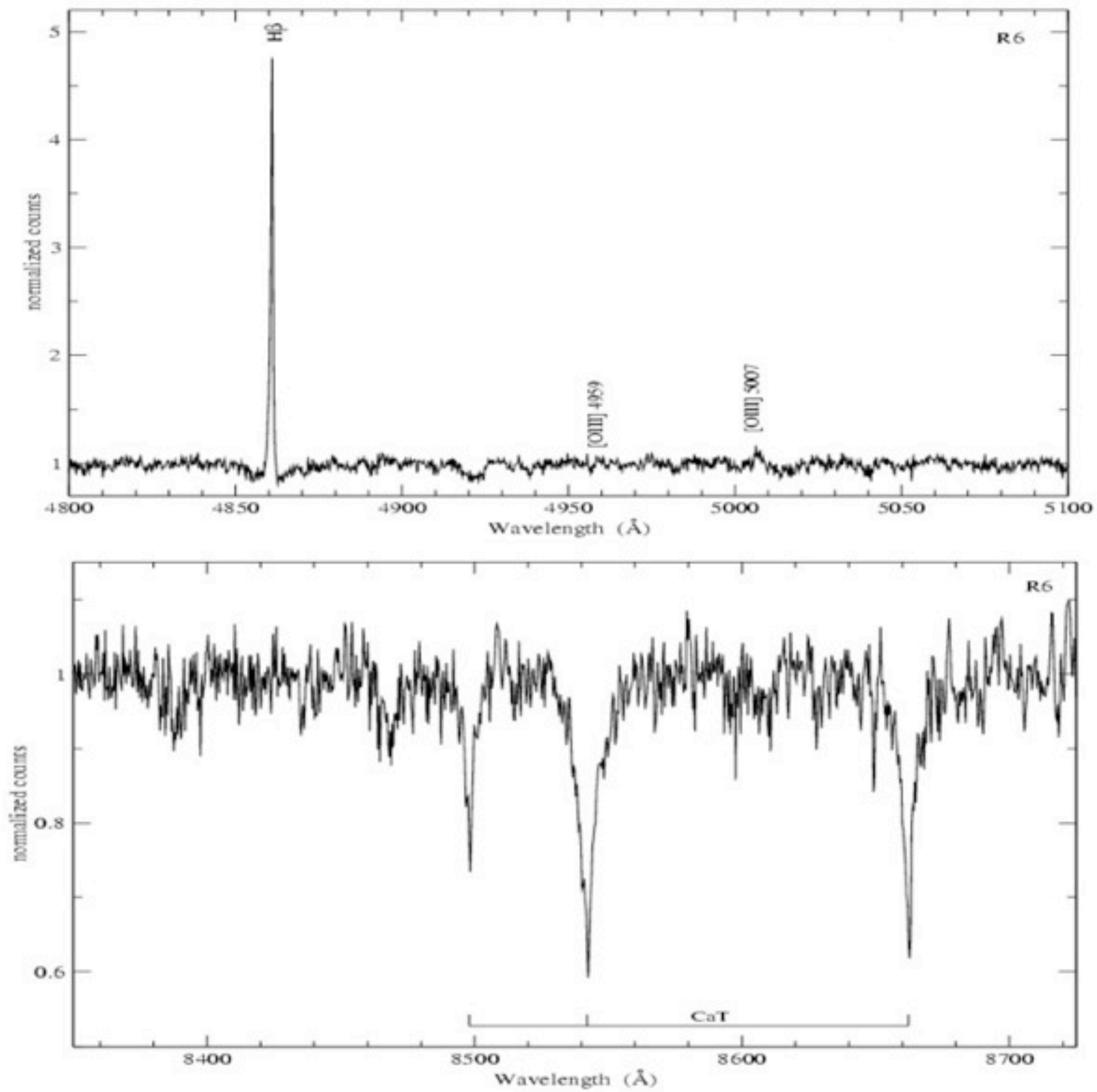


**Figure 3.** Blue (upper panel) and red (lower panel) rest frame normalised spectra of R6. Notice the absence of conspicuous emission lines in the red spectral range for this region.

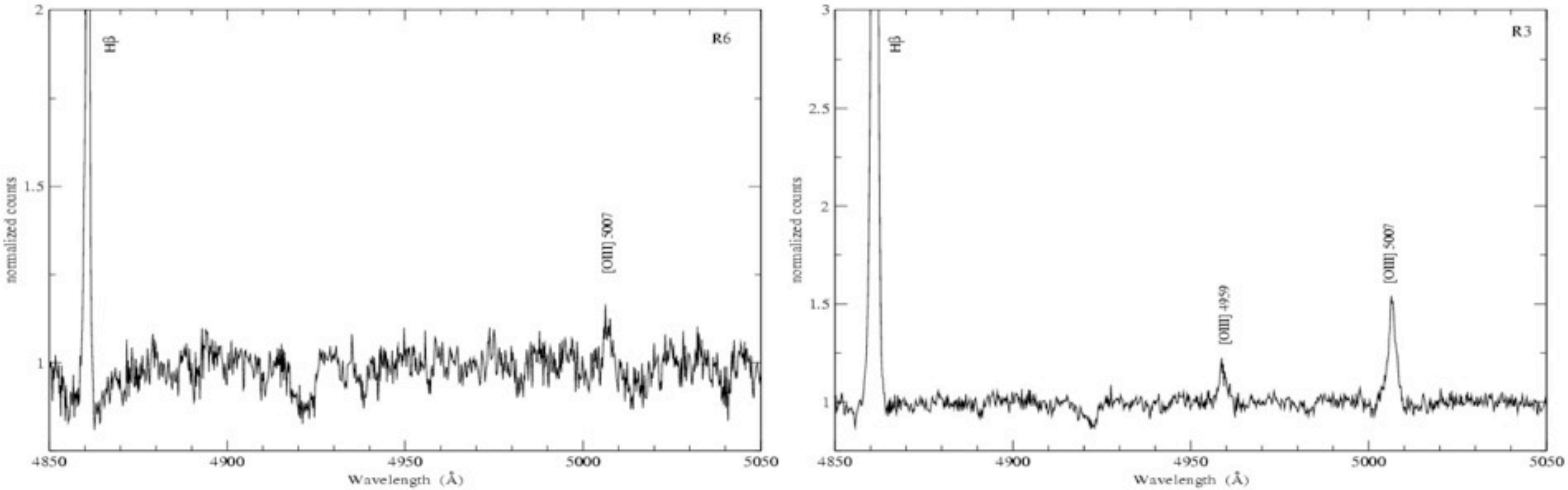


**Figure 5.** Enlargement of the blue rest frame normalised spectra of R6 (left) and R3 (right).

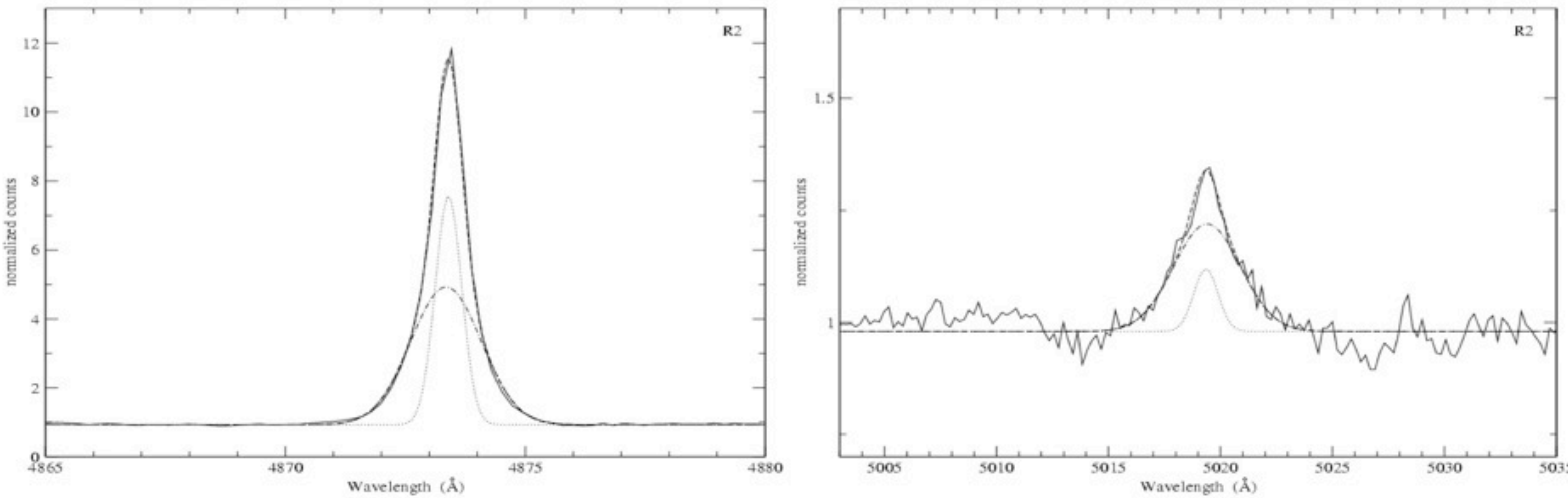


**Figure 9.** Sections of the normalised spectrum of R2. The left panel shows from 4865 to 4880 Å, containing H$\beta$ and the right panel, from 5003 to 5035 Å, containing the [OIII] $\lambda$ 5007 Å emission line. For both we have superposed the fits from the ngaussfit task in IRAF; the dashed-dotted line is the broad component, the dotted line is the narrow component and the dashed line is the sum of both.

Hägele et al 2007

NGC 3351

$\sigma_{gas} < \sigma_{*}$ by about 25 km/s

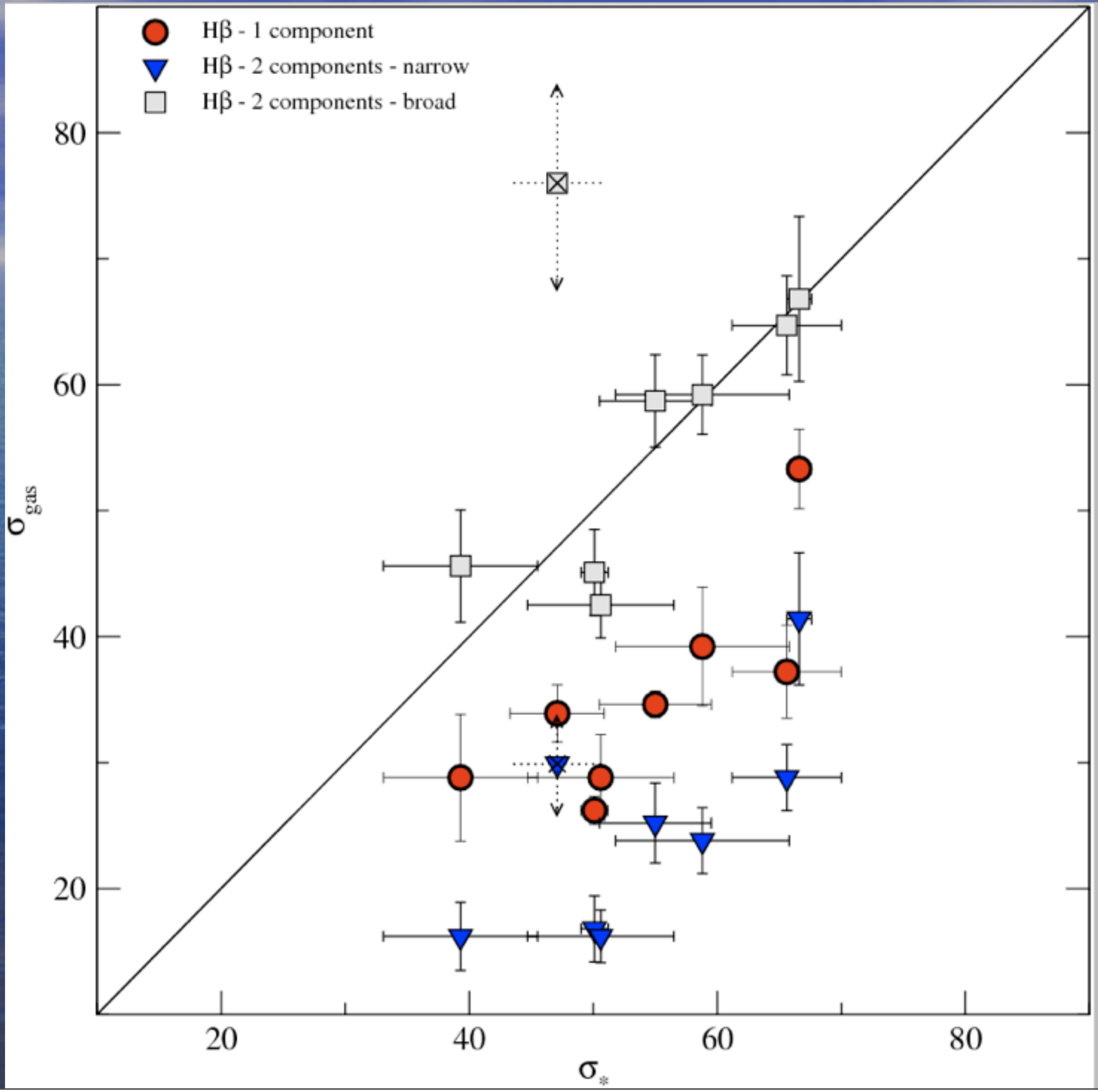


July 2013

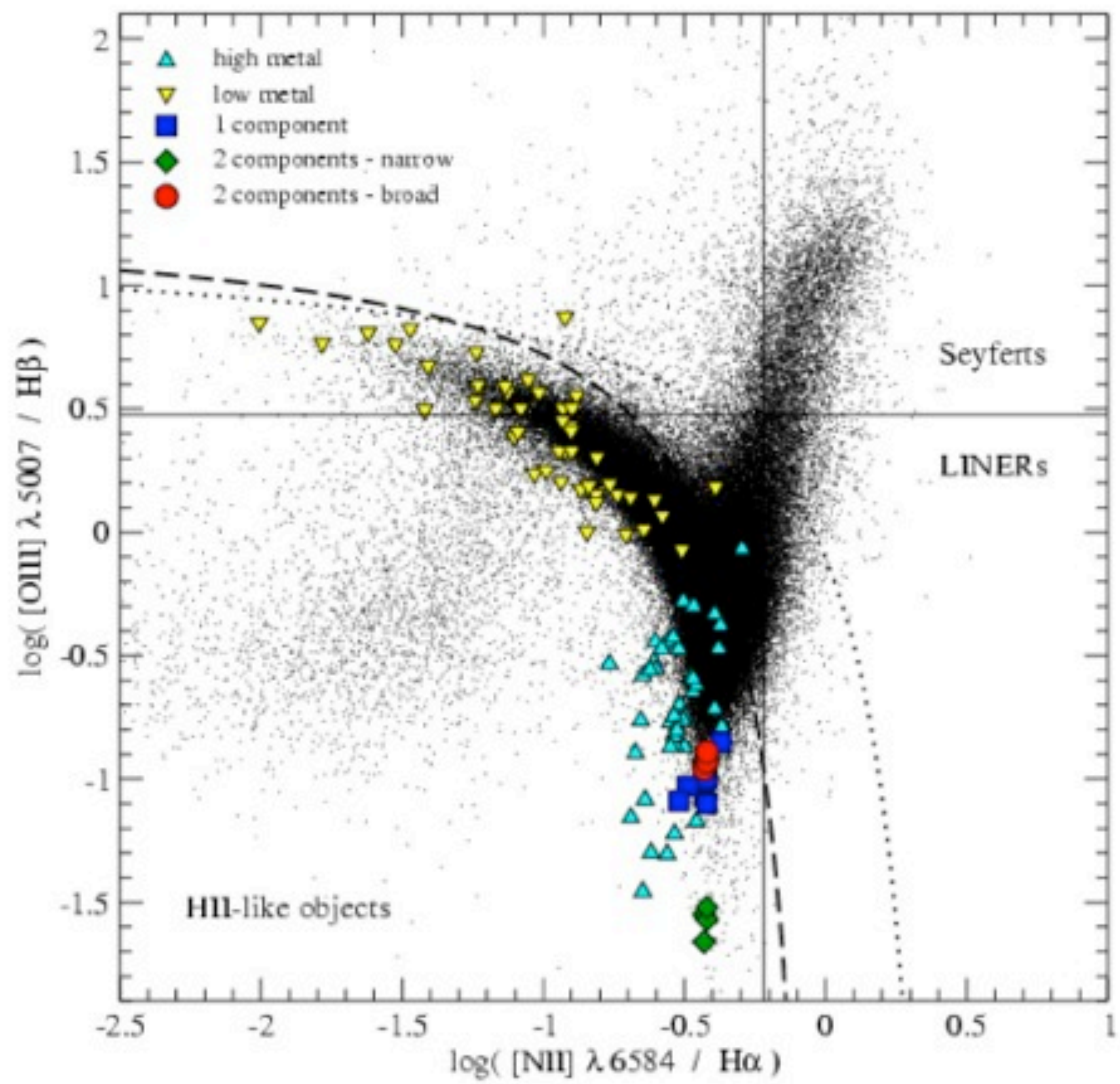


**Figure 12.** BPT diagram [OIII]/H$\beta$ *vs* [NII]/H$\alpha$. Squares correspond to the ratio of the emission intensities of [OIII] and H$\beta$ estimated using a single Gaussian fit, diamonds to the narrow components of the two Gaussian fits and circles to the broad components. Dotted and dashed curves are the boundary between Active Galactic Nuclei (AGNs) and HII galaxies defined by Kewley et al. (2001) and Kauffmann et al. (2003) respectively. The solid horizontal and vertical lines represent the division between Seyfert galaxies and LINERs according to Ho et al. (1997). Dots correspond to a subsample of emission line objects, including HII galaxies, from SDSS-DR3, from López (2005). Triangles correspond to HII regions from the sample of Pérez-Montero & Díaz (2005). They have been split into low metallicity (upside down triangles) and high metallicity regions (upward triangles) according to the criterion by Díaz & Pérez-Montero (2000) based on oxygen and sulphur abundance parameters.

# 17 circumnuclear star-forming regions in 3 early spiral galaxies, NGC 2903, NGC 3310 and NGC 3351

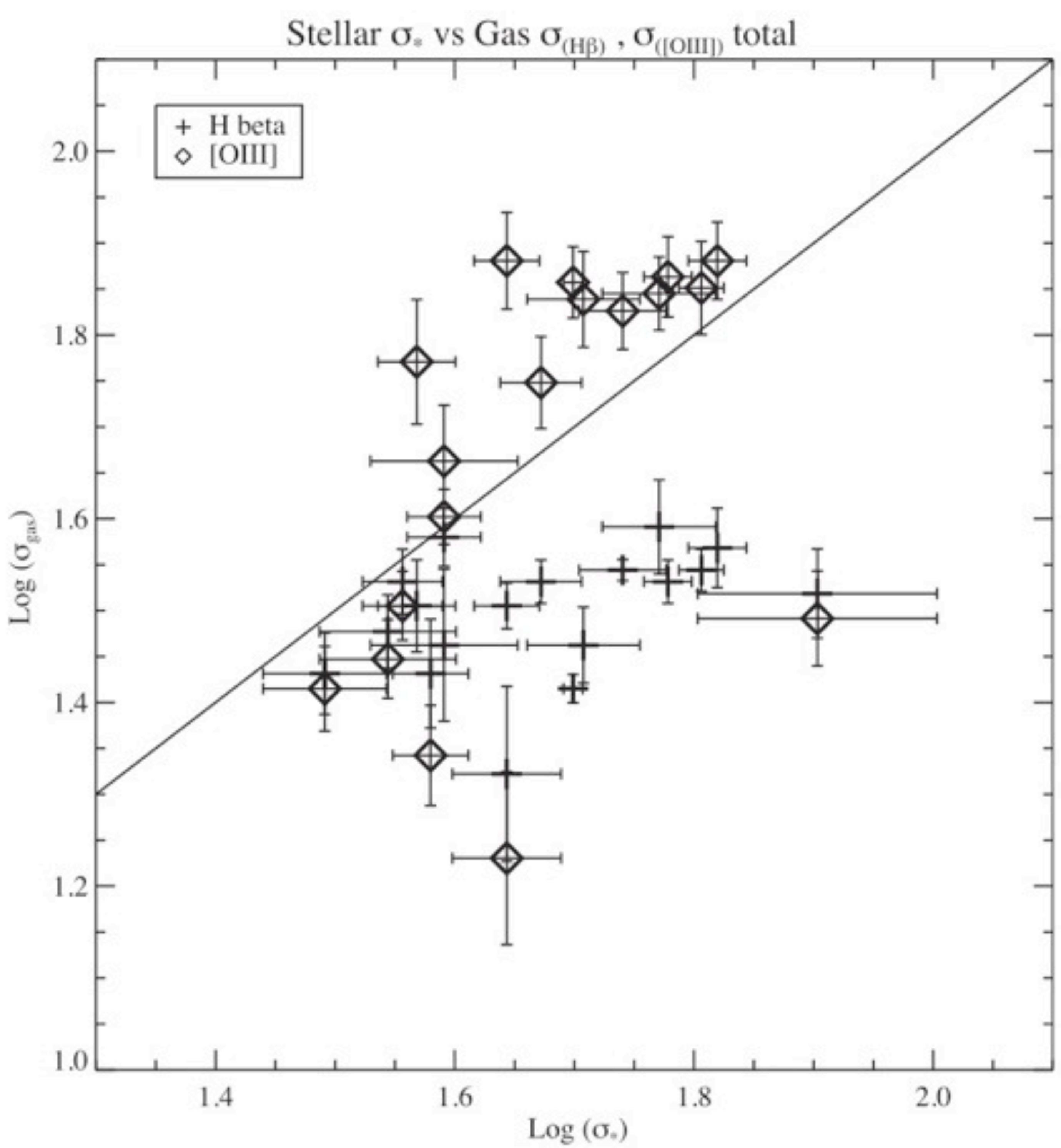


**Figure 3.** Gaseous versus stellar velocity dispersions from single-Gaussian fits. Pluses correspond to H$\beta$ while open diamonds correspond to [O III]. The continuous line represents $\sigma_{gas} = \sigma_{stars}$.

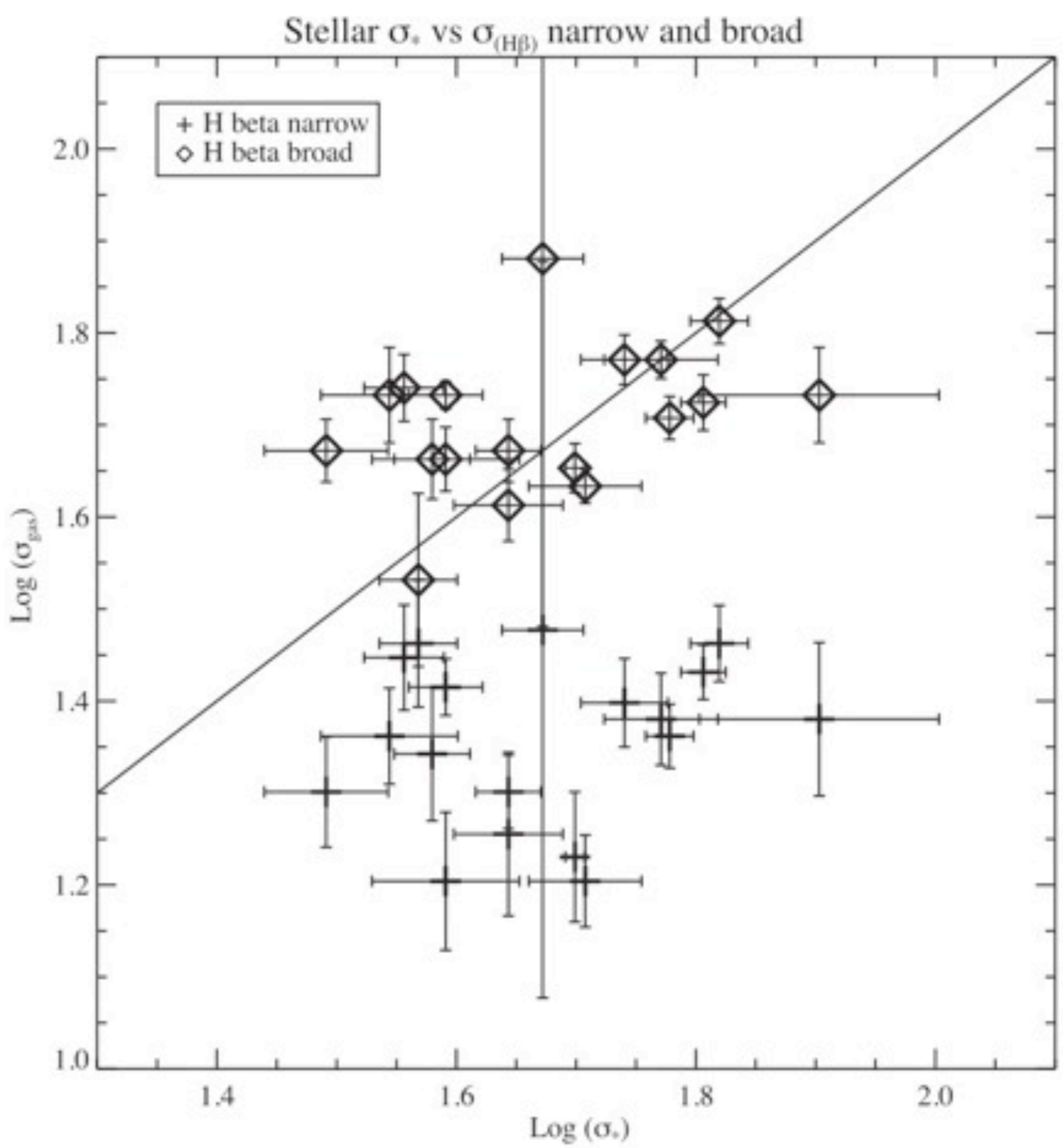


**Figure 4.** Gaseous (H$\beta$) versus stellar velocity dispersions for all the observed circumnuclear regions. The continuous line represents $\sigma_{\rm gas} = \sigma_{\rm stars}$.

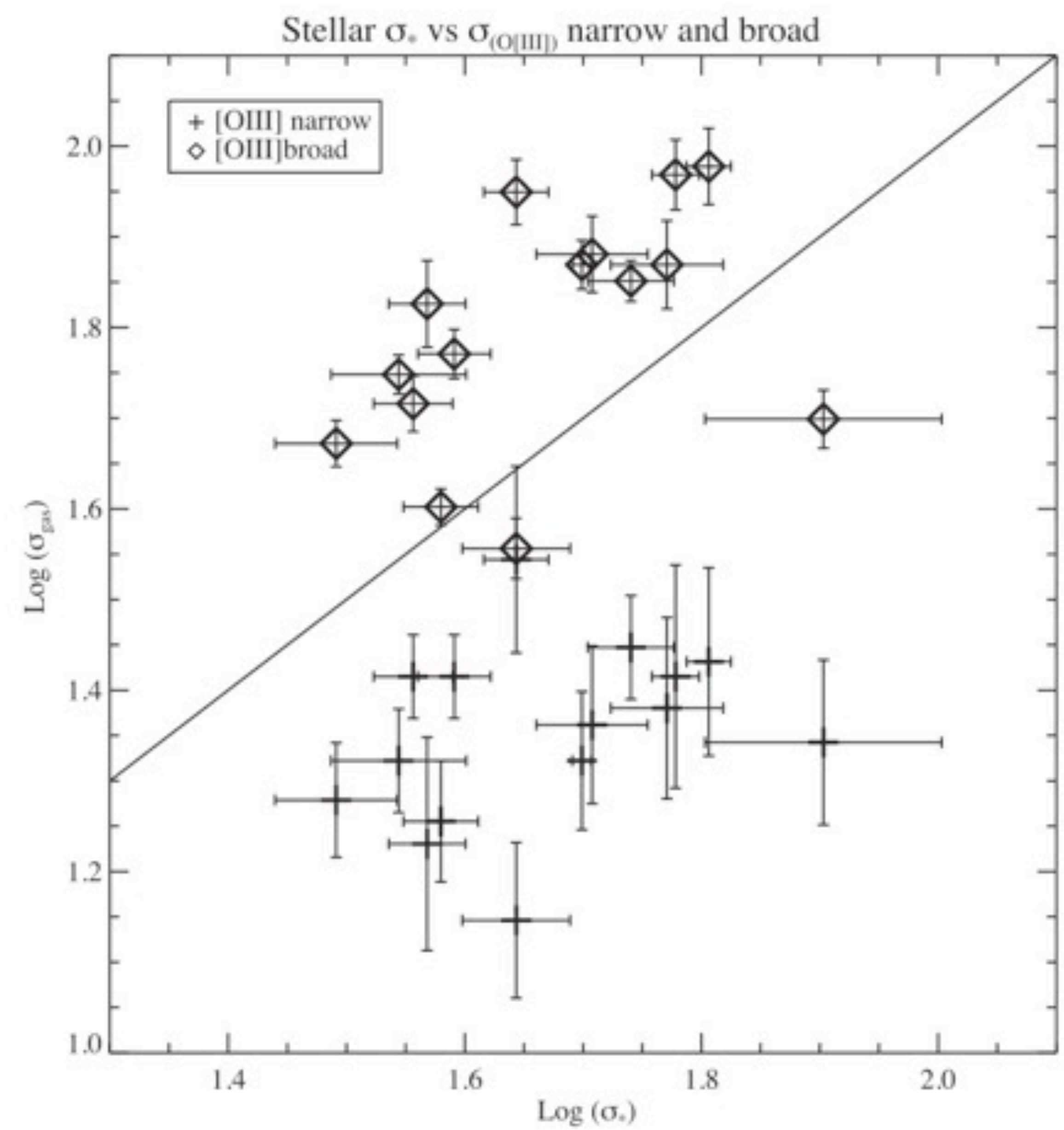


**Figure 5.** Gaseous (O[III]) versus stellar velocity dispersions for all the observed circumnuclear regions. The continuous line represents $\sigma_{\rm gas} = \sigma_{\rm stars}$.

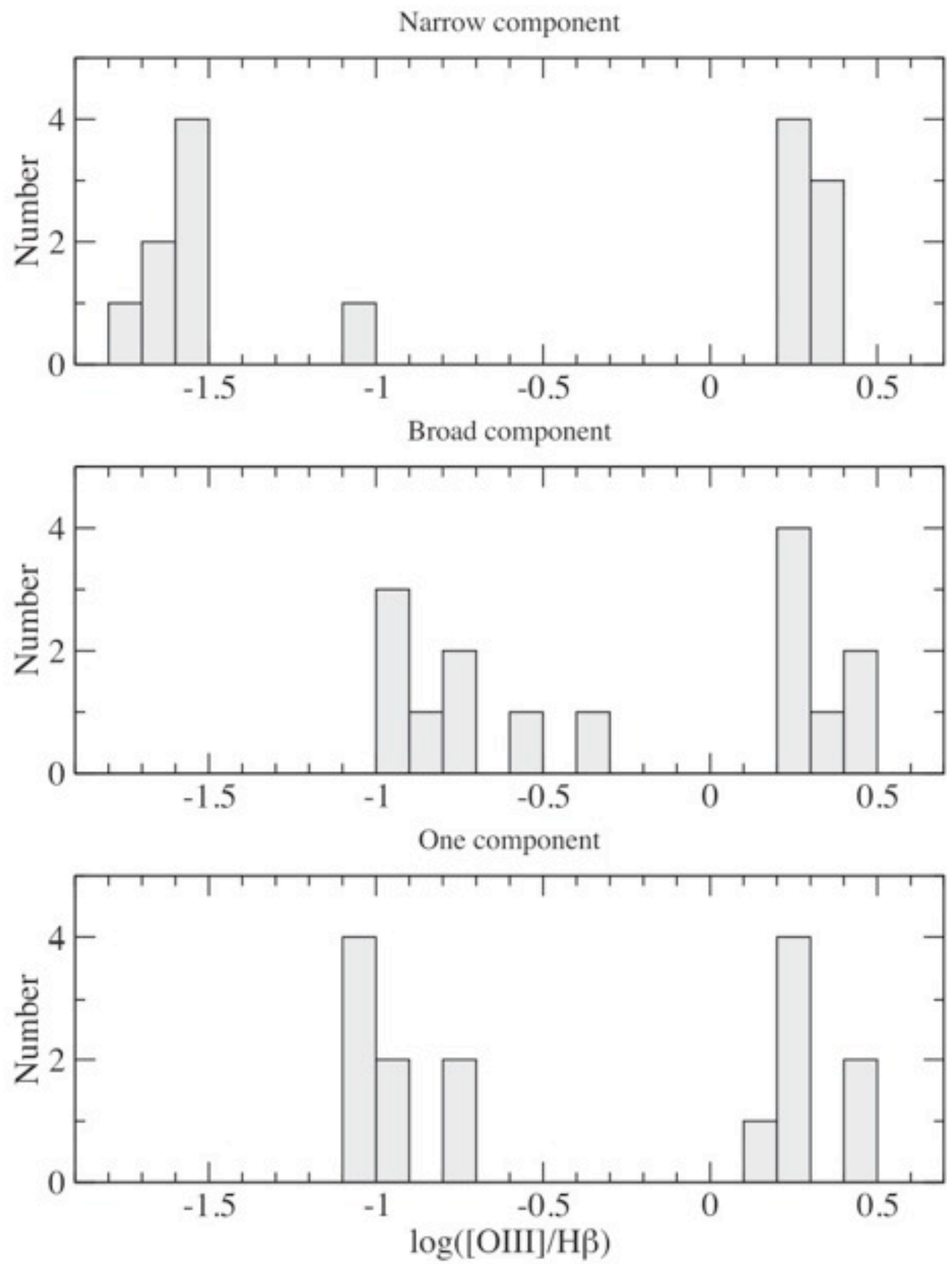


**Figure 6.** Histogram of the logarithmic [O III]/H$\beta$ ratio for the different gaseous kinematic components compared to values derived from single-Gaussian fits.



Wed, 24 Jul 2013

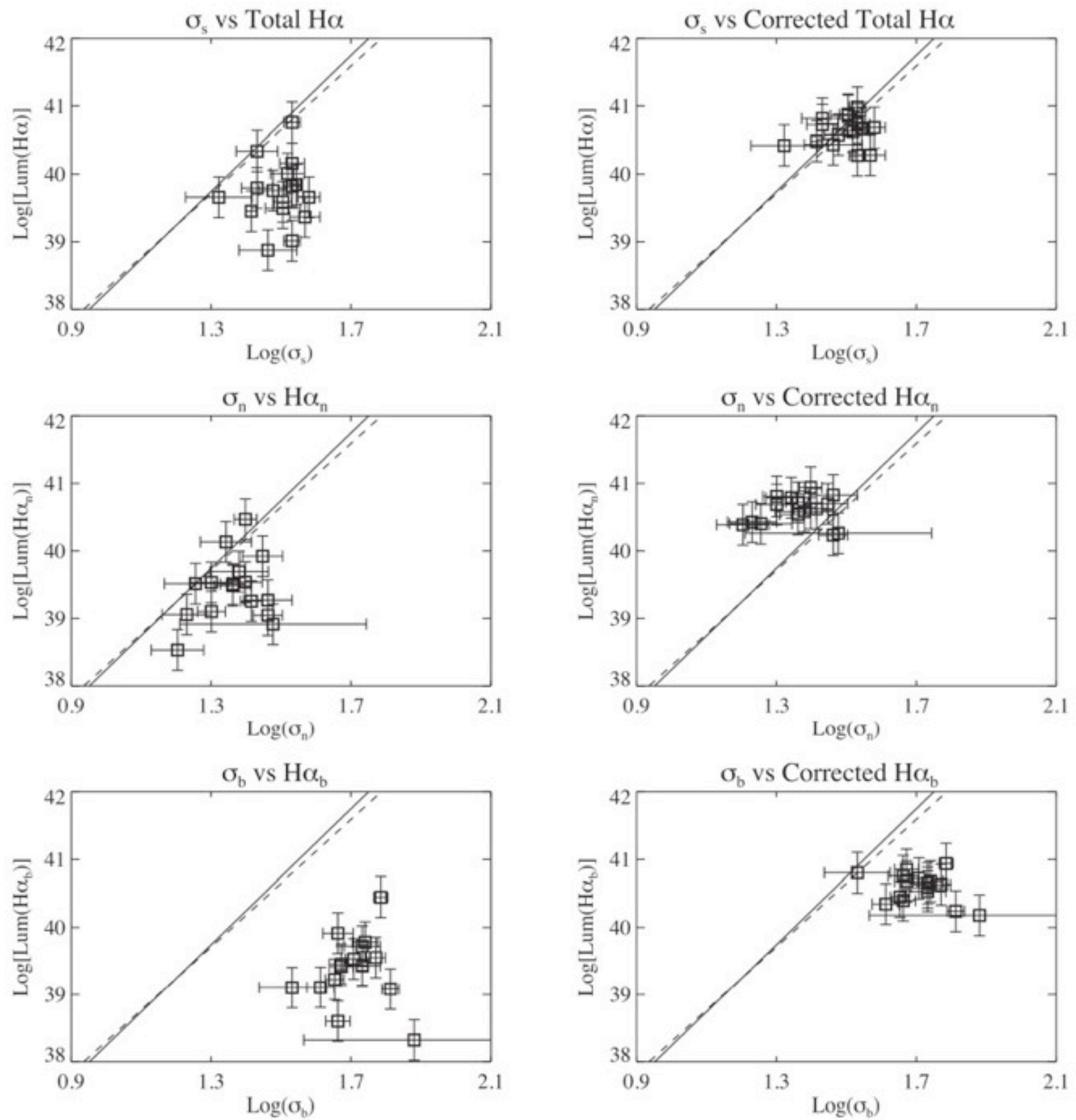


**Figure 7.** $\log(\sigma) - \log(L)$ relations for the observed CNSFRs. Panels show the relations derived for the velocity dispersions of the gas using a single-Gaussian fit (top), narrow components (centre) and broad components (bottom), respectively. The panels on the right show the result after correcting the luminosity for evolution (see the text). The lines correspond to a linear fit to 'young' giant H II regions, plotted as a reference value; B02 (dashed line) and Chávez et al. 2012

Jul

**Table 3.** Hα luminosities and derived quantities, and Hβ EWs.

| Region | $L(\mathrm{H}\alpha)_t$ | EM $f_n$ | EM $f_b$ | $L(\mathrm{H}\alpha)_n$ | $L(\mathrm{H}\alpha)_b$ | $M_{\mathrm{ion}}$ | $M_{\mathrm{H\,II}}$ | EW(Hβ) |
|---|---|---|---|---|---|---|---|---|
| | | | | NGC 2903 | | | | |
| R1+R2 | 66.3[a] | 49 | 51 | 32.3 | 34.0 | 18.9 | 0.79 | 12.1 |
| R1+R2 | – | 57 | 43 | 38.1 | 28.2 | – | – | 12.1 |
| R4 | 38.9[a] | 32 | 68 | 12.6 | 26.3 | 24.6 | 0.48 | 4.8 |
| R7 | 31.3[a] | 59 | 41 | 18.6 | 12.7 | 23.6 | 0.30 | 3.9 |
| | | | | NGC 3310 | | | | |
| R1+R2 | 102[b] | 48 | 52 | 49.3 | 52.7 | 13.9 | 3.38 | 28.6 |
| R4 | 144[b] | 58 | 42 | 83.5 | 60.5 | 17.6 | 4.78 | 32.4 |
| R4+R5 | 218[b] | 62 | 38 | 136 | 82.0 | 21.4 | 7.24 | 41.7 |
| R6 | 57.3[b] | 53 | 47 | 30.5 | 26.8 | 12.4 | 1.90 | 16.7 |
| S6 | 62.5[c] | 54 | 46 | 34.0 | 28.5 | 17.4 | 2.07 | 12.5 |
| R7 | 45.5[b] | 72 | 28 | 32.7 | 12.8 | 8.7 | 1.51 | 19.4 |
| R10 | 45.5[b] | 39 | 61 | 18.0 | 27.5 | 15.7 | 1.51 | 9.7 |
| J | 573[b] | 51 | 49 | 294 | 279 | 31.4 | 9.52 | 82.5 |
| | | | | NGC 3351 | | | | |
| R2 | 28.3[a] | 40 | 60 | 11.4 | 16.9 | 9.93 | 0.21 | 9.5 |
| R2 | – | 35 | 65 | 10.0 | 18.3 | – | – | 9.5 |
| R3 | 70.0[a] | 49 | 51 | 34.4 | 35.7 | 15.3 | 0.54 | 16.5 |
| R3 | – | 33 | 67 | 22.9 | 47.1 | – | – | 16.5 |
| R4 | 23.2[a] | 48 | 52 | 11.1 | 12.1 | 6.23 | 0.25 | 13.0 |
| R5 | 10.3[a] | 80 | 20 | 8.2 | 2.1 | 6.17 | 0.09 | 5.1 |
| R6 | 7.5[a] | 46 | 54 | 3.4 | 4.0 | 8.88 | 0.07 | 2.3 |

*Note*: EM$f$ in percentage, luminosities in $10^{38}$ erg s$^{-1}$, masses in $10^5$ M$_\odot$.
[a]From Planesas et al. (1997) corrected for the different adopted distances, and for reddening using $E(B-V)$ from Pérez-Olea (1996).
[b]From Díaz et al. (2000a).
[c]From Pastoriza et al. (1993).



Wed, 24 Jul 2013

Our main conclusion is that the presence of different kinematical components with similar total fluxes in the emission line spectrum of CNSFRs raises important doubts regarding the properties of the ionized gas derived from global line ratios obtained with low-resolution spectroscopy in star-forming regions in the central regions of early-type galaxies.

Given the ubiquity of these star-forming systems, ionized gas analyses should be done preferably from high-dispersion spectra with high spatial resolution.

# Outline

- Motivations
- Masses (photometric and dynamical)
- Drawbacks
- Difference between gas and stars
- Differences between photometric and dynamical
- 30-Doradus results
- What have we learnt? Implications

# Photometric Mass determination in young massive star clusters

From the luminosity → Photometric Masses;

Assumptions:

True stellar mass = model stellar mass

IMF (limits and slope)

Estimates :

age

metallicity

interstellar extinction

distance

# Dynamical Mass determination in young massive star clusters

- Based on the virial theorem ➔ dynamical masses, derived from projected $R_{hl}$ (~$R_{hm,}$ no mass segregation) and $\sigma_{los}$
- $M_{dyn} \;\alpha\; R_{hl} (\sigma_{los})^2$ (Spitzer 1987)
- Or (adapted by Kowenhoven + 2008, de Grijs et al. 2008)

$$M_{\rm dyn} = \eta \frac{r_{\rm hl}\sigma^2}{G},$$

Where $R_{hl}$ should be measured from the <u>continuum</u> light distribution and NOT from the Hα or any other emission line.

# Mass determination in young massive star clusters

- Dynamical masses

  Assumptions:

  ♥ The cluster follows a certain density model;

  ♥ equal-mass stars and no mass segregation;

  ♥ all stars are single;

  ♥ the cluster is in virial equilibrium;

# Drawbacks for young clusters

- The spectra of star-forming regions are dominated by hot stars and ionised gas emission.
- Winds and outflows, as well as gravity, affect the motion of the ISM (But baseline given by gravity).
- Rely on integrated spectra.
- Even if gravitational motions dominate, need to know full kinematic properties of the stellar component.

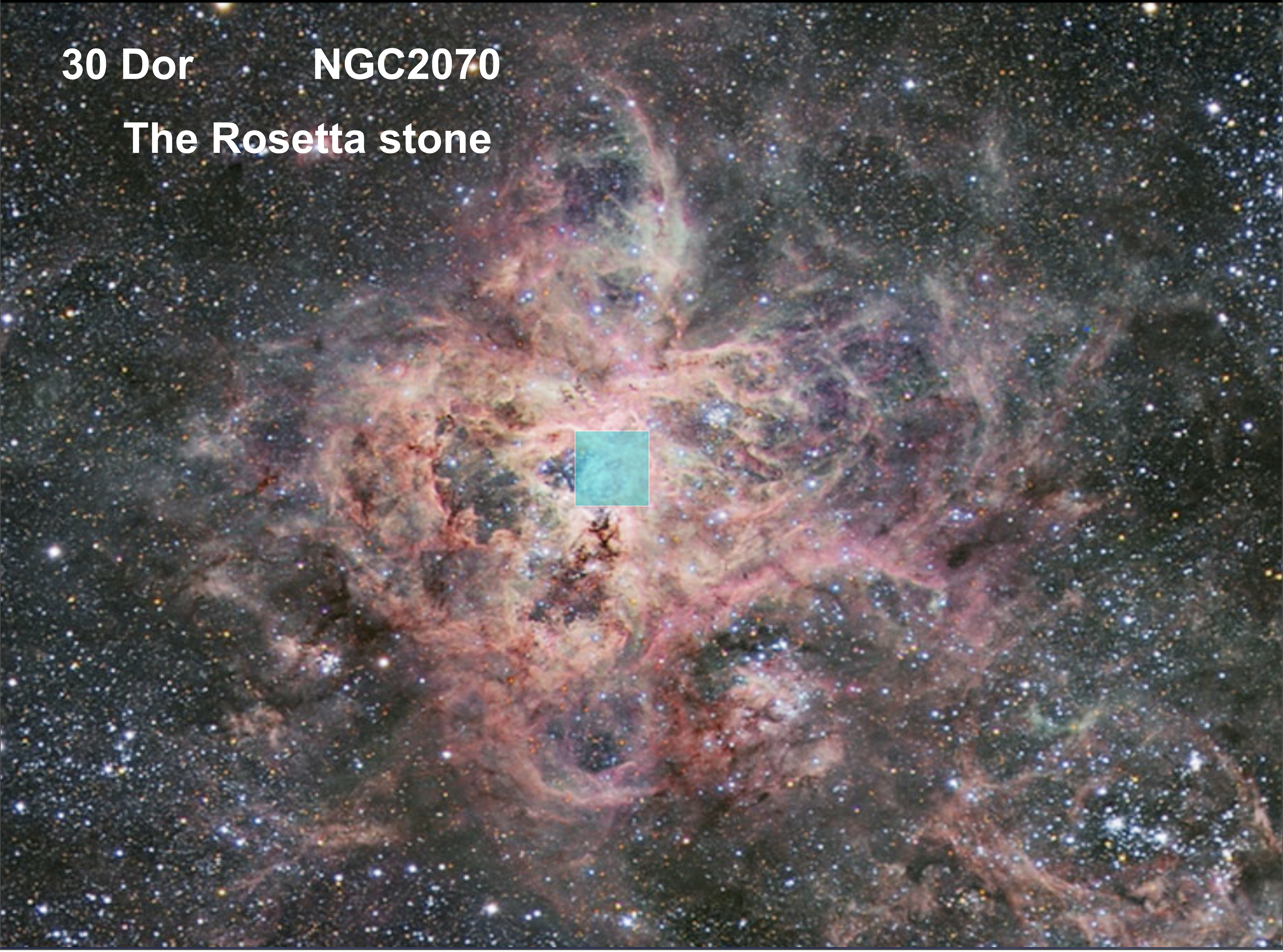
30 Dor NGC2070
The Rosetta stone

# 30-Doradus - NGC2070: The Rosetta stone

- Closest extragalactic massive starburst cluster (detailed studies)
- Binaries among massive stars?

  (known for some time).
- How common?

(Bosch et al. 1999,2001; single epoch mid-res. NTT-ESO spectra).

-- $\sigma$~35 km/s (OB * in NGC 2070);

-- while $M_{phot}$ ⇨ $\sigma$~10 km/s.

# 30 Dor Hα global profile

Flames observations by Torres-Flores et al 2013

FWHM = 56.7 km/s

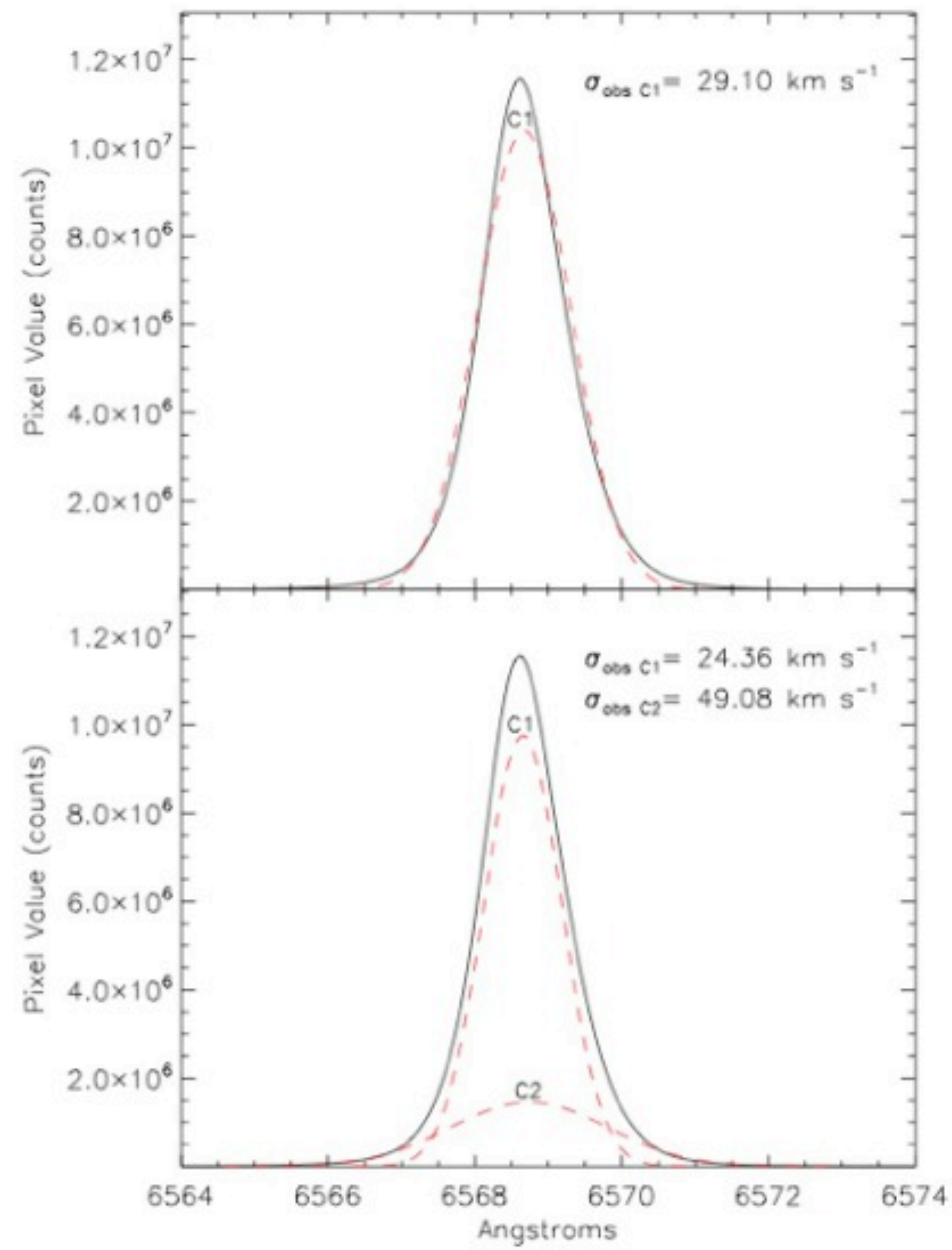


**Fig. 9.** Single and two-component Gaussian fits to the integrated Hα profile (upper and lower panels, respectively). The fitted components are shown by the red (dashed) lines and their widths are indicated in the upper right of each panel.

# *30 Dor H109α global profile*





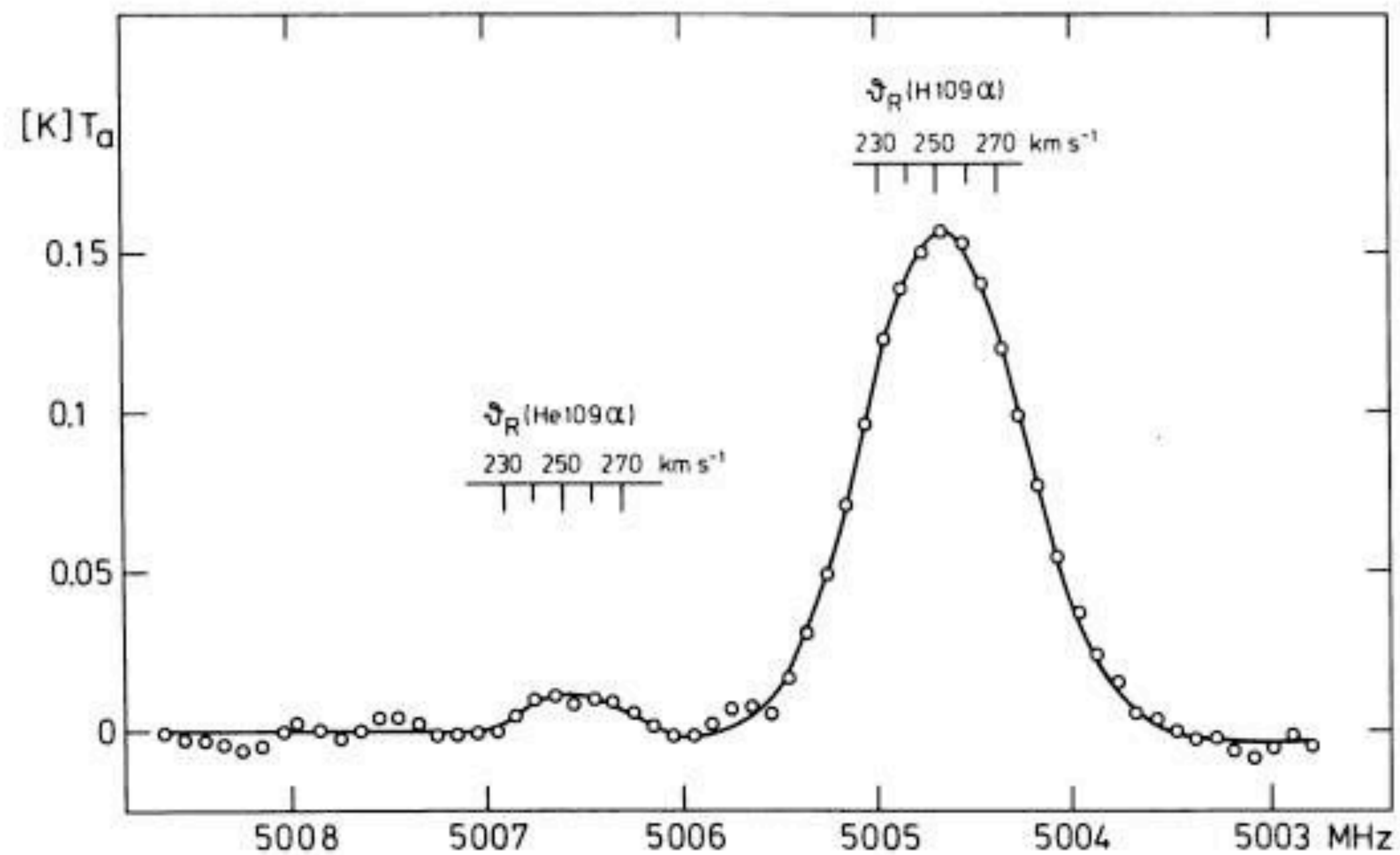


Fig. 1. The 109 α radio recombination lines of hydrogen and helium in 30 Dor as observed with the 64 m Parks radio telescope. The observed values are shown by open circles and the gaussian-fitted data are given by a solid line

Table 1

| | $T_L$ | $T_c$ | $T_L/T_c$ | $\Delta v_L$ | $V_r$ | HPW $\Theta_\alpha$ | HPW $\Theta_\delta$ | $T_{e_{LTE}}$ | $\langle N(He^+)/N(H^+)\rangle$ |
|---|---|---|---|---|---|---|---|---|---|
| | K | K | % | km s$^{-1}$ | km s$^{-1}$ | arc | arc | K | % |
| H 109 α | 0.162 ± 0.003 | 10.6 ± 0.3 | 1.5 | 57.6 ± 1.2 | 251 ± 3 | 3.0 | 3.0 | 11900 ± 1800 | 5–8 |
| He 109 α | 0.013 ± 0.003 | | | 38.2 ± 6.0 | 257 ± 9 | | | | |

# NGC 2070  IMF

Photometry for 1469 stars

Spectral types for 260 stars

From ESO NTT

Image:
130” or 35 pc each side



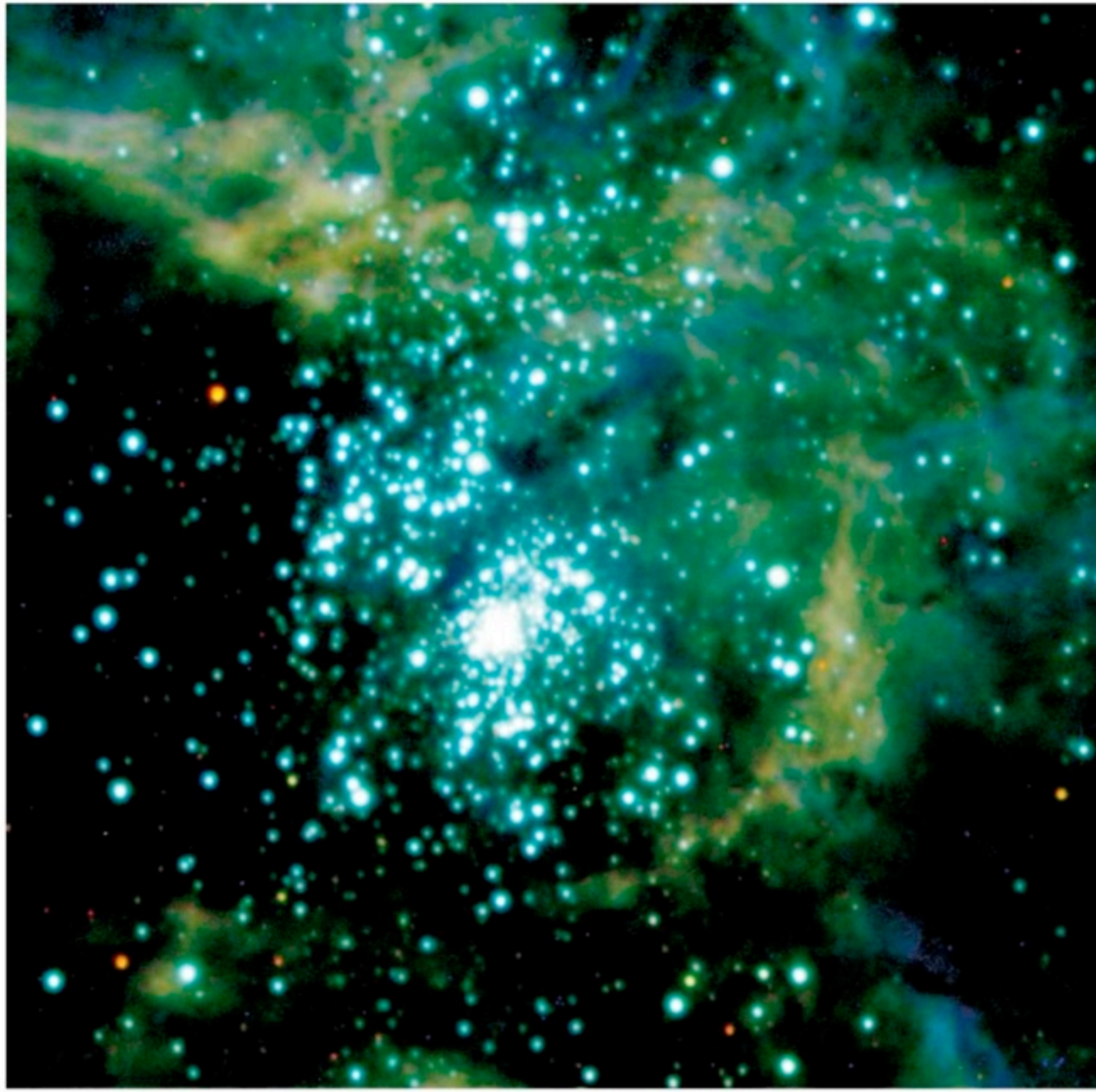

**Fig. 1.** Three–colour composite image of 30 Doradus showing the large number of hot blue stars. The V drives the red channel, the B drives the green channel, and the U drives the blue channel. The size of the field is 130″each side, corresponding to 35 pc for an adopted distance t
LMC of 55 kpc (Feast & Walker 1987). North is up, east to the left.

July 2013

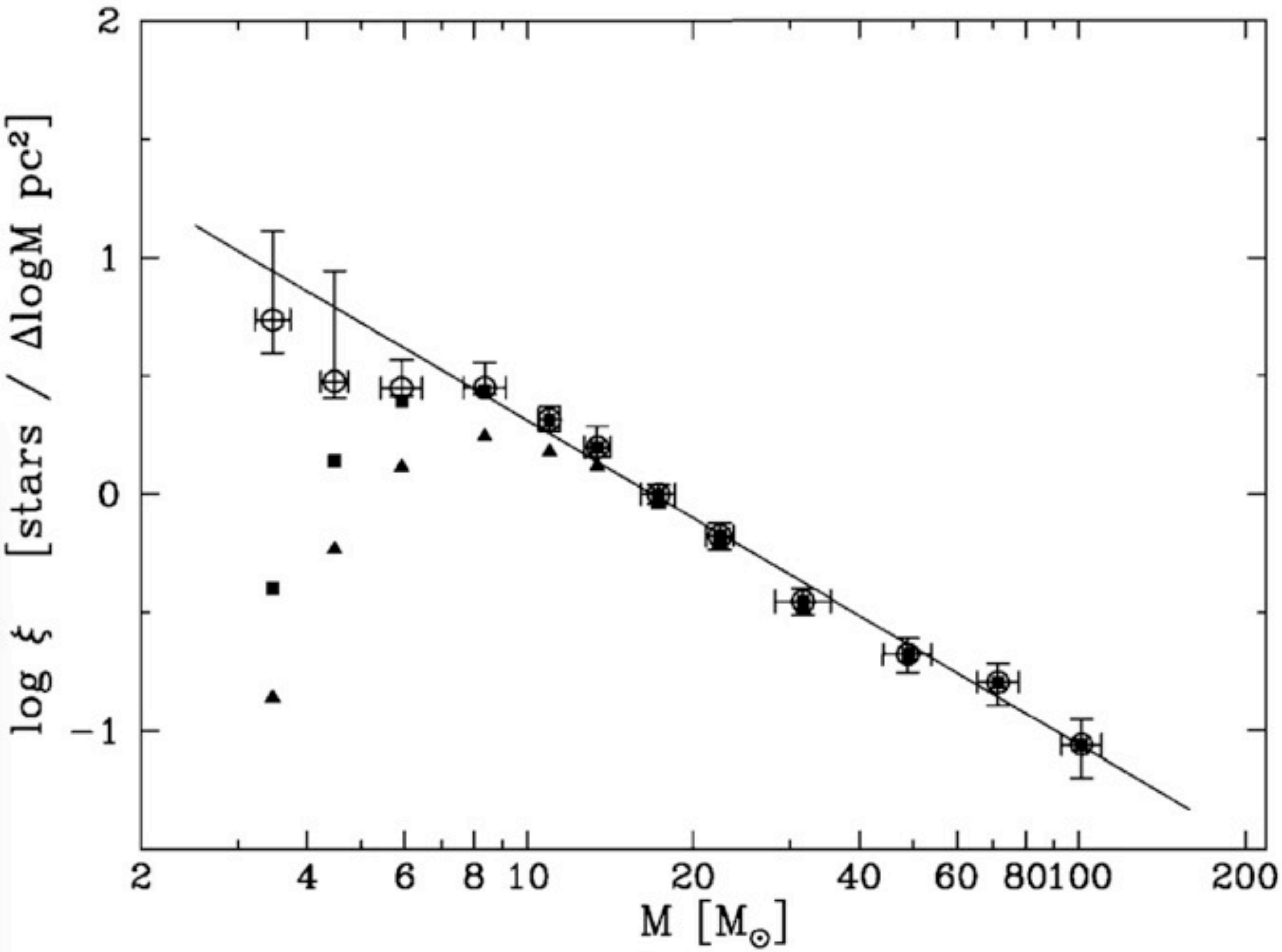


**Fig. 10.** The IMF of 30 Doradus for the sample of stars with $r > 15''$, calculated assuming equally likely isochrones below 3My. The line is a least squares fit to the data which gives $dN \propto M^{-2.37\pm0.08} dM$. The error bars consider counting statistics together with the errors in the incompleteness and magnitude-limit corrections.

# 30 Dor

Bosch et al (2002)

- NTT: Single epoch radial velocities for about 50 stars.
- Radial Velocity Dispersion (σ) ~ 32 km/s
  - Larger than the ionized gas! (~24 km/s)
  - Probably too large to be virialised.
- Indications of stellar mass segregation.
- Observational handicaps?
  - MOS tangled spectra
  - Red end unavailable (no reliable Rv for HeII 5411)
- Other source for a high stellar σ?
  - The presence of binaries ***could*** be introducing an enhancement of the observed velocity dispersion.

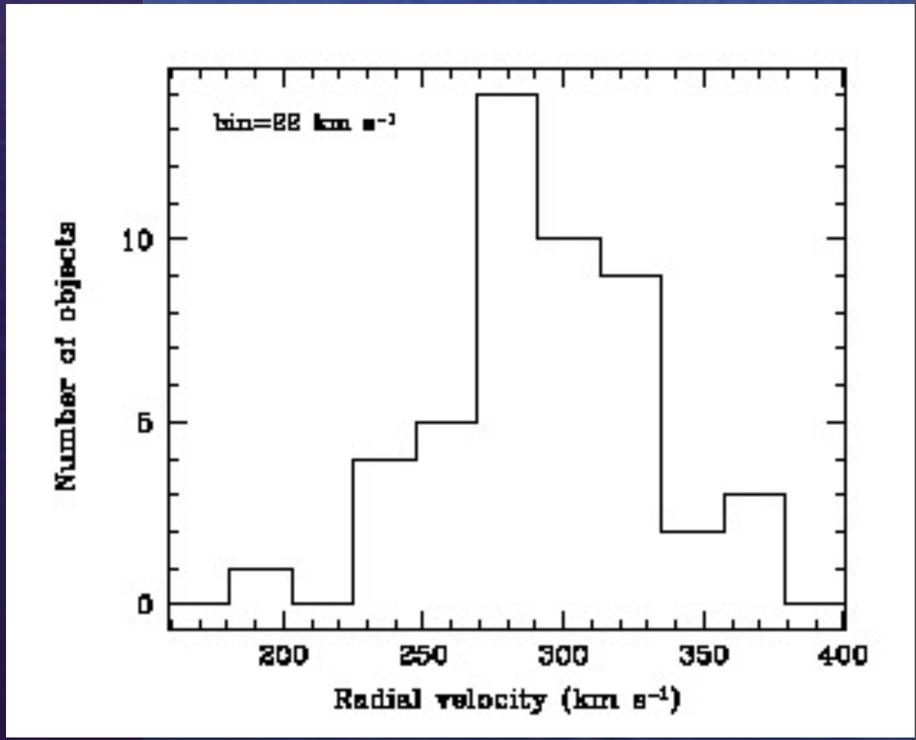

GEMINI OBSERVATORY

Images | Science | Public/Media | Jobs | About/Contact | Google™ Custom Search | Search

Change page styl

Default

# Binary Stars Abound in 30 Doradus Cluster

Home

A recent optical spectroscopic study led by Guillermo Bosch (Universidad de La Plata), Elena and Roberto Terlevich (INAOE, Tonantzintla) used the spectro-imager GMOS-South to reveal that a surprisingly high fraction (>50%) of the stars in the cluster NGC 2070 are binary. This massive cluster is responsible for ionizing the gas in the spectacular 30 Doradus nebula located in the Large Magellanic Cloud.

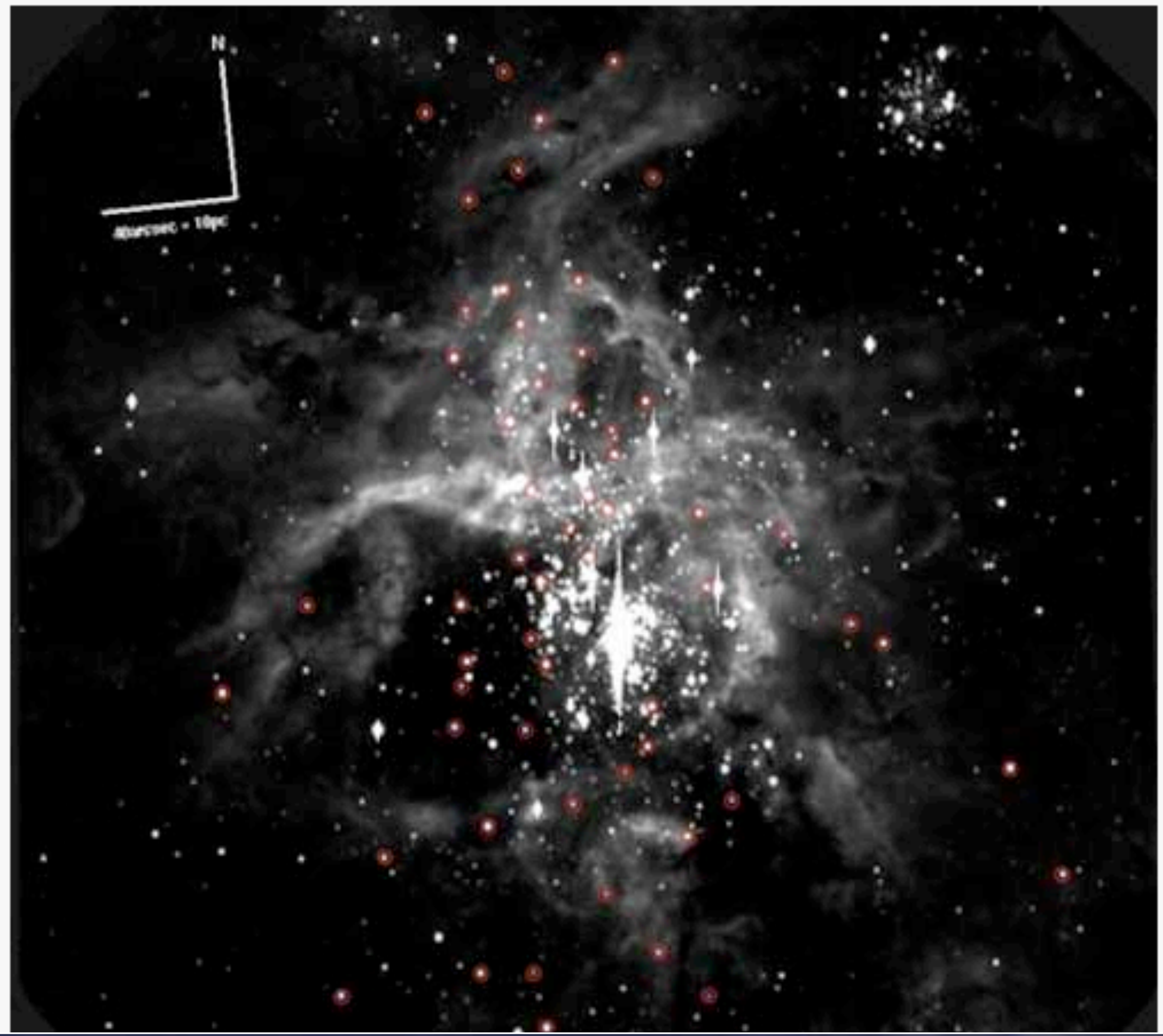


The fraction of binaries is an important factor influencing the initial mass function (IMF), the cluster's age, and dynamical mass determination. Although a large amount of work has been done on 30 Doradus and its ionizing cluster, little is known of it binary fraction.

Bosch and his colleagues obtained optical spectroscopy with the Gemini Multi-Object Spectrograph (GMOS) on Gemini South of 52 early-type stars on six epochs. Radial velocities derived for each night were very stable, with variation less than 1.0 km/sec. Twenty-five out of the 52 stars were found to be binary candidates. This is a very high mass fraction, considering that the finding here is only a lower limit.

The authors also derived the velocity dispersion for single mask epoch and found values as high as 30 km/sec. But after removing binary stars from the sample they were able to derive - for the first time - the velocity dispersion of NGC 2070 free

# 30-Doradus GMOS data

- Our Gemini-S GMOS (multi obj. spectrograph) optical observations

  50 early type * observed at 7 epochs in 2006 and 2007 ➪
  radial velocity variations ➪ spectroscopic binaries.

- Nebular emission lines used as anchor for zero point

  $\Delta V_{neb} \leq 1.0$ km/s; $\sigma_{neb} = 3.1$ km/s
  ➪ no systematic velocity shifts between epochs.

# GMOS data

Actual uncertainty in individual radial velocity measurements for each line (from IRAF ngauss task) ~ 5 km/s

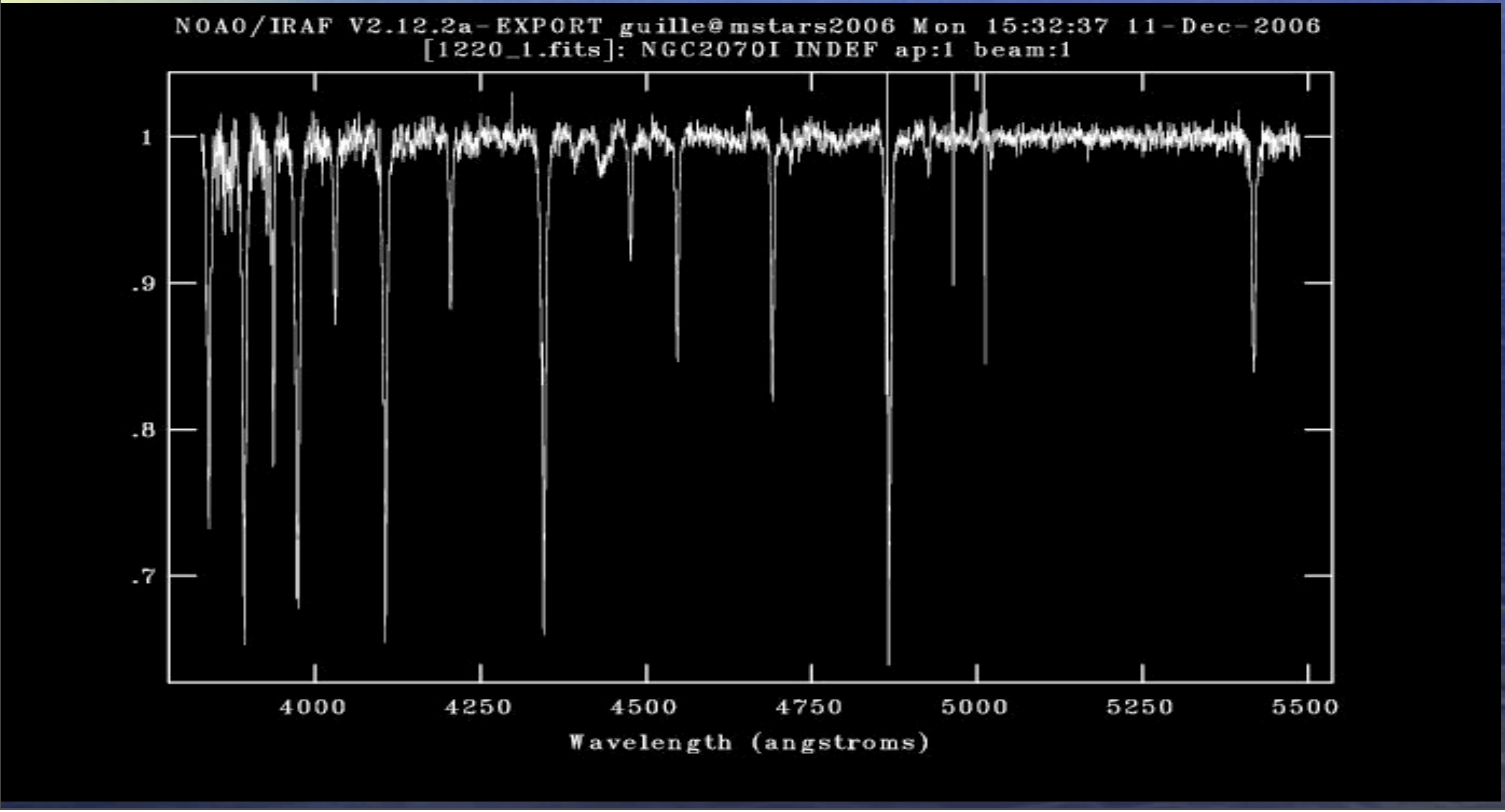

# Measurements

- Individual radial velocity for each absorption line (each ion/element separately), chosen according to the stellar type (same ones at all epochs for each star).
- Fitting uncertainties ~ 5 km/s.
- Differences in radial velocities between epochs, weighted by the internal error define binaries

  (Abt et al. 1972).

  Caveat: atmospheric turbulence and winds, both in early stars. But in that case, large internal errors.
- Also several double-lined binaries.

2 epochs:
profile changes
HeI λλ 4026, 4387Å;

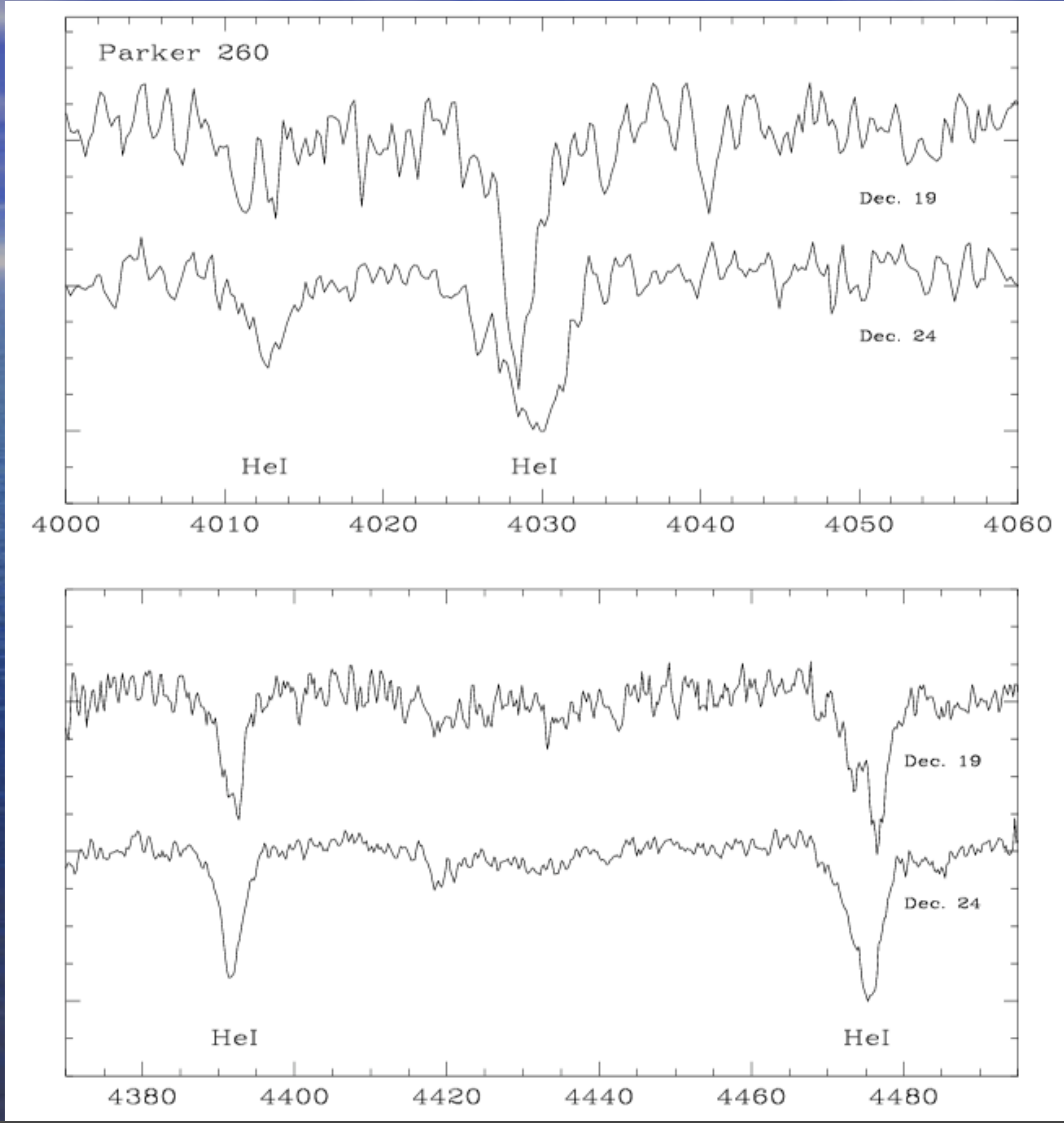


July 2013

# Results

- 48% of the stars are binaries
- Consistent with a 100% population being binaries (num. sim. Bosch & Meza 2001)
- More epochs will allow us to determine orbits and to confirm some of the candidates. (need very good S/N).

# Young cluster kinematics

- Multiple-Epoch velocity dispersion, i.e. after removing binary orbital motion, $\sigma_r$ = 8.3 km/s
- Single-epoch velocity dispersion typically $\sigma_r$ ~ 30 km/ are overestimates of the cluster velocity dispersion $\sigma_{cl}$.
- Single epoch measurements of the velocity dispersion are completely dominated by binary orbital motion.
- On the other hand because the stellar velocity dispersion $\sigma_r$ is determined by the most luminous stars motions, if the cluster is mass segregated $\sigma_r$ will be an underestimate of the cluster velocity dispersion $\sigma_{cl}$.
- ***In young clusters massive stars are not good test particles.***

# Cluster kinematics

- $M_{phot} \sim 4.5 \times 10^5 M_\odot$ (Selman et al. 1999)

$$\sigma_r^2 = \frac{4.5\ 10^{-3}\ M}{3\ R_c}$$

(Binney and Tremain. 1987; assuming isotropy)

For the total mass of 30Dor, $R_{1/2}$=12pc ➔

$\sigma_r$ = 8 km/s (consistent within observational and sampling uncertainties with our value)

Slight reduction expected but not dramatical, if more binaries Discovered.

- The binary corrected $M_{vir}$ is comparable to the $M_{phot}$ ➔

# Conclusions 1

- Binary fraction among massive stars in NGC 2070 (30Dor) (from 7 epochs) may be > 50%, and consistent with 100%.
- Important effects on:
  - ★ Virial masses of young clusters may be overestimated by large factors if binaries are neglected,
  - ★ Massive end of IMF?
  - ★ Formation process of massive stars
  - ★ Star cluster stability (de Grijs et al. 2008)
- $\sigma_r$ for ionizing cluster coincides (within errors) with stellar kinematics if cluster is virialized and Mass derived from photometric + ionized mass → cluster stands as a globular cluster progenitor (far from

# Conclusions 2

- Taken together, measurements of the photometric and dynamical masses can allow constraints on the stellar IMF and the dynamical state of the objects.
- If there is stellar mass segregation, $\sigma_{gas}$ may be a better estimator of $\sigma_{cl}$ than $\sigma_{*}$ from massive stars.
- If $\sigma_{gas} < \sigma_{*}$ that in itself could be a diagnostic for the presence of binaries.

To study the properties of young massive clusters we need high resolution, both spatial and spectral.

*Because the S/N of weak line increases almost linearly with resolution, the ideal resolution is given by the need to just resolve the ionized gas sound speed.*

*Minimum resolution given by H sound speed at*

*$T_e$ ~ 10,000 K, i.e. R > $c/c_s$ ~ 30,000*

*And, we need this from 3500 Å to 2.4*

# Thanks